Rotational dynamics of viscoelastic planetary bodies

Important note
To cite this publication, please use the final published version (if applicable).
Please check the document version above.

Rotational Dynamics of Viscoelastic Planetary Bodies

Rotational Dynamics of Viscoelastic Planetary Bodies

Proefschrift

ter verkrijging van de graad van doctor

aan de Technische Universiteit Delft,

op gezag van de Rector Magnificus prof.dr.ir. T. H. J. J. van der Hagen,

voorzitter van het College voor Promoties,

in het openbaar te verdedigen op

woensdag 2 mei 2018 om 12:30 uur

door

Haiyang Hu

Ingenieur Luchtvaart en Ruimtevaart,
Technische Universiteit Delft, Nederland,

geboren te Chengdu, China.

Dit proefschrift is goedgekeurd door de promotoren.

Samenstelling promotiecommissie bestaat uit:

Rector Magnificus,	voorzitter
Prof. dr. L. L. A. Vermeersen,	Technische Universiteit Delft, promotor
Prof. dr. ir. P. N. A. M. Visser,	Technische Universiteit Delft, promotor
Dr. ir. W. van der Wal,	Technische Universiteit Delft, co-promotor

Onafhankelijke leden:

Prof. dr. N. Rambaux	IMCCE, France
Prof. dr. T. van Hoolst	Royal Observatory of Belgium, België
Dr. I. Matsuyama	The University of Arizona, USA
Prof. dr. -ing. Habil R. Klees	Technische Universiteit Delft
Prof. dr. E. K. A. Gill	Technische Universiteit Delft, reservelid

An electronic version of this dissertation is available at
http://repository.tudelft.nl/.

一叶秋风，
清庭芳满，
舟行江上，
日落天涯.
The peacefullness on the voyage into the unkown.

胡海洋 轩辕 少游

CONTENTS

PREFACE

Solving a problem is always fun to me. It is like a game: specific rules are given, you make your moves to reach the goal.

I was very fond of mathematics and physics when I was in primary and middle school. For this reason, I chose theoretical mechanics for my bachelor study, which I thought was a nice combination of both and did a second-major in fundamental mathematics. I finished these studies but did not get the thrill I expected.

I came to the Netherlands in 2009 and went to Hogeschool Fontys in Eindhoven to study something completely new, electrical engineering. Because of this, I found the excitement and willingness to devote myself to something, again. The most helpful experience in this year was the internship at GE security in Weert. I worked with Math Pantus, a great engineer and a radar geek (people who would build a radar in their backyard and stay up in the night to communicate with people on the other side of the Earth). The task given to me was to build a functionality in a motion radar so that it can distinguish a human from a dog (usually a pet is not allowed if a motion radar is installed). This work made me understand that the deployment of mathematics, physics and programming to solve a concrete and complex real life problem in is the true passion for me.

I decided to stay in the Netherlands for a master study. And I chose the "coolest" major I could found here: aerospace engineering in TU Delft. Since I had no background in this major, in the beginning, I did not even know what *angle of attack* was (it is not the best attack angle for a fighter plane as I thought). I had great help from Dr. Qiping Chu and Dr. Erik-Jan van Kampen who gave courses on control theory and later became my MSc. thesis supervisors. I chose a topic which was to use interval analysis to analyse the stability of an uncertain system. It was a challenging task which gave me a taste of the joy in scientific research and led to my decision to continue a PhD study.

At the beginning of the search for a PhD position, I sent my application to many fields. I just needed an interesting problem to solve and I had the feeling that if the topic required the fundamental skills I have, then I would be able to do it. However, not many potential employers would see it in this way, they probably only saw a guy with no background knowledge for the specific position. It is still a mystery to me why my PhD supervisor prof. Bert Vermeersen chose me to carry out the PhD project for which he had funding, except that Dr. Chu and Erik-Jan gave me very good references. But thanks to Bert, I could start my four year PhD here in TU Delft, which is one of the happiest experiences in my life so far, I got to do the thing I like most: solving a challenging problem while getting paid (yeah!). It was not easy in the beginning, for someone who could not name the nine (now eight) planets in our solar system in sequence to conduct a scientific research in planetary science. I got great help from Bert through my entire PhD study. I was quite lucky for me that my promoter is also an expert in this field. I still remember that once after a short presentation of my results in a group meeting, Bert immediately pointed out a factor I missed in the formulation of the problem which turned out to be very significant. One thing I appreciate most is the

freedom Bert gave me to carry out the research in my own way. The content of this thesis is different from the original proposal of this project. After the first two years in which I finished the finite-element model (FEM), I discovered that it was not possible to get a complete dynamic solution for the reorientation of tidally deformed bodies, and all methods for calculating large angle polar wander only results in approximated solutions. As a result, I decided to develop a method for solving this problem, during which Bert provided me with both support and advice.

This thesis could also not have been completed without the help of Wouter van der Wal, my daily supervisor. Wouter gave me the most direct help throughout my PhD study. A draft paper which I had read for five times myself and which I did not want to lay even one eye on anymore, Wouter was willing to read and help correct again and again. Without Wouter's help, none of my publications would have gained their current scientific level. The help from Wouter was not only in scientific issues but also in daily life. I still have many naive perspectives on many issues, both in daily life and in science. Wouter always gave me suggestions on various issues. I argued with Wouter the most during my PhD study and I also learned from him the most.

This period of my PhD would have been much less fun without all my colleagues in this friendly and multi-cultural group of Astrodynamics and Space Missions. Hermes shared the office with me for two and half years and helped me a lot at the beginning of my PhD. Hermes' expertise on icy moons and general geophysics gave me the first guidance into this field. Work with Hermes was easygoing. We could say no words to each other except "morning" and "see you", or we could drink beer and talk for 5 hours. Dominic was the first person who welcomed me in this group. The intensive discussion about the rotation matrix through e-mail is still memorable for me. I also thank him a lot for proofreading this thesis. Bas and Teresa shared a different office later with me, it was quite an interesting and enjoyable experience for me to work with a "non-Dutch" Dutch and a "non-German" German.

I also appreciate the help of many people along the journey of my PhD, prof. Zdeněk Martinec gave me my first lecture on rotational dynamics. During my short stay in UC Berkeley, I had many nice discussions with Prof. Imke de Pater, the author of the textbook Fundamental Planetary Science, which was like a bible in the beginning of my PhD. I also give my deepest thanks to our secretary Relly, who takes care of all the bureaucratic issues that I dislike. I thank Prof. Pieter Visser for being the committee member of my defence and leading this dynamic group. And I also thank The Netherlands Organisation for Scientific Research (NWO) for funding this project. Finally, I sincerely thank my PhD defence committee for taking the time to read my thesis and be part of the defence, especially those coming from outside the Netherlands.

During my stay here in the Netherlands, I had lots of fun with my friends and high school classmates Shiyan and Lijin, and their lovely partners Zhongkai and Guannan. It was amazing to reunite with people you knew from teenage years in a country so far away. And last and most important, thank you, Mom and Dad, for watching over me all these years, through all the difficulties, providing endless patience and support, even if it meant that your only son was staying on the other side of the planet.

Haiyang
Delft, April 2018

SUMMARY

True polar wander (TPW), the secular part of the displacement of the rotation axis with respect to surface topography or internal signatures, has been proposed to explain many geologic features on various planets and moons, e.g, the Tharsis plateau on Mars (Schultz and Lutz, 1988), the tiger stripes on Enceladus (Nimmo and Pappalardo, 2006) and the Sputnik Planitia on Pluto (Keane et al., 2016). The theoretical study of polar wander can be dated back to the 18th century when Euler predicted the free precession of the Earth. Gold (1955) introduced the modern concept and general mechanism of TPW. Goldreich and Toomre (1969) gave a early quantitative treatment of the problem. After the development of the normal mode method for viscoelastic media, Love numbers can be obtained which describe the deformation of a stratified viscoelastic planetary body for surface and tidal loads (Farrell, 1972). With such a description, the moment of inertia (MoI) equation, which gives the change in the MoI of the body, can be explicitly expressed in terms of the rotational vector components. Together with the Liouville equation, a time-dependent solution for TPW on a visco-elastic multi-layer model can be obtained. Due to the mathematical difficulty to solve these two equations, an exact analytical solution for TPW could not be achieved in previous studies. Instead, three types of approximated methods were adopted:

- Linear method. Early studies focused on the present day TPW on the Earth and small angular change. A linear approach, which applies the linearised form of the Liouville equation (Munk and MacDonald, 1960), was adopted. This can be used to calculate TPW for the case that the rotational axis is not too far away (less than 10 degrees) from the initial position (Nakiboglu and Lambeck, 1980; Sabadini and Peltier, 1981; Wu and Peltier, 1984).

- Non-linear method with the quasi-fluid approximation. In order to deal with the long-term rotational variation of Earth which may include large (more than 10 degrees) angle TPW, non-linear methods have been developed. They adopt the quasi-fluid approximation which assumes that the variation of the driving force for TPW is much slower than the characteristic viscous relaxation. Mathematically, the quasi-fluid approximation is an approximation taking the first order terms in the Taylor expansion of the tidal Love number (Spada et al., 1992a; Ricard et al., 1993; Cambiotti et al., 2011).

- Fluid limit method. The reorientation on a rotating tidally deformed body can not be dealt with by current theories, linear or non-linear because when the body is tidally deformed, we have a triaxial body (no symmetry around the rotational axis). Reorientation of such bodies involves not only the displacement of the rotational axis but also the tidal axis. Most studies concerning TPW of a tidally deformed body only focus on the fluid limit of the visco-elastic response which gives the final position of the rotational and tidal axes (Willemann, 1984; Matsuyama and Nimmo, 2007).

For these approximated solutions, several issues concerning their applicability have not been studied yet. Firstly, the linearised form of the Liouville equation is derived in the body-fixed frame where the rotational axis coincides with the axis of the maximum MoI in the beginning (Munk and MacDonald, 1960). Since the loading (the inertia tensor representing the extra mass applied on the solid model) is also defined in the body-fixed fame, the linear theory actually also assumes that the relative location of the loading with respect to the rotational axis does not change during TPW. The error caused by this assumption can theoretically invalidate this method as the location of the loading approaches the equator or the poles. When a point mass is located near the poles or equator, the effect of a change in colatitude of the point mass is larger than when the point mass is placed at 45(135) degree colatitude, for example. As a result, the valid applicable range for the linear methods should decrease as the loading approaches the pole or the equator. Currently, no study gives the expected error in the linear theory as a function of the angle of TPW and the position of the load.

Secondly, the non-linear approach is currently the only general way to calculate large-angle (more than 10 degrees) TPW. As a result, the effect of the quasi-fluid approximation, which is applied in many previous studies (Spada et al., 1992a, 1996; Ricard et al., 1993; Harada, 2012; Chan et al., 2014; Moore et al., 2017), has not been tested. So it is not clear what the effect is of taking the quasi-fluid approximation and ignoring the effects of the slow relaxation modes on the TPW behaviour.

Thirdly, since the fluid limit solution does not provide dynamic solutions, we do not have a clear insight in how the reorientation of a tidally deformed body is accomplished. Studies which concern the direction of polar wander of tidally deformed bodies driven by either a positive mass anomaly such as ice caps on Triton (Rubincam, 2003) or a negative mass anomaly such as a diapirism induced low density area on Enceladus (Matsuyama and Nimmo, 2007; Nimmo and Pappalardo, 2006), assume that the polar motion is directly targeting its end position, or in other words, moving towards the end position along a great circle. However, these assumptions are not tested in these papers because a theory to provide a time-dependent solution is lacking.

In order to tackle these problems, this thesis presents a more general method to study the rotational variation of planetary bodies and evaluate the approximations taken in previous studies. We first established a numerical iterative procedure which can be combined with a finite element package where also lateral heterogeneity and complex rheology can be adopted. Then a semi-analytical approach was also established with which the influence of the lithosphere and hydrostatic state of the body can be taken into account. Compared to previous approaches, the new method can calculate both small (less than 10 degrees) and large (larger than 10 degree) angle TPW as well as the long-term secular trend and short-term Chandler wobble for fast-rotating bodies such as Earth and Mars. As a result, the long-term mega wobble for slow-rotating objects such as Venus can also be dealt with. Most importantly, our new method provides a dynamic solution for reorientation of tidally deformed bodies. The effect of the lithosphere can be directly included and models which are not in hydrostatic equilibrium can also be simulated.

With the help of the new method, we can demonstrate that, firstly, the linear rotation theory leads to a bias which can be infinitely large when the initial position of the mass anomaly causing the true polar wander approaches the poles or the equator. This significantly limits the applicable range of the linear method if loads are close to poles or equator. Secondly,

the quasi-fluid approximation can introduce a large error in the transient response for a time-dependent solution. For instance, the TPW speed on Mars calculated based on the quasi-fluid approximation can be underestimated by a factor of 4, while the speed of the rotational axis approaching the end position on Venus is overestimated. Thirdly, a tidally deformed rotating body has a preference for reorientation around the tidal axis rather than the rotational axis. Rotational axis motion driven by a positive mass anomaly near the poles tends to first rotate around the tidal axis instead of towards it. For tidally locked bodies, positive mass anomalies are more likely to be found around the equator and the great circle perpendicular to the tidal axis, while negative mass anomalies tend to be around the great circle that contains the tidal and rotational axes.

Finally, we introduce a dimensionless fluid limit process number $\mathscr{F}$ which can be obtained from the Love numbers of the planet model and TPW speed. With this number, we provide a simple criterion to test if the fluid-limit solution or the quasi-fluid approximation can be adopted given a specific interior model and estimated maximum reorientation speed. It is shown in this thesis that this number $\mathscr{F}$ needs to be less than 0.001 for the reorientation path of a tidally deformed body obtained by the fluid limit solution to match the path of the dynamic solution close enough for practical purposes. The same criterion also applies for results obtained by the quasi-fluid approximation.

The new method is applied to various planetary bodies and new insights are obtained on the rotational behaviour of these bodies.

Earth. For a mass load on a layered Earth derived from the Preliminary Reference Earth Model (PREM) (Dziewonski and Anderson, 1981) together with a reasonable viscosity profile such as the SG6 model (Wu and Wang, 2006), both the linear method and our approach can yield an accurate present day TPW. However, due to the intrinsic error of the linear method, predicting TPW behaviour for more than 0.8 degree with this approach can result in more than 2% error.

Mars. Due to the adoption of the quasi-fluid approximation, previous estimates of the TPW speed (about 1 degree/Ma), e.g. Chan et al. (2014); Bouley et al. (2016), can be underestimated up to a factor of 4.6 given the possible range of the Martian viscosities (10^{19} to 10^{22} Pa s).

Venus. The rotational behaviour of Venus is dominated by a mega wobble, which is a slow wobble with large amplitude (Spada et al., 1996). Spada et al. (1996) overestimated the speed of a mass anomaly on Venus approaching the pole or equator due to the effect of applying the quasi-fluid approximation. If we assume that Venus has similar viscosity as the Earth or Mars, a positive mass anomaly of the same relative scale will take much longer time (10-15 times) on Venus to reach the equator than on the Earth or Mars.

Icy moons. Most icy moons are tidally locked to a much more massive body. For example, the mass of Jupiter is about 37500 times the mass of its moon Europa. We show that the reorientation of these tidally deformed bodies triggered by a positive mass anomaly has a preference of first reorienting around the tidal axis to place the mass anomaly close to the equator. Then the speed of the reorientation slows down and the mass anomaly moves slowly towards the sub-host or anti-host points. Consequently, TPW on an icy moon, such as Triton, Enceladus and Europa, triggered by large ice caps on the poles would see the body reorient around the tidal axis first, different from what is predicted in (Rubincam, 2003) and (Matsuyama and Nimmo, 2007) with the fluid-limit method. The presence of a lithosphere

mostly determines to what extent positive mass anomalies can be relocated towards the sub- and anti-host points but the mass anomalies are still more likely to be found around the equator.

Pluto. Although Pluto is tidally locked with the orbiting moon Charon, the mass of Charon is only about 12% of that of Pluto which creates a smaller tidal bulge than that of the icy moons. As a result, the reorientation path on Pluto does not have a strong preference to first reorient around the tidal axis. Instead the path of the mass anomaly is almost along a great circle. This means the reorientation path obtained in previous studies based on the fluid-limit method, e.g. (Keane et al., 2016), can be very close to a complete solution. However, the speed of the reorientation is still biased by the fluid limit method depending on the viscosity of the planet and the load history, e.g. how fast the volatile accumulates in the Sputnik Planitia (Keane et al., 2016) and the ocean upwells (Nimmo et al., 2016).

To summarize, the new method established in this thesis provides a more advanced tool for planetary scientists to properly interpret manifestations of rotational variations on various bodies.

SAMENVATTING

Poolbeweging, ook wel bekend als true polar wander (TPW), is de langdurige verplaatsing van de rotatie-as ten opzichte van de oppervlaktetopografie of interne signaturen. TPW wordt gesteld als verklaring voor geologische kenmerken op verschillende planeten en manen zoals het Tharsis plateau op Mars (Schultz and Lutz, 1988), de tijgerstrepen op Enceladus (Nimmo and Pappalardo, 2006) en de Sputnik Planitia op Pluto (Keane et al., 2016). Het theoretisch onderzoek naar poolbeweging dateert uit de 18e eeuw toen Euler de precessie van de Aarde wist te voorspellen. Gold (1955) heeft het moderne concept en het algemene mechanisme van TPW geïntroduceerd. Goldreich and Toomre (1969) zijn pioneers geweest in de kwantitatieve aanpak van het probleem. Nadat men de NormaalModeanalyse voor verschillende visco-elastische media heeft uitgeschreven, kunnen Love getallen gevonden worden die de vervorming op een gelaagd visco-elastisch planetair lichaam beschrijven voor oppervlakte- en getijdebelastingen (Farrell, 1972). Met deze beschrijving kan de "traagheidsmomentvergelijking", die de verandering van het traagheidsmoment van het lichaam geeft, expliciet worden uitgedrukt in componenten van de rotatievector. In combinatie met de Liouville vergelijking kan vervolgens een tijdsafhankelijke oplossing voor TPW op een visco-elastisch gelaagd lichaam gevonden worden. Door de wiskundige complexiteit die samenhangt met het oplossen van deze twee vergelijkingen is een exacte analytische oplossing voor TPW nooit gevonden in voorgaande onderzoeken. In plaats daarvan zijn 3 methodes ontwikkeld om tot een benaderde oplossing te komen.

- Lineaire oplossing: De eerste onderzoeken richtten zich vooral op hedendaagse TPW van de Aarde en kleine hoekveranderingen. Een lineaire aanpak, die de gelineariseerde vorm van de Liouville vergelijking (Munk and MacDonald, 1960) gebruikte, werd aangenomen. Deze methode kan gebruikt worden om de TPW te berekenen voor gevallen waarbij de rotatie-as zich niet ver beweegt (minder dan 10 graden) van zijn beginpositie (Nakiboglu and Lambeck, 1980; Sabadini and Peltier, 1981; Wu and Peltier, 1984).

- Niet-lineaire oplossing met een quasi-vloeibare benadering: Om ook met lange termijn veranderingen van de Aardrotatie om te kunnen gaan (meer dan 10 graden verandering van de rotatie-as), zijn niet-lineaire methodes ontwikkeld. In deze methodes werd de quasi-vloeibare benadering gebruikt waarin wordt aangenomen dat de variatie van de drijvende kracht achter TPW vele malen langzamer is dan de karakteristieke viskeuze relaxatie. Wiskundig gezien is de quasi-vloeibare benadering een benadering waarbij de eerste orde termen van de Taylor-reeks van de getijde Love getallen worden gebruikt (Spada et al., 1992a; Ricard et al., 1993; Cambiotti et al., 2011).

- Vloeistoflimiet methode: De heroriëntatie van een roterend, door getijde vervormd lichaam kan niet beschreven worden met huidige methodes, de lineaire methode en de niet-lineaire methode. Dit omdat, wanneer het lichaam vervormd is door de getijden, het niet langer rotatie symmetrisch is. Bij de heroriëntatie van zulke lichamen is

niet alleen de verplaatsing van de rotatie-as maar ook van de getijde-as van belang. De meeste onderzoeken over TPW van een door getijden vervormd lichaam richten zich enkel op de vloeistoflimiet van de visco-elastische respons die slechts de eindpositie geeft van de rotatie- en getijde-as (Willemann, 1984; Matsuyama and Nimmo, 2007).

Voor deze benaderingen zijn verscheidene aspecten wat betreft de toepasbaarheid van de benaderingen nog niet onderzocht. Ten eerste, de gelineariseerde vorm van de Liouville vergelijking is afgeleid binnen een assenstelsel dat aan het lichaam is bevestigd, waarbij de rotatie-as in het begin samenvalt met de hoofdtraagheidsas (Munk and MacDonald, 1960). Omdat de belasting (de traagheidstensor die de extra massa op het vaste lichaam representeert) ook gedefinieerd is binnen een aan het lichaam gefixeerd assenstelsel, zal automatisch in de lineaire benadering ook aangenomen worden dat de relatieve locatie van de belasting ten opzichte van de rotatie-as niet verandert tijdens de TPW. De fout die door deze aanname wordt veroorzaakt kan theoretisch gezien oneindig groot worden wanneer de locatie van de belasting de pool of de evenaar benadert. Wanneer een puntmassa zich in de buurt van de polen of de evenaar bevindt zal het effect van een verandering in de breedtegraad van de puntmassalocatie groter zijn dan wanneer de puntmassa zich bijvoorbeeld bevindt op een breedtegraad van 45 of -45 graden. Hierdoor wordt het toepassingsgebied van de lineaire benadering kleiner wanneer de belasting de pool of de evenaar benadert. Op dit moment geeft geen enkel onderzoek de verwachte fout als een functie van de TPW hoek en de locatie van de belasting.

Ten tweede is de niet-lineaire methode nu de enige algemene manier om TPW over een grote hoek (meer dan 10 graden) te berekenen. Als gevolg hiervan is het effect van de quasi-vloeibare benadering, die in veel onderzoeken wordt toegepast (Spada et al., 1992a, 1996; Ricard et al., 1993; Harada, 2012; Chan et al., 2014; Moore et al., 2017), niet getest. Daarom is het onduidelijk wat het effect is van de quasi-vloeibare benadering en het negeren van de effecten van langzame relaxatiemodes op het gedrag van TPW.

Ten derde, omdat de vloeistoflimiet oplossing geen dynamische oplossingen verschaft hebben we geen duidelijk inzicht in hoe heroriëntatie van een door getijden vervormd lichaam tot stand komt. Onderzoeken die zich bezig houden met de richting van de poolbeweging van door getijden vervormde lichamen nemen aan dat de poolbeweging rechtstreeks is, en met andere woorden via een een grootcirkelpad naar hun eindbestemming bewegen. Dit is zowel het geval bij onderzoeken over TPW die worden gedreven door positieve massa-anomalieën zoals de ijskappen op Triton (Rubincam, 2003) als bij negatieve massa-anomalieën zoals de door diapirisme ontstane gebieden met een lage dichtheid op Enceladus (Matsuyama and Nimmo, 2007; Nimmo and Pappalardo, 2006). De aanname dat poolbeweging zich altijd langs een grootcirkelpad beweegt wordt niet getest in deze onderzoeken omdat een theorie die een tijdsafhankelijke oplossing verschaft ontbreekt.

Om deze problemen te kunnen oplossen wordt er in dit proefschrift een meer algemene methode gepresenteerd om rotatieveranderingen van planetaire lichamen te kunnen bestuderen en worden de benaderingen die gedaan zijn in voorgaand onderzoek geëvalueerd. We stellen een numeriek iteratieve procedure op die gecombineerd kan worden met een eindige-elementensoftwarepakket. Op deze manier kunnen laterale heterogeniteit en complexe rheologie geïmplementeerd worden. Ook wordt in dit proefschrift een semi-analytische methode gepresenteerd waarin de invloed van de lithosfeer en de hydrostatische toestand van het lichaam meegenomen kunnen worden. In vergelijking met eerdere

methodes kan deze nieuwe aanpak zowel kleine hoeken (kleiner dan 10 graden) als grote
hoeken (meer dan 10 graden) van TPW berekenen en is deze methode in staat de aparte
lange termijn en korte termijn Chandler wobble voor snel draaiende lichamen, zoals de
Aarde en Mars, door te rekenen. Hierdoor kan de lange termijn mega wobble voor traag ro-
terende lichamen zoals Venus ook behandeld worden. Bovenal biedt onze nieuwe methode
een dynamische oplossing voor de heroriëntatie van door getijden vervormde lichamen.
Het effect van de lithosfeer kan direct meegenomen worden en modellen die zich niet in
een hydrostatisch evenwicht bevinden kunnen ook gesimuleerd worden. Door middel van
deze nieuwe methode kunnen we aantonen dat, ten eerste, de lineaire rotatietheorie leidt
tot een fout die relatief groter wordt wanneer de beginpositie van de massa anomalie, die de
poolbeweging veroorzaakt, de pool of evenaar benadert. Dit limiteert het gebied waarin the
lineaire methode van toepassing is als de belasting zich dicht bij de evenaar of pool bevindt.
Ten tweede, de quasi-vloeibare benadering kan grote fouten introduceren in de eindige res-
pons voor een tijdsafhankelijke oplossing. De snelheid van de TPW op Mars, bijvoorbeeld,
die op basis van de quasi-vloeibare benadering is berekend, kan een onderschatting opleve-
ren van een factor 4, terwijl de snelheid van de rotatie-as die op Venus naar haar eindpunt
beweegt met de quasi-vloeibare methode overschat wordt. Ten derde, een door getijden
vervormd lichaam heeft een voorkeur voor heroriëntatie rondom de getijde-as in plaats van
rondom de rotatie-as. De beweging van de rotatie-as die wordt gedreven door een positieve
massa-anomalie in de buurt van de polen, heeft de neiging om eerst rondom de getijde-as te
draaien in plaats van direct ernaartoe te bewegen. Voor lichamen die zich in een synchrone
rotatie bevinden is het waarschijnlijker dat positieve massa anomalieën rond de evenaar en
op de grootcirkel in het vlak loodrecht op de getijde-as gevonden kunnen worden, terwijl
negatieve massa-anomalieën de neiging hebben om zich te bevinden rond de grootcirkel
die zowel de rotatie-as als de getijde-as snijdt Tot slot introduceren we een dimensieloos
vloeistoflimietgetal $\mathscr{F}$, dat verkregen kan worden met behulp van het Love getallen van het
planeetmodel en de TPW-snelheid. Met dit getal kunnen we een simpel criterium opstel-
len om te testen of de vloeistoflimietoplossing en de quasi-vloeibare benadering gebruikt
kunnen worden voor een gegeven inwendig model en maximale heroriëntatiesnelheid. Dit
proefschrift toont aan dat dit getal $\mathscr{F}$ minder dan 0.001 moet zijn voor een heroriëntatie
pad dat gevonden is met behulp van de vloeistoflimietoplossing voor een door getijden ver-
vormd lichaam om voldoende overeen te komen met het pad van een dynamische oplos-
sing voor praktische toepassingen. Hetzelfde criterium is ook van toepassing op resultaten
die verkregen zijn door middel van de quasi-vloeibare benadering. De nieuwe methode
wordt toegepast op verschillende planetaire lichamen en nieuwe inzichten zijn verkregen
over het gedrag van de rotatie van deze lichamen.

Aarde. Voor een massa belasting op een gelaagde Aarde die gebaseerd is op het Preliminary
Reference Earth Model (PREM) (Dziewonski and Anderson, 1981) samen met een gangbaar
viskeus profiel zoals dat van het SG6 model (Wu and Wang, 2006) kan zowel de lineaire
methode en onze methode een precieze hedendaagse TPW opleveren. Echter, door de in-
trinsieke fout van de lineaire methode kan deze bij een voorspelde TPW van meer dan 0.8
graden een fout van meer dan 2% geven.
Mars. Vanwege het gebruik van de quasi-vloeibare benadering kunnen eerdere schattingen
van de TPW snelheid (ongeveer 1 graden/Ma) (e.g. Chan et al., 2014; Bouley et al., 2016) een
onderschatting opleveren van een factor 4.6 gegeven de variaties in de viscositeit van Mars

van 10^{19} tot 10^{21} Pa s.

Venus. Het rotatiegedrag van Venus wordt gedomineerd door een mega wobble, wat een langzame wobble is met een grote amplitude (Spada et al., 1996). Spada et al. (1996) overschat de snelheid waarmee de massa anomalie op Venus de pool of de evenaar benadert doordat de quasi-vloeibare benadering wordt toegepast. Als we aannemen dat Venus een vergelijkbare viscositeit heeft als de Aarde of Mars dan zal een positieve massa-anomalie van dezelfde orde grootte er veel langer over doen (10-15 keer) om de evenaar op Venus te bereiken dan op Mars of de Aarde.

IJsmanen. De meeste ijsmanen hebben een synchrone rotatie ten opzichte van een veel zwaarder lichaam. De massa van Jupiter is bijvoorbeeld 37500 keer zo groot als die van zijn maan Europa. We tonen aan dat de heroriëntatie van deze door getijden vervormde lichamen, die in gang gezet zijn door een positieve massa anomalie, eerst zal plaatsvinden rondom de getijde-as om de massa anomalie dicht bij de evenaar te plaatsen. Daarna vertraagt de heroriëntatie en de massa anomalie beweegt zich dan langzaam richting het sub-host of anti-host punt. Als gevolg hier van zal TPW, die in gang gezet is door grote ijskappen op de polen van een ijsmaan, zoals Triton, Enceladus of Europa, er voor zorgen dat het lichaam zich als eerst heroriënteert rondom de getijde-as, in tegenstelling tot wat voorspeld is in (Rubincam, 2003) en (Matsuyama and Nimmo, 2007) met behulp van de vloeistoflimiet methode. De aanwezigheid van een lithosfeer bepaalt in welke mate positieve massa-anomalieën verplaatst kunnen worden naar de sub- en anti-host punten, echter het zal nog steeds waarschijnlijker zijn dat de massa-anomalieën zich in de buurt van de evenaar bevinden.

Pluto: Hoewel Pluto zich in een synchrone rotatie bevindt met zijn maan Charon, is de massa van Charon slechts 12% van die van Pluto. Dit creëert een kleinere getijdebult dan op de ijsmanen. As gevolg hiervan heeft de heroriëntatie van Pluto geen sterke voorkeur om eerst rondom de getijde-as te draaien. In plaats daarvan zal het pad van de massa anomalie zich bijna perfect langs een grootcirkel bewegen. Dit betekent dat het heroriëntatie pad dat is verkregen in voorgaande, op vloeistoflimiet gebaseerde onderzoeken, bijvoorbeeld (Keane et al., 2016), de werkelijkheid dicht zal benaderen. Echter, de snelheid van de heroriëntatie is nog steeds vertekend door de vloeistoflimiet, afhankelijk van de viscositeit van de planeet en het verloop van de belasting in de tijd, bijvoorbeeld hoe snel volatiele stoffen zich in Sputnik Plantinia hebben verzameld (Keane et al., 2016) en hoe snel de oceaan opgeweld is (Nimmo et al., 2016).

Samenvattend, de niuwe methode die wordt gepresenteerd in dit proefschrift is een geavanceerdere methode voor planeetwetenschappers om op een juiste methode manifestaties van veranderende rotatie van verscheidene lichamen te interpreteren.

1

INTRODUCTION

This chapter presents an introduction on the theory for long-term rotational variations of planetary bodies. It answers the following questions: why do we need to study rotational variations? What kind of rotational variations is the focus of this study? Which factors can affect the variations? The physics behind these issues is explained in a schematic way. Also some observed geophysical features caused by the rotational variations of the body are introduced.

1.1. Rotation: pulse of a planet

Figure 1.1: A demonstration of planetary rotation.

Before the modern medical system was developed, especially before advanced diagnostic equipment such as X-ray and MRI was invented, Chinese medicine was one of the leading medical systems in the world. A famous technique it relied on is the pulse diagnosis. The pulse is a periodic signal which reflects the performance of our body. By studying the change in this signal, one can know if various organs function normally. The pulse diagnosis provides information of significant diagnostic value without directly looking into the body.

In planetary science, we are in the same situation as medicine in ancient times. Technologically, we still lack the equipment to directly look into the interior of planetary bodies. We also can not probe them: the deepest scientific drilling for the Earth, Kola Superdeep Borehole, is about 12 km which is less than the average thickness of the crust. All the information obtained about the interior of a planetary body is from indirect observations: its orbit, (near) surface gravity, various radiational signals, magnetics and seismic studies. Also the periodic behaviour of every celestial body, rotation, provides information about its interior, just like diagnosing a person in Chinese medicine. By studying the rotational variations and combining this with the geographic features, we can obtain information about the planetary interior or explain the formation of certain surface features. There is a daily-life example of the concept that the rotational behaviour can reflect the internal properties: a simple method to distinguish between a boiled egg and a raw egg is to rotate both and let them spin on a surface. The boiled egg will keep rotating much longer than the raw egg. The physics behind this simple experiment can be very complex and concerns differential rotation, stability of a static flow and viscosity. It is necessary to establish a physical/mathematical model which links the rotational states and the interior conditions. The main purpose of this PhD thesis is to further develop the rotational theory for planetary

bodies, which can be used to link various observed geophysical features, such as the Tharsis plateau on Mars and Sputnik Planitia on Pluto, to rotational behaviours of the body which also reflect their interior properties. This thesis focuses on a particular rotational behaviour which will be introduced in the next section.

1.2. POLAR WANDER: THE WANDERING POLE AND ITS PATH

ROTATIONAL behaviour of a planetary body can be very complex, as it contains both torque-induced and torque-free rotational variations. Furthermore, planetary bodies are deformable, or more precisely: viscoelastic, which means that they act like elastic bodies on a short time scale but like a fluid over long time scales. As a result, the short-term rotational behaviour of planetary bodies and the long-term one are quite different. In this thesis, we focus on the torque-free case which contains the mechanism that explains the locations of many observed surface features on various planetary bodies: true polar wander.

1.2.1. INTRODUCING POLAR WANDER AND TRUE POLAR WANDER

When no external torque is exerted on the body, the rotational axis is fixed in the inertial frame because of the conservation of angular momentum. The moments of inertia of the body can be changed by many geophysical processes, such as mantle convection, a meteorite forming a crater, volatile accumulation or ocean upwelling on the icy moons. These processes give a perturbation which relocates the mass of the body. As a result, the body will reorient itself and the rotational velocity may also change to keep the angular momentum the same. For an observer on the surface of the planet, such reorientation appears as if the rotational axis is moving around. For this reason, this phenomenon is referred to as polar wander.

On the Earth, it is well known that the north/south pole is constantly moving and the study of this phenomenon can be dated back to 19th century (Evans, 1866). As shown in figure 1.2, the movement of the poles has two kinds of temporal behaviour: a short-term periodic behaviour and a long-term secular drift. The short-term movement contains a wobble with a one year period and a wobble with 14 month period which is called Chandler wobble. The averaged long-term movement is referred to as true polar wander (TPW).

Physically, the Chandler wobble is an eigenmotion of the body and its frequency is the natural frequency of the rotating system. Such frequency is different from the free nutation of a rigid Earth and the difference is induced by the fact that the Earth is deformable. The yearly wobble comes from the excitation which has a period of one year, e.g. flow in the ocean and atmosphere (Wahr, 1983; Gross, 2000). In section 2.2, the mathematical description of these two periodical behaviours will be shown. The long-term drift, TPW, is also the consequence of the deformation of the rotating body. The detailed physical explanation for TPW will be presented in section 1.3.2.

1
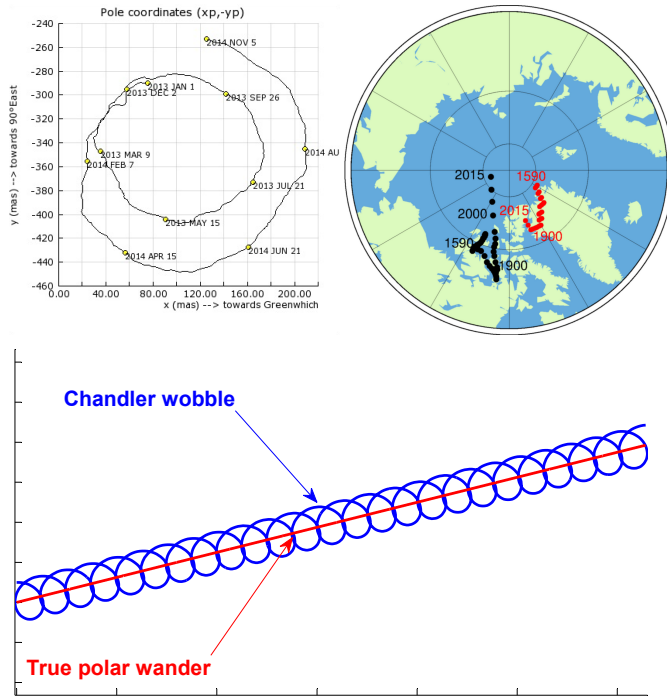
Figure 1.2: Upper left: Short-term pole movement (2 years) on the Earth. (from *The International Earth Rotation Service (IERS), https://www.iers.org/*)
Upper right: Long-term pole movement (400 years) on the Earth. The red dots are the geometric north poles in different years. (from *German Research Centre For Geoscience (GFZ), http://www.gfz-potsdam.de*)
Bottom: A schematic illustration of the Chandler wobble and true polar wander in the body-fixed frame.

1.2.2. CASES OF TPW

Due to the availability of orbiting satellites and ground stations, TPW on the Earth can be directly observed by measuring the position of the rotational axis in a body fixed frame (figure 1.2). However, TPW on most of the planetary bodies can only be inferred from the location of certain geological features because we lack the (ground based) instruments to measure their orientation in the same way as for the Earth (Seidelmann, 1982). As will be shown in section 1.3.2, TPW tends to relocate a positive mass anomaly (such as mountains) to the equator and a negative mass anomaly (such as impact craters) to the poles. As a result, it is more likely to find huge mountains or plateaus which are not in isostasy close to the equator. When we indeed observe these features near the equator of a certain planetary body, it is often assumed that TPW relocated the feature to its current position. Of course it is still possible that they originally formed at their current locations but the probability is very low. In this section, we discuss several well-known geographic features on planetary bodies of our solar system which are widely believed to indicate past TPW. The significance of modelling TPW in order to link the observed features to their formation and the interior properties of the planetary body is discussed in the end.

The first example is the Tharsis plateau on Mars where the largest volcanoes in our Solar System reside. As shown in figure 1.3, the surface area of Tharsis is about 10–30 million km^2 which is 8 to 25 percent of the entire surface of Mars (Williams et al., 2008). The total mass of Tharsis is estimated to be $10^{19} \sim 10^{20}$ kg (Hynek and Phillips, 2001; Nimmo and Tanaka, 2005) which is large enough to trigger large angle TPW (Arkani-Hamed, 2009). As a result, it is assumed that the Tharsis region could have formed somewhere else rather than at its current position near the equator and was subsequently relocated by TPW (Murray and Malin, 1973; Kite et al., 2009; Bouley et al., 2016). However, the original position and the formation epoch of Tharsis are still under debate: theories of both an early formation (Arkani-Hamed, 2009) and a late formation (Bouley et al., 2016) can be found in the literature.
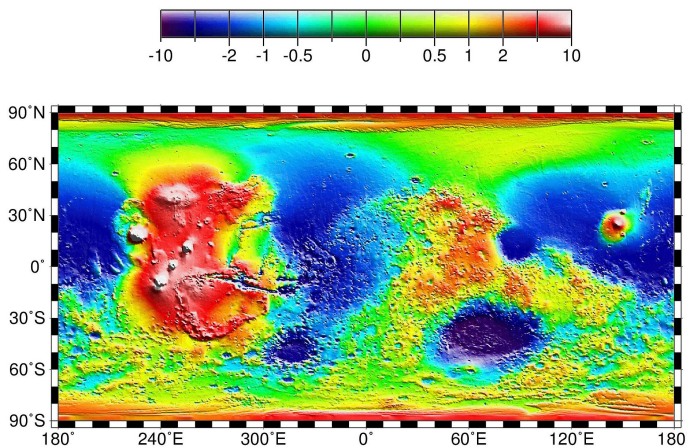
Figure 1.3: Global topography of Mars. The Tharsis plateau is the large red area on the left. The unit for the scale bar is km. Image taken from (Smith et al., 1999).

The second example is the south polar region on Enceladus as shown in figure 1.4. This area shows four almost parallel ice cracks with an average length of 130 kilometres and a depth of 500 meters. Accompanying the tiger stripes are the highest observed geysers in this region which eject water vapor, molecular hydrogen, and solid material into space (Spencer and Nimmo, 2013). Such active behaviour, which is also confirmed by thermal images of this area (Spencer and Nimmo, 2013), suggests a subsurface ocean. Some studies assumed that the ocean is limited to the south pole (Iess et al., 2014; McKay et al., 2014) which proved to be inconsistent with the observed short-term wobble which was found during the Cassini mission (Showman et al., 2013; Tajeddine et al., 2017). As a result, it is currently assumed that a global ocean of average thickness of 30 to 40 kilometres is present within Enceladus (Showman et al., 2013; Tajeddine et al., 2017). The large libration amplitude provides a strong constraint for the global ocean (Thomas et al., 2016). Nonetheless, the active south pole compared to a quiet north pole suggests that the internal structure and activity at the south pole are different from the rest of the body. It is assumed that this local activity created a negative mass anomaly which reoriented Enceladus so that the area where the tiger stripes formed was relocated to the south pole (Nimmo and Pappalardo, 2006).

Figure 1.4: A close view of the tiger stripes at the south pole of the Enceladus. This image was obtained during the Cassini mission in 2005 by the Cassini imaging team.

The third case is Pluto and its Sputnik Planitia which covers a large part of the heart-shaped surface feature, see figure 1.5. Pluto is tidally locked with its largest moon Charon. As shown in figure 1.5, the location of Sputnik Planitia is ver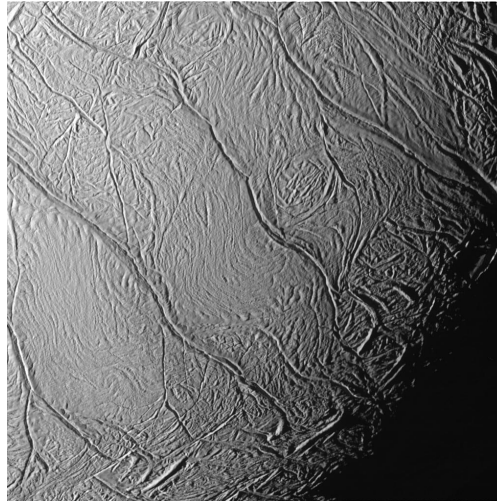y close to the anti-Charon point. Similar to Tharsis on Mars, the reason that it is located near the equator is assumed to be the fact that this area forms a positive mass anomaly. Studies show that two processes, volatile accumulation and ocean upwelling, created a large enough positive mass anomaly which reoriented Pluto so that Sputnik Planitia was relocated to its present day position (Nimmo et al., 2016; Keane et al., 2016). Section 1.3.3 will show why the tidal force pushes a positive mass anomaly to the sub-host or the anti-host point.

Besides the cases presented above, many other planetary bodies in our solar system are also believed to have experienced TPW such as the Earth e.g. (Besse and Courtillot, 1991; Lambeck, 2005), Earth's Moon (Siegler et al., 2016) and icy satellites like Europa and Ganymede (Schenk et al., 2008).
Understanding TPW is crucial to provide a link between observations and the formation of the observed features and the interior properties. For instance, the mass of the Tharsis area can be derived from gravity data (Goossens et al., 2017) together with the surface topography (Hynek and Phillips, 2001; Nimmo and Tanaka, 2005). This provides the load which triggers TPW on Mars. On the other hand, the displacement history of the poles can be obtained from many resources, such as surface hydrogen distribution (Feldman et al., 2004) or valley networks which suggest the surface stress pattern (Bouley et al., 2016). The load and TPW history together constrain the interior properties of Mars, e.g. the thickness of the crust and the viscosity of the mantle. Such constraint is provided by the reorientation (TPW) theory. Or the other way around, if the interior properties are constrained by other information than based on the rotation theory, the speed of the TPW or the formation history of the surface feather which triggered TPW, could be constrained.
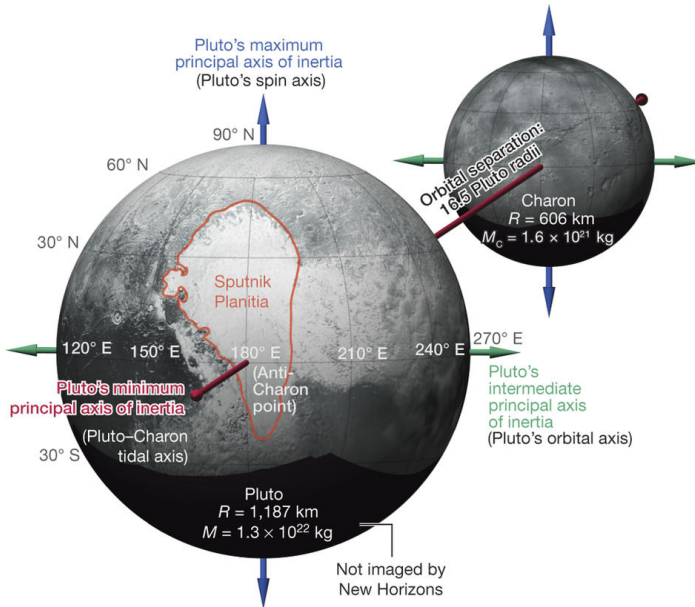
Figure 1.5: Orthographic spherical projections of Pluto and Charon. Base map: NASA/Johns Hopkins University Applied Physics Laboratory/Southwest Research Institute. Image taken from (Keane et al., 2016).

1.3. PHYSICAL BACKGROUND

Before we go into the mathematical description of the problem, we illustrate the physics of TPW with schematic drawings. In this section, also other factors which significantly affect the rotational behaviour, such as the tidal force and the lithosphere of a planet, will be presented.

1.3.1. DEFORMATION BEHAVIOUR OF PLANETS

As mentioned in the previous section, TPW can only happen on bodies that are deformable. The deformation of terrestrial planets and icy satellites consists of an elastic and viscous component. In the short term, planetary bodies behave like an elastic material where the deformation due to a given stress, and the recovery after the removal of this stress, happens instantaneously. In the long term, viscous behaviour becomes dominant and planetary bodies respond like fluid. The long-term viscous behaviour is the reason why the shape of most planetary bodies is close to spherical under their self-gravitation. We will introduce in this section the fundamental rheological model, the Maxwell model, which describes the viscoelasticity of planetary bodies.

The choice for a particular rheology model depends on three criteria (Sabadini et al., 2016): (1) the mathematical difficulty, (2) the quality of the geophysical data, (3) our knowledge of the behaviour of the medium. Based on these three criteria, first, a Maxwell model is the most simple model for which the Love numbers of the planetary body can be directly

obtained by the normal mode theory (Peltier, 1974). Secondly, the time scale for TPW behaviour of a planetary body is usually in millions of years, e.g. the TPW speed on the Earth is about 1 degree per million years (Ricard et al., 1993). It is very difficult to obtain a precise reorientation history of a planetary body for such slow TPW speed. Thirdly, as will be shown in chapter 5, TPW is mainly controlled by the long-term viscous response of the body and the load which triggers the TPW, such as volatile accumulation, ocean upwelling and mantle convection, usually does not have short-term periodic behaviour such as the tidal deformation due to an eccentric orbit. Consequently, for the study of TPW, we can expect a small impact from replacing Maxwell rheology by a more advanced model such as Andrade rheology which has been shown to result in a large difference in a study of tidal dissipation (Renaud and Henning, 2017). As a result, the Maxwell rheology is chosen for the study of the long-term rotational behaviour of planetary bodies.
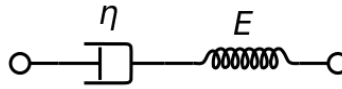
Figure 1.6: Representation of the Maxwell rheology

The schematic representation of the Maxwell rheology is the spring-damper system shown in figure 1.6. With this model, if the material is given a constant strain, the stress relaxes and eventually becomes zero due to the damper. When put under a constant stress, the two components act independently as follows: the spring has an instantaneous deformation which stays as long as the stress remains. Once the load is removed, the spring recovers instantaneously. On the other hand, the damper extends linearly with time when the stress remains and will not recover after the load is removed. The total deformation of viscoelastic material is the sum of these two components.
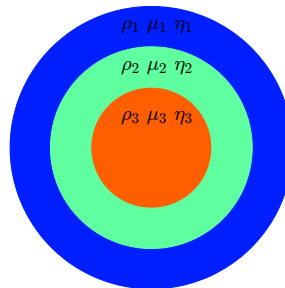
Figure 1.7: Illustration of a uniformly stratified planetary interior model.

The interior model of a planetary body is usually simplified into a stratified sphere. In each layer, the physical properties, which include the density ρ, shear modulus μ and viscosity η, are given, as shown in figure 1.7. Physically, each layer can be represented by a spring-damp system and the entire model becomes a series connection of all these subsystems. For a laterally homogeneous model, which means the thickness of each layer is constant, the de-

formation of the model can be analytically calculated by the normal mode method (Peltier, 1974) which results in the Love numbers. For a heterogeneous model, the deformation can usually only be obtained by a numerical method such as a finite element method.

The viscoelasticity of the planetary body determines that in the long-term the resistance of the body against deformation will vanish and this is the reason why a positive mass anomaly on the body can eventually reach the equator and a negative mass anomaly can reach the pole. This will be explained in detail in section 1.3.2.
Furthermore, for a viscoelastic body, since the material can fully relax, the equilibrium shape of a rotating body is determined only by the centrifugal potential and the self-gravitation if no third body is considered. When these two forces are in balance, the planetary body is in hydrostatic equilibrium when the compressibility of the planet model is ignored. The hydrostatic state of the entire body, or simply speaking: the "background shape", is crucial to the TPW behaviour as will be demonstrated in section 4.5. As will be discussed in section 1.3.4, if a certain part of the body, usually the lithosphere which has very high viscosity, cannot relax during the TPW, this will prevent the mass anomalies from reaching the equator or poles.

1.3.2. PROCESS OF TPW

In this section the process of TPW due to a positive mass anomaly will be explained schematically. The process of TPW on an Earth-like object was first studied by Gold (1955). Figure 1.8 gives a schematic depiction of the long-term rotational behaviour of a viscoelastic body for the condition that its Chandler wobble period is much shorter than the dominant relaxation time of the body. This is the case for the Earth and Mars. For instance, the Chandler wobble on Earth has a period of around 400 days while the dominant relaxation time of the Earth is about 1000 to 10,000 years. It will be explained later in this section why this condition is necessary. The process of TPW can be decomposed in the following steps:

Step 1, figure 1.8a. In the body-fixed co-rotating frame, a rotating viscoelastic body in hydrostatic equilibrium is flattened or, in other words, it has an equatorial bulge which is centered at the equator. The black dots represent the original north and south poles.

Step 2, figure 1.8b. When a positive mass anomaly within or on the body is created, the rotational stability is broken and, due to the centrifugal potential, an extra force ΔF is exerted on the body which makes the body reorient in the direction of the force until a new equilibrium position is reached. We should be aware that the direction of the movement becomes different when the rotational behaviour is like a mega wobble such as on Venus (Spada et al., 1996).

Step 3, figure 1.8c. After the reorientation, the centrifugal force is applied to the body at a new position. Since the body is deformable, under the centrifugal force, the equatorial bulge will readjust so it becomes perpendicular to the rotational axis again. This process is
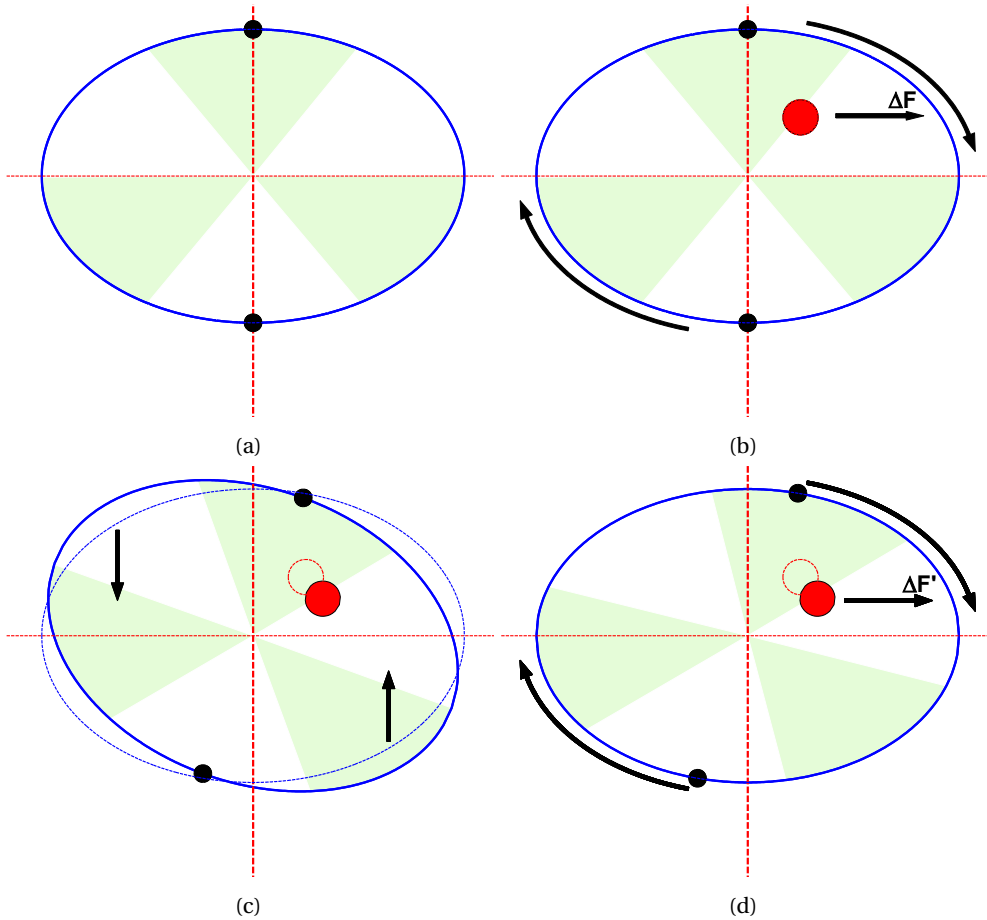
Figure 1.8: A schematic process of the TPW of an Earth-like object viewed in the cross-section of the body in the body-fixed frame. The black dots are the original north and south poles. The solid red dot represents the mass anomaly. The vertical red dashed line is the rotational axis.

called equatorial bulge readjustment.

Step 4, figure 1.8d. When the bulge is readjusted, the balance is broken again by the extra mass anomaly and a new unbalanced force $\Delta F'$ appears. As a result, the situation returns to step 2. This iteration will continue until the positive mass anomaly reaches the equator.

During TPW, the second step (reorientation of the rotational axis) and the third step (equatorial bulge readjustment) happen at the same time. So in reality, during TPW the reorientation of the rotational axis can never achieve the new equilibrium position and the equatorial readjustment can never cause the bulge to be perpendicular to the rotational axis again. These two processes work in opposite directions and the net effect only vanishes when the mass anomaly is at the equator or at the poles.

If we view this process in terms of the moment of inertia, a rotating body is stable when its rotational axis coincides with the axis of maximum moment of inertia (AOM), which is the case before the mass anomaly is applied to the body. The existence of the mass anomaly changes the position of the AOM and the rotation becomes unstable. As a result, the rotational axis tries to "follow" the AOM which is the process of reorientation of the rotational axis. However, the equatorial bulge readjustment moves the positive mass anomaly away from the rotational axis which pushes the AOM further away. As a result, *the process of TPW can be seen as a process of the rotational axis "chasing" the AOM.*

Before the illustration shown in figure 1.8, we stated the condition that the Chandler wobble period needs to be much shorter than the dominant relaxation time of the body. It will be explained in the following why this condition is necessary.

In the second step of previous illustration, it is stated that the rotational axis will move away from from the load in the opposite direction. This is only true when secular behaviour is not dominated by the Chandler wobble. As shown in figure 1.2, the rotational variation contains both the periodic component, the Chandler wobble, and the secular TPW. When the period of the former is short enough, the periodic behaviour can be ignored when considering long-term rotational changes. However, as the rotational speed of the planet slows down, the equatorial bulge shrinks. Consequently, the period of the Chandler wobble becomes longer. When this period becomes comparable to the dominant relaxation time of the body, the rotational change is dominated by this periodic phenomenon and the rotational behaviour looks completely different. Since the rotation rate of Venus is only about 0.0041 times that of the Earth, TPW on Venus shows completely different patterns compared to that on the Earth. We present a schematic illustration of the rotational behaviour changing from an Earth-like fast rotating object to a Venus-like slow rotating object in figure 1.9. As the rotational speed slows, four trends appear:

1. The average secular behaviour (red line in figure 1.9) becomes curly instead of staying within a great circle.

2. The length of the secular behaviour becomes shorter.

3. The magnitude of the Chandler wobble becomes larger.

4. The period of the Chandler wobble becomes longer.

These changes can be explained mathematically which will be shown in section 4.3.

Mega wobble is very similar to the free nutation of a rigid body. The theory for the rotational variation of a rigid body will be briefly discussed in section 2.2. The determination of the period of the Chandler wobble and the mega wobble case will be shown in section 2.2 and chapter 4, respectively.
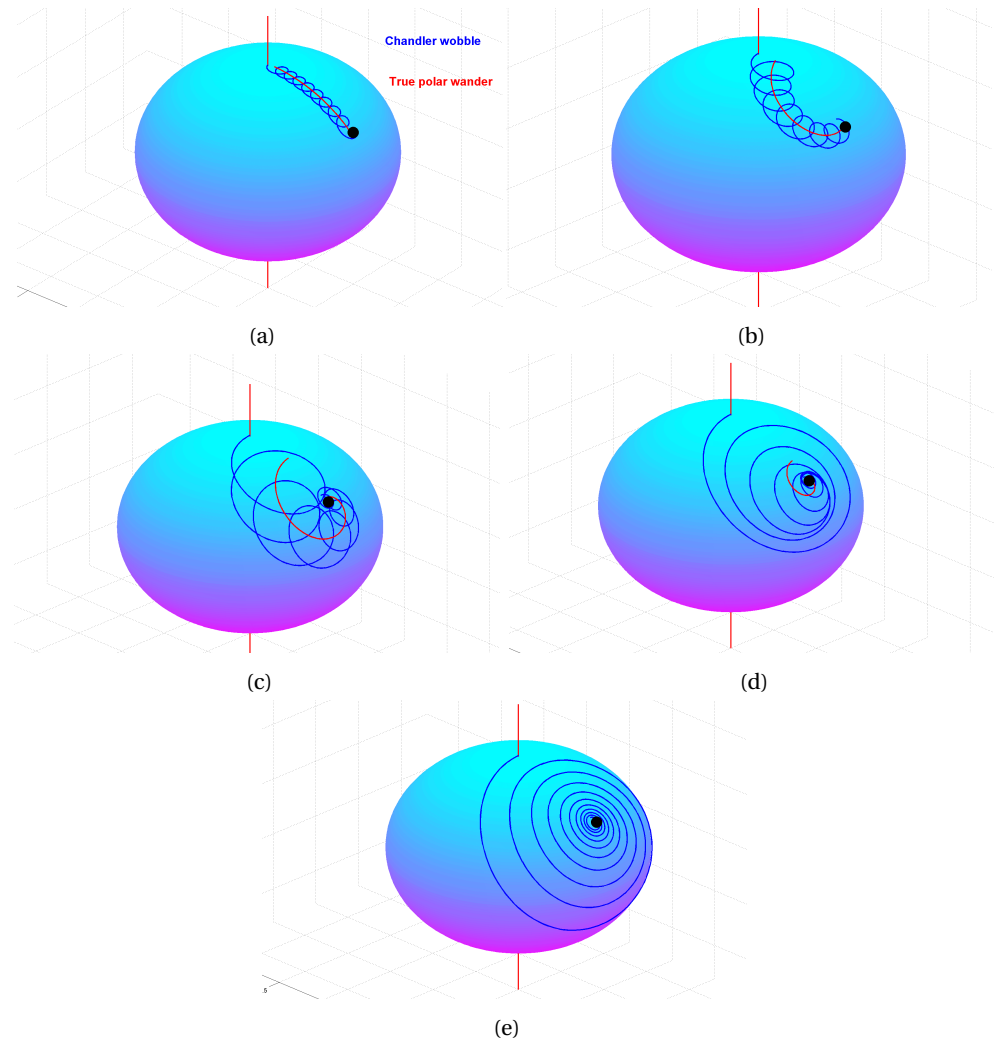
Figure 1.9: A schematic illustration of the rotational behaviour for an object with an Earth-like interior and its rotational speed decreasing from (a) Earth-like to (e) Venus-like. The vertical red line is the original rotational axis and the black dot represents a negative mass anomaly.

1.3.3. EFFECT OF A TIDAL BULGE

Since a moon or planet orbits around a planet or sun, the body not only experiences the centrifugal force but also the tidal force from the host body. For three of the four terrestrial planets in our solar system, the Earth, Mars, and Mercury, the rotational period is much shorter than the orbital period. As a result, the tidal force applied on them is much smaller than the centrifugal force and the tidal force due to the Sun is usually ignored when describing rotational behaviour. However, most of the moons, e.g. the Moon of the Earth, Europa and Enceladus, and the dwarf planet Pluto are tidally locked to either their host planet or

its largest moon. In this case, the magnitude of the tidal force becomes comparable to the centrifugal force. It will be shown in section 2.1 that when the mass of the orbiting host is much larger than the body, which is true for most tidally locked moons, the tidal force is three times the magnitude of the centrifugal force which will create a large tidal bulge besides the centrifugal bulge. Consequently, we cannot ignore the tidal force when calculating the reorientation of the body. In this thesis, we consider tidally locked bodies whose orbital eccentricity and axial tilt (obliquity) can be ignored.

For this kind of tidally deformed bodies, we introduce the bulge-fixed coordinate system
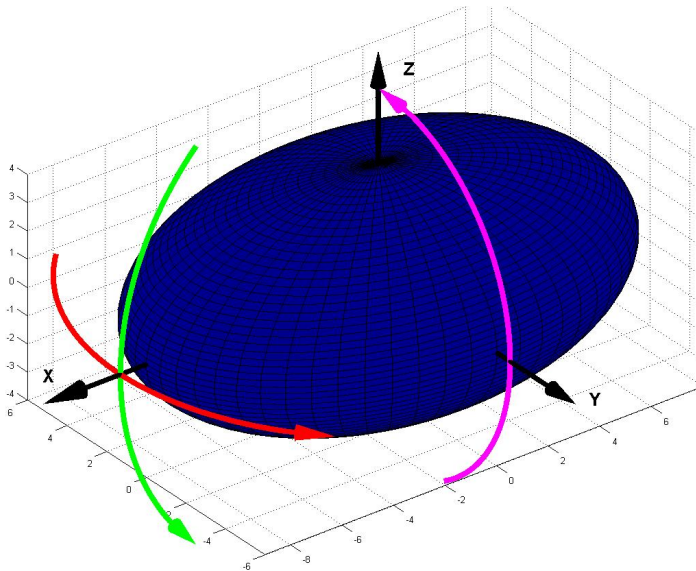
Figure 1.10: The bulge-fixed coordinate system in a tidally deformed rotating body. The X-axis is the tidal axis that points towards the central body. The Z-axis is the rotation axis, and the Y-axis completes a right-handed coordinate system. The coloured arrows show three reorientations around the axes, which will be labelled as X-, Y- and Z-reorientation.

where the X-axis and Z axis always coincide with the tidal and rotational axis, respectively, as shown in figure 1.10. As we can see, the reorientation of a tidally deformed body is much more complex than when only the centrifugal force is present, because we need to consider the movement of not only the rotational axis but also the tidal axis. We are not aware of a published dynamic solution for TPW on a tidally deformed body. Most previous studies (Matsuyama and Nimmo, 2007; Matsuyama et al., 2014; Keane et al., 2016) only consider the final reorientation of the body with a lithosphere. The method in these studies will be introduced in section 2.4. Before that, it is necessary to know why the lithosphere of a body can influence its final reorientation. Therefore, in the next section, the effect of the lithosphere with very high viscosity will be discussed.

1.3.4. EFFECT OF AN ELASTIC LITHOSPHERE

The statement that a positive mass anomaly will eventually reach the equator and a negative mass anomaly will reach one of the poles as well as the schematic demonstration shown in figure 1.8 requires one crucial condition: the entire body should be able to fully relax after the considered period. This means that the viscosity of the entire body should be lower than a certain value. If part of the planetary body, usually the lithosphere, has a very high viscosity, then this part can not sufficiently relax during the TPW process and it will accumulate stress which prevents the equatorial bulge to readjust fully. The effect of the lithosphere is shown schematically in figure 1.11.

In figure 1.11, on the left and right columns are bodies without and with a lithosphere, respectively. In the beginning, the entire body is in hydrostatic equilibrium in both cases, as shown in figure 1.11a and 1.11b, so the whole body is fully relaxed (Stress level 0).

When a positive mass anomaly is attached to the surface, as shown in figure 1.11c and 1.11d, the body without a lithosphere can sufficiently relax, in which case the body itself does not show significant resistance to the reorientation. On the other hand, for the body with a lithosphere, stress starts to accumulate in the lithosphere due to deformation which generates a restoring force $\Delta F"$ that counters TPW.

In the long term the body without a lithosphere does not give any resistance to the reorientation. The mass anomaly is pushed to the equator and the body reaches a new hydrostatic equilibrium in this new position, as shown in figure 1.11e. On the other hand, for the body with a lithosphere, the restoring force within the lithosphere will eventually become big enough to cancel the extra centrifugal force applied on the mass anomaly and the TPW stops. As a result, the mass anomaly cannot reach the equator in this case, as shown in figure 1.11f. The magnitude of the TPW angle is determined by the MoI of the mass anomaly and by the lithosphere.

Next we consider the behaviour of the body following removal of the mass anomaly during the TPW or after it is finished. The direction of the rotational axis of the body without the lithosphere, since a new equilibrium has been established on the final position, will not change, as shown in figure 1.11g. In contrast with this, for the body with a lithosphere the restoring force will try to reorient the body back to its original orientation since the stress remains within the lithosphere, as shown in figure 1.11h. This process is almost exactly the same as TPW triggered by an apparent mass anomaly, but in this case the unrelaxed lithosphere plays the role of the mass anomaly to trigger the TPW.

The new equilibrium position for both cases are shown in figure 1.11i and 1.11j. While the body without an lithosphere keeps the new orientation, the body with an elastic lithosphere will end up with the rotational axis back at its original position. If the lithosphere can partially relax during the entire TPW, then the restoring force will vanish during the process and the final reorientation will be somewhere between the start position and the maximum

displacement. This will be demonstrated with modelling in chapter 4.

In this chapter, the process of TPW and relevant issues such as a tidal bulge and lithosphere is explained without including mathematics. The next chapter will show the mathematical representation for the process of TPW. Most importantly, we will introduce and describe the limitations of various types of solutions to the TPW problems which are used in previous studies.

1
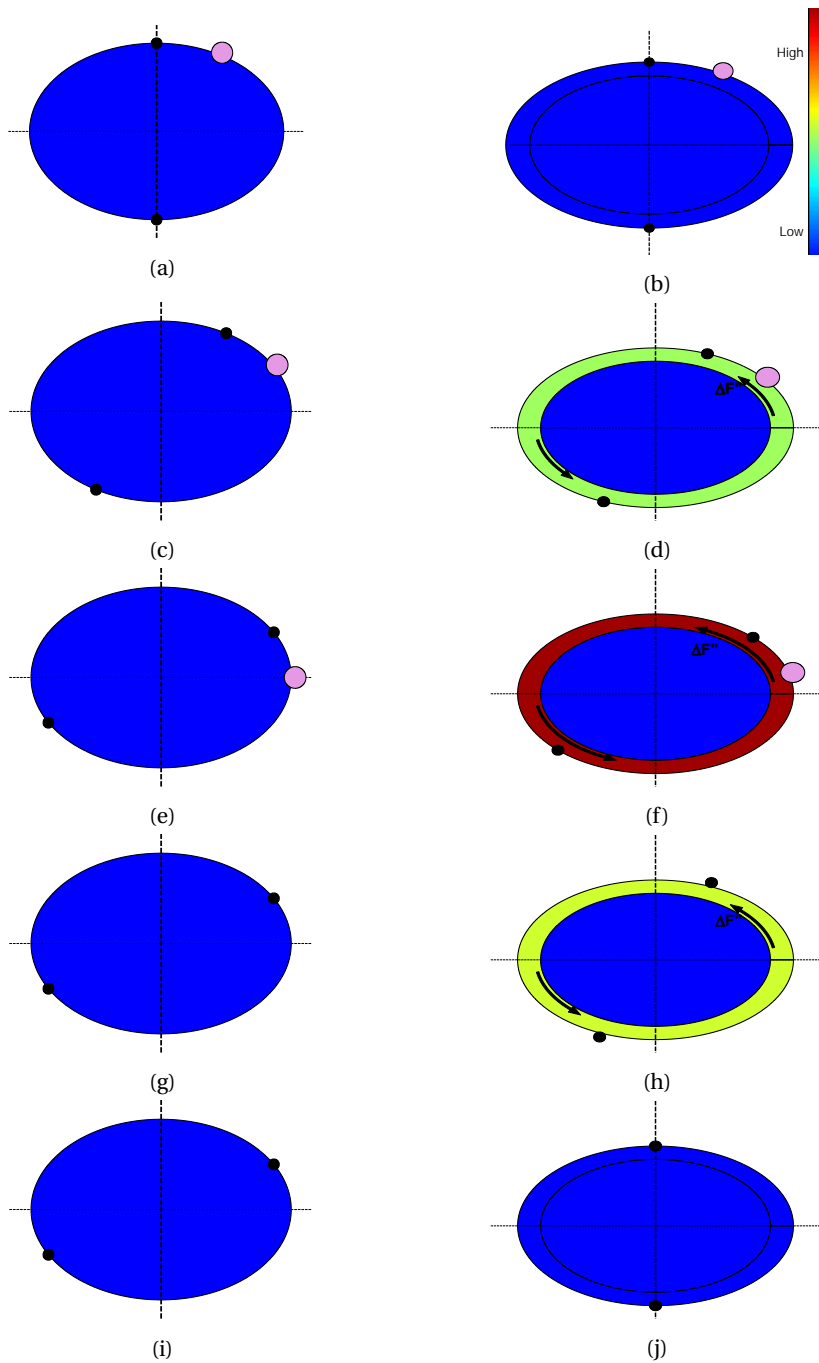
Figure 1.11: Left column (a-c-e-g-i): Reorientation of a body without lithosphere due to a positive mass anomaly and its removal.
Right column (b-d-f-h-j): Body with a lithosphere.
Black dots are the original north and south poles and the magenda dot is the mass anomaly. The colorbar indicates the relative stress level.

2

REVIEW OF ROTATIONAL THEORIES AND PROBLEM STATEMENT

This chapter presents three types of analytical solutions for long-term TPW which are widely used in previous studies: linear, non-linear and fluid-limit. First, the governing equations, the Liouville equation and moment of inertia equation, are introduced. Then each solution is introduced, focusing on: the accuracy and applicability. Based on the evaluation of previous methods, the goal of this thesis and the research questions are presented.

2.1. LIOUVILLE EQUATION AND MOMENT OF INERTIA EQUATION

In this section, the governing equations for the rotational variations of a spherical viscoelastic body are presented. The mathematical representation of the effect of a tidal bulge and a lithosphere, which was introduced in the previous chapter, is also discussed.

TPW, or the reorientation of a rotating body, can be represented by the change in its rotational vector in a body-fixed frame, which we define as $\boldsymbol{\omega} = (\omega_1, \omega_2, \omega_3)$ where $\omega_i, i = 1, 2, 3$ are the components in the body-fixed frame. The change in the rotational state of the body must satisfy the conservation of angular momentum, which in the rotating body-fixed frame is represented as the well-known Euler's equation. For the torque-free case, it reads (Lambeck, 1988):

$$\frac{d}{dt}(\mathbf{I} \cdot \boldsymbol{\omega}) + \boldsymbol{\omega} \times \mathbf{I} \cdot \boldsymbol{\omega} = 0 \tag{2.1}$$

where $\mathbf{I}$ is the moment of inertia (MoI) tensor of the body. When the body is deformable, $\mathbf{I}$ becomes $\mathbf{I}(t)$ and equation 2.1 is usually referred to as the Liouville equation (Sabadini et al., 2016). This is a non-linear equation which we need to solve to obtain the value of $\boldsymbol{\omega}$ for a prescribed change in the MoI tensor $\mathbf{I}$. As a result, we need another equation to describe the change in the MoI.

Generally, the MoI of a planetary body can be changed in three ways:

1. The direct contribution from a geophysical feature which can be represented as a relocation of the mass of the body. Such feature is modelled as a mass anomaly whose inertia tensor will be labelled as $\Delta\mathbf{I}_1$.

2. The deformation of the body due to the mass anomaly. Due to the gravity, the presence of this extra mass anomaly upon a body will cause the body to deform until a hydrostatic equilibrium state is reached. The change in the inertia tensor of this process will be labelled as $\Delta\mathbf{I}_2$.

3. Equatorial bulge readjustment. Due to the centrifugal force, an equatorial bulge is created. The shape of this bulge alters following the rotational axis. The change in MoI of the equitorial bulge will be labelled as $\Delta\mathbf{I}_3$.

To calculate TPW, the MoI tensor of the mass anomaly, $\Delta\mathbf{I}_1$, should be known. This is the input for our calculation. We label MoI of this part as $\mathbf{C}(t)$, so $\Delta\mathbf{I}_1 = \mathbf{C}(t)$. In order to describe how the body deforms due to the load of the mass anomaly and the centrifugal force, we need the Love numbers of the planetary body.

Love numbers were first introduced by Augustus Edward Hough Love to describe the overall elastic response of the Earth to the tidal potential (Dehlinger, 1978). Similar to the simple Hooke's law for a spring, for an elastic Earth the degree two potential Love number k_2 gives a simple linear relation between the degree two load potential Φ_c and the second degree

perturbation in the self gravitational potential Φ_g at radius a (Farrell, 1972):

$$\Phi_g(a) = k_2\Phi_c(a) \tag{2.2}$$

Here $\Phi_c(a)$ is the centrifugal potential which is a function of the rotational vector $\boldsymbol{\omega}$ which will be given in equation 2.9. From the gravitational potential $\Phi_g(a)$ the change in the inertia tensor can be obtained. For this part of the derivation, we refer to chapter 3 of (Sabadini et al., 2016), which gives:

$$\Delta I_{3,ij} = \frac{k_2 a^5}{3G}[\omega_i\omega_j - \frac{1}{3}\Omega^2\delta_{ij}] \tag{2.3}$$

where $\Delta I_{3,ij}$ are the components of tensor $\Delta\mathbf{I}_3$. G is the gravitational constant and a is the radius of the planet. This time-invariant form of $\Delta I_{3,ij}$ provides the instantaneous equatorial bulge readjustment due to an applied centrifugal potential Φ_c.

The definition of Love numbers can be extended when the viscoelasticity of the body and load are considered. The Correspondence Principle states that a linear viscoelastic problem in the time domain is equivalent to an elastic problem in the Laplace domain (Peltier, 1974). As a result, we have (Peltier, 1974):

$$\Phi_g(s, a) = k_2(s)\Phi_c(s, a) \tag{2.4}$$

similar to the relationship shown in equation 2.2, where $\Phi_c(s, a)$ and $\Phi_g(s, a)$ are the corresponding Laplace transformations of $\Phi_c(t, a)$ and $\Phi_g(t, a)$, respectively. Following the same procedure, we can obtain the relationship between the change in the inertia tensor $\Delta I_{3,ij}$ and the rotational vector ω similar to equation 2.3 in the Laplace domain. In time domain, where multiplication becomes convolution, we have

$$\Delta I_{3,ij}(t) = \frac{k_2(t)a^5}{3G} * [\omega_i(t)\omega_j(t) - \frac{1}{3}\Omega(t)^2\delta_{ij}] \tag{2.5}$$

which describes the viscoelastic response of the equatorial bulge as a function of the rotational vector.

The concept of the Love numbers can also be extended to describe the body's response to a surface or internal load. In this case, the Love number is called the load Love number, in contrast with the tidal Love number which is introduced above. To distinguish these two types of Love numbers, we label the tidal Love number in equation 2.5 as k^T and label the load Love number as k^L. The Load love number directly gives the relationship between the MoI of the applied mass anomaly and the change in the MoI of the body (Sabadini et al., 2016):

$$\Delta I_{2,ij}(t) = k^L(t) * C_{ij}(t) \tag{2.6}$$

As a result, the MoI of the entire body can be obtained as

$$\begin{aligned} I_{ij}(t) &= I_0\delta_{ij} + \Delta I_{1,ij} + \Delta I_{2,ij} + \Delta I_{3,ij} \\ &= I_0\delta_{ij} + \frac{k^T(t)a^5}{3G} * [\omega_i(t)\omega_j(t) - \frac{1}{3}\Omega(t)^2\delta_{ij}] \\ &\quad + [\delta(t) + k^L(t)] * C_{ij}(t) \end{aligned} \tag{2.7}$$

where I_0 is the MoI of the unperturbed spherical planetary body and δ_{ij} is the Kronecker delta function. Equation 2.7 gives the change in the MoI of the entire planetary body as a function of rotational vector $\boldsymbol{\omega}$ and the input load $\mathbf{C}(t)$. We will name this equation in the following as *moment of inertia (MoI) equation*, which is the second governing equation.

For a stratified spherical self-gravitating visco-elastic body with a Maxwell rheology, Love numbers can be obtained by the normal mode method (Peltier, 1974; Sabadini et al., 2016). In this thesis, it is not discussed in detail how Love numbers are computed by the normal mode method. Tidal and load Love numbers of a Maxwell stratified viscoelastic body in the Laplace domain have the form (Peltier, 1974):

$$k(s) = \quad k_e + \sum_{i=1}^{M} \frac{k_i}{s - s_i} \tag{2.8}$$

where k_e is the elastic Love number, k_i are the residues of each mode and s_i are the inverse relaxation times. This form of the Love number describes how a stratified viscoelastic body deforms. The elastic response of the body is characterized by the elastic Love number k_e which in the time domain is a delta function. Due to the difference between the properties of layers, several viscous relaxations follow the elastic response and are characterized by the relaxation strengths $k_i/(s - s_i), i = 1, 2..M$, which in the time domain is the exponential function $k_i e^{s_i t}$.

When the tidal and load Love numbers of the body and the direct contribution to the MoI from a geophysical feature, $\mathbf{C}(t)$, are given, equations 2.1 and 2.7 can be solved to obtain the rotational changes.

The MoI equation 2.7 can only be applied to bodies for which the influence of the tidal deformation can be ignored. If the tidal force can not be ignored, the effect of the tidal bulge needs to be added to equation 2.7. First we compare the tidal potential with the centrifugal potential. For an incompressible model with linear rheology, the effective centrifugal potential is (Murray and Dermott, 2000)

$$\Phi_c = \frac{1}{3}\Omega^2 r^2 P_2^0(\cos\theta) \tag{2.9}$$

with θ being the colatitude and P_2^0 the associated Legendre function of degree 2 and order 0.

When the distance between the source body of the tidal potential and the target planetary body is much larger than the radius of the target planetary body ($a >> r$ in figure 2.1), the tidal potential due to the source body can be written as (Murray and Dermott, 2000)
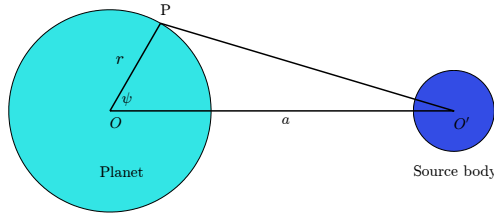
Figure 2.1: The relationship between the radius of the planetary body, r, the semi-major axis of the source body of the tidal potential, a, and the angle between the radius vector $\overrightarrow{OP}$ and the direction of the tidal bulge $\overrightarrow{OO'}$, ψ.

$$\Phi_t = -\frac{GM_T}{a^3} r^2 P_2^0(\cos\psi) \tag{2.10}$$

Here ψ is the angle between the radius vector and the direction of the tidal bulge, as shown in figure 2.1. If we define an equivalent angular speed of the tidal potential as:

$$\Omega' = \sqrt{\frac{3GM_T}{a^3}} \tag{2.11}$$

then the expression of the tidal potential becomes the same as the centrifugal potential except for the negative sign. As a result, the effect of applying a tidal potential to a certain object is the same as applying the centrifugal potential of the same magnitude but with opposite direction. When a tidal potential is present, the MoI equation 2.7 becomes

$$I_{ij}(t) = I\delta_{ij} + \frac{k^T(t)a^5}{3G} * \left[\omega_i^R(t)\omega_j^R(t) - \frac{1}{3}\omega_l^R\omega_l^R\delta_{ij}\right]$$
$$- \frac{k^T(t)a^5}{3G} * \left[\omega_i^T(t)\omega_j^T(t) - \frac{1}{3}\omega_l^T\omega_l^T\delta_{ij}\right] + [\delta(t) + k^L(t)] * C_{ij}(t) \tag{2.12}$$

where $\boldsymbol{\omega^T} = (\omega_1^T, \omega_2^T, \omega_3^T)$ is the tidal vector which points to the source of the tidal potential and whose magnitude satisfies

$$|\boldsymbol{\omega^T}| = \sqrt{\frac{3GM_T}{a^3}} \tag{2.13}$$

When the body contains a lithosphere, equations 2.7 and 2.12 may need to be modified, depending on whether the lithosphere is considered as elastic or as viscoelastic with very high viscosity. If a model with a viscoelastic lithosphere is considered, there will be a very slow buoyancy mode in the Love number which represents the relaxation of the lithosphere. The MoI equation 2.7 or 2.12 keeps the same form. If the lithosphere is elastic or the slowest buoyancy mode associated with the lithosphere is ignored when calculating the Love number, then the Love number does not contain the contribution from the lithosphere. Consequently the MoI obtained from equation 2.7 or 2.12 lacks the influence of the lithosphere which needs to be added. For this part we refer to section 4.4.

The rotational variation of a planetary body is obtained by the solution of the two governing equations introduced above. However, analytically solving a non-linear equation 2.1 together with equation 2.7 which contains convolution is not feasible. As a result, various approximations were adopted in previous studies to simplify either the Liouville equation or the MoI equation. In the following three sections, we will show these approximations and discuss their applicability and limitation of the methods based on these approximations.

2.2. LINEAR METHOD

In this section, we will first introduce the linearized Liouville equation along with a brief discussion about the short-period periodic rotational behaviour, namely the Chandler and the 1-year wobble. Then the linear solutions for TPW from Sabadini and Peltier (1981) and Wu and Peltier (1984) are introduced.

The linear method only considers the case where the TPW happens on bodies which are in hydrostatic equilibrium and the perturbation does not change the state too far away from the equilibrium. As a result, we first need to obtain the state of a viscoelastic body in hydrostatic equilibrium. Basically, when a viscoelastic spherical body starts to rotate with a constant speed, the body will gradually flatten due to the centrifugal force. This process continues until the centrifugal force and the self-gravitational force are balanced. The influence of such a process on the MoI of the body is described by equation 2.5, which is the change of MoI, $\Delta \mathbf{I}_3$, as a function of rotational vector, $\boldsymbol{\omega}(t)$. If we set $\boldsymbol{\omega}(t) = \Omega(0,0,1)$, the difference in the inertia tensor of the body in hydrostatic state and a spherical body can be obtained by the infinite time limit of equation 2.5:

$$\Delta \mathbf{I_h} = \lim_{t \to \infty} \Delta \mathbf{I}_3(t) \tag{2.14}$$

which can be solved by Laplace transform with the final value theorem: $f(\infty) = \lim_{s \to 0} F(s)$. Let $\mathbf{I}_3(s)$ be the Laplace transformation of $\mathbf{I}_3(t)$. Substituting equation 2.8 into $\mathbf{I}_3(s)$ results in

$$\begin{aligned}
\Delta \mathbf{I_h} &= \mathscr{L}^{-1} \lim_{s \to 0} \Delta \mathbf{I}'(s) \\
&= \begin{pmatrix} \Delta A & 0 & 0 \\ 0 & \Delta B & 0 \\ 0 & 0 & \Delta C \end{pmatrix} \\
&= \frac{k_f^T \Omega^2 a^5}{3G} \begin{pmatrix} -\frac{1}{3} & 0 & 0 \\ 0 & -\frac{1}{3} & 0 \\ 0 & 0 & \frac{2}{3} \end{pmatrix}
\end{aligned} \tag{2.15}$$

where $\mathscr{L}^{-1}$ stands for the inverse Laplace transform, ΔA, ΔB and ΔC are the change of MoI at the three principle axes. k_f^T is the infinite time limit of the tidal Love number which is equivalent to substituting $s = 0$ in equation 2.8. This number is often called the fluid Love

number and can be written as

$$
\begin{aligned}
k_f^T &= && k^T(0) \\
&= && k_e^T - \sum_{i=1}^{m} \frac{k_i^T}{s_i}
\end{aligned}
\tag{2.16}
$$

In this case, since only the centrifugal force is considered, the body is symmetric around the rotational axis and the MoI around the three principle axes can be obtained as

$$
\begin{aligned}
A = I_0 + \Delta A &= I_0 + \Delta B = B \tag{2.17a} \\
C &= I_0 + \Delta C \tag{2.17b}
\end{aligned}
$$

The size of the equatorial bulge can be characterized by the difference $C - A$ which is (Mitrovica et al., 2005)

$$
C - A = \frac{k_f^T a^5 \Omega^2}{3G}
\tag{2.18}
$$

When perturbations happen to the inertia tensor of the planetary body in hydrostatic equilibrium, the MoI of the body can be written as

$$
\mathbf{I} = \begin{pmatrix}
A + \Delta I_{11} & \Delta I_{12} & \Delta I_{13} \\
\Delta I_{21} & B + \Delta I_{22} & \Delta I_{23} \\
\Delta I_{31} & \Delta I_{32} & C + \Delta I_{33}
\end{pmatrix}
\tag{2.19}
$$

where ΔI_{ij} is the sum of $\Delta I_{1,ij}$, $\Delta I_{2,ij}$ and $\Delta I_{3,ij}$ as introduced in the previous section. If we assume that the rotational variation is small, we can define the perturbed rotational axis as

$$
\boldsymbol{\omega} = \Omega(m_1, m_2, 1 + m_3)^T
\tag{2.20}
$$

where m_1, m_2 and m_3 are small real numbers and Ω is the norm of the vector $\boldsymbol{\omega}$. Substituting equation 2.19 and 2.20 into the Liouville equation 2.1, and ignoring the higher order terms (see section 3.3 for the detailed process) results in the linearized Liouville equation (Sabadini et al., 2016)

$$
\begin{aligned}
\dot{m}_1 &= -\frac{C - B}{A} \Omega m_2 + \frac{\Omega}{A} \Delta I_{23} - \frac{\Delta \dot{I}_{13}}{A} \tag{2.21a} \\
\dot{m}_2 &= \frac{C - A}{B} \Omega m_1 - \frac{\Omega}{B} \Delta I_{13} - \frac{\Delta \dot{I}_{23}}{B} \tag{2.21b} \\
\dot{m}_3 &= -\frac{\Delta \dot{I}_{33}}{C} \tag{2.21c}
\end{aligned}
$$

For planets like the Earth and Mars, the tidal force is much smaller than the centrifugal force. And if we do not consider lateral heterogeneity, it can be assumed that $A = B$. By

defining $\boldsymbol{m} = m_1 + i m_2$ where i is the imaginary unit, the first two equations in 2.21 can be written as

$$i \frac{\dot{\boldsymbol{m}}}{\sigma_r} + \boldsymbol{m} = \boldsymbol{\Phi}_L \qquad (2.22)$$

where the load function $\boldsymbol{\Phi}_L$ and the Eulerian free precession frequency σ_r are defined as

$$\boldsymbol{\Phi}_L = \frac{\Delta I_{13}}{C - A} + i \frac{\Delta I_{23}}{C - A} \qquad (2.23)$$

$$\sigma_r = \frac{C - A}{A} \Omega \qquad (2.24)$$

We should be aware that the load function $\boldsymbol{\Phi}_L$ here contains contributions from all three factors ($\Delta \mathbf{I} = \Delta \mathbf{I}_1 + \Delta \mathbf{I}_2 + \Delta \mathbf{I}_3$) introduced in the previous section. If the load function $\boldsymbol{\Phi}_L$ is time-invariant, namely if the body is rigid ($\Delta \mathbf{I}_2 = \Delta \mathbf{I}_3 = 0$) and the relative position and the magnitude of the mass anomaly do not change ($\Delta \mathbf{I}_1$ is a constant), equation 2.22 can be solved analytically which results in a periodic behaviour: the free nutation (Lambeck, 1988). The frequency of the free nutation is different from that of the Chandler wobble introduced in section 1.3.2 due to the fact that the deformation of the body is not taken into account (Lambeck, 1988).

Combining equations 2.18 and 2.5 and ignoring the second order terms of m_i, we have

$$\Delta I_{3,13} = \frac{C - A}{k_f^T \Omega^2} k^T(t) * [\omega_1(t)\omega_3(t)] \approx \frac{C - A}{k_f^T} k^T(t) * m_1(t) \qquad (2.25a)$$

$$\Delta I_{3,23} = \frac{C - A}{k_f^T \Omega^2} k^T(t) * [\omega_2(t)\omega_3(t)] \approx \frac{C - A}{k_f^T} k^T(t) * m_2(t) \qquad (2.25b)$$

which gives the change in the MoI due to equatorial readjustment as a function of m_i. Substituting equations 2.25 and 2.6 in the linearized Liouville equation 2.22 gives

$$i \frac{\dot{\boldsymbol{m}}}{\sigma_r} + \boldsymbol{m} - \frac{k^T}{k_f} * \boldsymbol{m} = \boldsymbol{\Phi}_l \qquad (2.26)$$

where $\boldsymbol{\Phi}_l$ becomes

$$\boldsymbol{\Phi}_l(t) = \left(\delta + k^L \right) * \frac{\Delta C_{13} + i \Delta C_{23}}{C - A} \qquad (2.27)$$

which only contains the parts $\Delta \mathbf{I}_1$ and $\Delta \mathbf{I}_2$ now. This is the linear form of the governing equation which combines the Liouville equation and MoI equation. Providing an input $\mathbf{C}(t)$ which describes certain geophysical processes, the rotational change, $\mathbf{m}$, can be obtained. The result contains both short-term periodic behaviour as well as long-term TPW for small angle perturbations.

Equation 2.26 can be used to determine the period of the Chandler wobble. If we only consider the instantaneous behaviour of the body instead of its long-term viscous response, then the Love number k^T can be simplified to contain only the elastic part k_e^T, which in the Laplace domain is a constant whose convolution with $\boldsymbol{m}$ becomes a multiplication. As a result, equation 2.26 becomes

$$i\frac{\dot{\boldsymbol{m}}}{\sigma_r} + (1 - \frac{k_e^T}{k_f})\boldsymbol{m} = \boldsymbol{\Phi}_l \tag{2.28}$$

Compared to equation 2.22 whose natural frequency is σ_r, the periodic behaviour obtained from 2.28 has frequency

$$\sigma_0 = \left(1 - \frac{k_e^T}{k_f^T}\right)\sigma_r \tag{2.29}$$

And this value represents the frequency of the Chandler wobble. Since it depends on both the elastic and fluid Love number of the body, the period of the Chandler wobble is generally understood as the free nutation of the body modified by the fluidity of the core, the elasticity and anelasticity of the mantle and the oceans (Lambeck, 1988). The magnitude of the Chandler wobble is dependent on the excitation, which contains both non-periodic geological processes such as earthquakes (Mansinha and Smylie, 1967; Press and Briggs, 1975) and periodic processes such as ocean flow and atmospheric pressure change (Wahr, 1983; Gross, 2000). These seasonal excitations also generate the extra one year periodic wobble besides the Chandler wobble.

In order to solve equation 2.26 in a more general way Laplace transformation is applied. With $\boldsymbol{m}(s)$ and $\boldsymbol{\Phi}(s)$ being the transformed quantities of $\boldsymbol{m}(t)$ and $\boldsymbol{\Phi}_l(t)$ respectively, we have

$$\left(i\frac{s}{\sigma_r} + 1 - \frac{k^T(s)}{k_f}\right)\boldsymbol{m}(s) = \boldsymbol{\Phi}(s) \tag{2.30}$$

Substituting the Love number $k^T(s)$ and fluid Love number k_f^T defined in equation 2.8 and 2.16 leads to

$$\boldsymbol{m}(s) = -\frac{i\sigma_r\boldsymbol{\Phi}(s)}{s\left(1 + i\sum_{j=1}^M \frac{x_j}{s-s_j}\right)} \tag{2.31}$$

where $x_i = (\sigma_r k_i)/(k_f s_i)$. To solve equation 2.31, Sabadini and Peltier (1981) and Wu and Peltier (1984) took different approaches. Sabadini and Peltier (1981) directly applied partial fraction decomposition for the parameter s on the right side and obtained

$$\frac{1}{s\left(1 + i\sum_{j=1}^M \frac{x_j}{s-s_j}\right)} = \frac{A_0}{s} + \sum_{j=1}^M \frac{A_j}{s - a_j} \tag{2.32}$$

Here A_i and a_i are complex numbers. Combining this equation with equation 2.27 to replace $\boldsymbol{\Phi}(s)$ changes equation 2.31 into

$$\boldsymbol{m}(s) = -i\sigma_r\left(\frac{A_0}{s} + \sum_{j=1}^M \frac{A_j}{s - a_j}\right)\left(1 + k^L\right)\frac{\Delta C_{13}(s) + i\Delta C_{23}(s)}{C - A} \tag{2.33}$$

Since A_i and a_i are complex numbers, for a stationary load, where $C(t)$ is constant and $k^L = 0$, $m(t)$ typically has the form

$$m_1 = \beta_0 + \beta_1 t + \sum_{j=2}^{M} \beta_j \sin(\alpha_j t) e^{\alpha_j t} \tag{2.34a}$$

$$m_2 = \beta'_0 + \beta'_1 t + \sum_{j=2}^{M} \beta'_j \cos(\alpha_j t) e^{\alpha_j t} \tag{2.34b}$$

where β_i, β'_i and α_i are real numbers. This form suggests that each of the M relaxation modes will give rise to a rotational mode with damped periodic behaviour. Usually only one of the rotational modes, which is associated with the mantle and often referred to as the M_0 mode, has a very large imaginary part and this corresponds to the observed Chandler wobble (Sabadini et al., 2016).

In contrast with the approach by Sabadini and Peltier (1981), Wu and Peltier (1984) assume that all rotational modes have a much longer relaxation time than the Chandler wobble. By taking $|s| << \sigma_0$, the unit in the denominator of equation 2.33 can be ignored. This approximation changes equation 2.33 into a real equation in which the Chandler wobble is filtered out. The next procedure is exactly the same as in Sabadini and Peltier (1981) where partial fraction decomposition is applied. Here we compare both approaches with an example. A mass anomaly of 2×10^{19} kg is attached on the surface of the SG6 Earth model (see table 3.2 for the physical properties) and we do not consider the deformation of the Earth due to the mass anomaly ($k^L = 0$). The rotational variation is calculated by both methods. The results are shown in figure 2.2. As can be seen, in the result obtained by Wu and Peltier (1984), the Chandler wobble is replaced by an elastic jump in the beginning and the magnitude of this jump represents the amplitude of the initial wobble. Other than this, these two approaches obtain the same secular behaviour in the long term. The equivalence of these two approaches has been analytically studied by Vermeersen and Sabadini (1996).

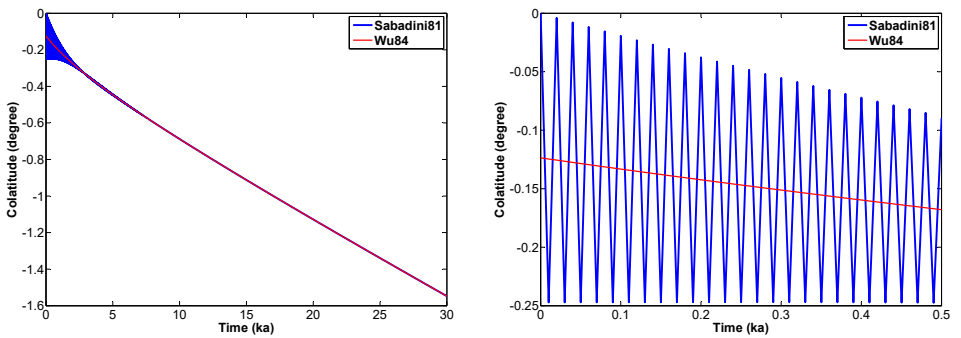Figure 2.2: Polar wander in the x-z plane for the SG6 Earth model triggered by a point mass of 2×10^{19} kg attached at the surface at 45° colatitude. Rotational variations calculated by both Sabadini and Peltier (1981) and Wu and Peltier (1984) are included. On the left, the time range is 30 ka and on the right 500 years.

The following summarizes the applicability of the linear method:

- The linear methods fully adopt the rheology behind the model (no approximation on the MoI equation) which means that for small angle TPW, the linear method provides accurate TPW behaviour of a Maxwell body. As a result, the linear methods should be the first candidate for validating a new method. More specifically, if the result from the new method contains the short-term periodic behaviour, the method by Sabadini and Peltier (1981) should be used for validation. Otherwise, the method by Wu and Peltier (1984) is chosen.

- The applicable range for the linear method is limited to a small angle due to the linearisation of the Liouville equation. During the linearisation process, two assumptions are taken: (1) the axis of maximum MoI is close to the rotational axis (C>A and C>B must be satisfied after the perturbation), (2) During the TPW, the MoI of the equatorial bulge does not change (C-A is constant). These two assumptions limit the linear method to only the case where the contribution of the mass anomaly to the MoI is very small compared to that of the equatorial bulge. This can be true for terrestrial planets such as the Earth and Mars, but not necessarily for Venus, which has an extremely small equatorial bulge.

- An intrinsic error is present due to the fact that the MoI of the mass anomaly C is calculated in the body fixed frame. Thus C is not updated during the TPW (see equation 2.33). This means that for the mass anomalies placed near the pole or the equator, the results from the linear method can contain a large error. For instance, in the beginning, a positive mass anomaly is placed at 1 degree colatitude. Then after TPW of 1 degree, the colatitude of the mass anomaly is changed to 2 degrees, for which the contribution of the load is almost doubled. However, in the linear method, this change is not considered since its position in the body-fixed frame is fixed. This issue is further discussed in section 3.3.

2.3. NON-LINEAR METHOD

For large angle TPW, the linearized Liouville equation cannot be applied anymore. Instead, the original non-linear equation needs to be solved. Sabadini and Peltier (1981) first formulated the problem in a non-linear way which was further developed by Spada et al. (1992a) and Ricard et al. (1993).

Due to the mathematical difficulty of solving the Liouville equation 2.1 together with the MoI equation 2.7, an approximation is adopted in non-linear methods. As we can see from the MoI equation 2.7, the most difficult part is the convolution for the tidal Love number which describes the viscous behaviour of the equatorial bulge. If we assume that the rotation is studied for time scales much larger than the characteristic relaxation times of the model, we can assume that $|s| << |s_i|$ which leads to an approximation of the Love number

in the form of equation 2.8: (Ricard et al., 1993)

$$
\begin{aligned}
k^T(s) &= k_e^T + \sum_{i=1}^{M} \frac{k_i^T}{s - s_i} \\
&\approx k_e^T - \sum_{i=1}^{M} \left(\frac{k_i^T}{s_i} + \frac{k_i^T s}{s_i^2} \right) \\
&= k_f^T (1 - T_1 s)
\end{aligned}
\tag{2.35}
$$

The constant T_1 is

$$
T_1 = \frac{1}{k_f^T} \sum_{i=1}^{M} \frac{k_i^T}{s_i^2}
\tag{2.36}
$$

Mathematically, this approximation is the first order term of a Taylor expansion of the Love number in the Laplace domain. With this new form of the Love number, we want to see how it responds to a linearly changing load to the body. In the time domain, this is to convolute equation 2.35 with a linear function $F(t) = At$. This load function can resemble a changing load such as accumulation of volatiles. The response in the time domain reads:

$$
\begin{aligned}
R(t) &= k^T(t) * F(t) \\
&= \mathcal{L}^{-1}[k_f^T(1 - T_1 s)F(s)] \\
&= k_f^T F(t) - A k_f^T T_1
\end{aligned}
\tag{2.37}
$$

which shows that if the change of the load, A, is very small, the body immediately reaches its fluid limit $k_f^T F(t)$ without the delayed viscous response. As a result, this formulation of the Love number as shown in equation 2.35 is called the quasi-fluid approximation. With the time domain transformation of $s\omega_i(s)$ being $\dot{\omega}_i(t)$, substituting equation 2.35 into 2.7 gives (Ricard et al., 1993)

$$
\Delta I_{i,j}(t) = \frac{k_f^T a^5}{3G} [\omega_i(t)\omega_j(t) - \frac{1}{3}\Omega(t)^2 \delta_{ij}]
$$
$$
- \frac{k_f^T a^5}{3G} T_1 [\dot{\omega}_i(t)\omega_j(t) + \omega_i(t)\dot{\omega}_j(t) - \frac{2}{3}\omega_l(t)\omega_l(t)\delta_{ij}] + E_{ij}
\tag{2.38}
$$

where $E_{ij} = [\delta(t) + k^L(t)] * C_{ij}(t)$. Combining equation 2.38 and 2.1 and neglecting $\ddot{\omega}$ and $\dot{\omega}^2$ for consistency with the assumption of the approximation in 2.35 results in (Ricard et al., 1993):

$$
A_{ij}(\boldsymbol{\omega})\dot{\omega}_j + B_{ij}(\boldsymbol{\omega}, \mathbf{E}, \dot{\mathbf{E}})\omega_j = 0
\tag{2.39}
$$

where

$$A \quad = \quad \frac{k_f^T a^5 T_1}{3G} \begin{pmatrix} \frac{3GI}{k_f^T a^5 T_1} & \omega^2 \omega_3 & -\omega^2 \omega_2 \\ -\omega^2 \omega_3 & \frac{3GI}{k_f^T a^5 T_1} & \omega^2 \omega_1 \\ \omega^2 \omega_2 & -\omega^2 \omega_1 & \frac{3GI}{k_f^T a^5 T_1} \end{pmatrix} \tag{2.40}$$

$$B \quad = \quad \begin{pmatrix} \dot{E}_{11} & \Sigma_3 & -\Sigma_2 \\ -\Sigma_3 & \dot{E}_{22} & \Sigma_1 \\ \Sigma_2 & -\Sigma_1 & \dot{E}_{33} \end{pmatrix} \tag{2.41}$$

and $\Sigma_k = E_{ki}\omega_i$. Thus the governing equations become a system of first order differential equations 2.39 which can be solved by numerical integration methods.

Since the Liouville equation is not linearized, the non-linear method has better applicability compared to the linear methods for two cases: (1) large-angle TPW, (2) Bodies with very a small equatorial bulge, such as Venus.

On the other hand, since the non-linear method takes the quasi-fluid approximation 2.35, the result does not fully represent the response of a Maxwell body. As will be discussed in section 4.2, the quasi-fluid approximation underestimates the equatorial readjustment speed in normal TPW case, depending on the model. Consequently, the TPW obtained by non-linear methods for the Earth or Mars has a much slower transient response than that of a Maxwell body. If we compare the results of the linear method from Wu and Peltier (1984) and the non-linear one from Ricard et al. (1993), as shown in figure 2.3, it is clear that for short term small angle TPW, where the linear method is accurate, the non-linear method can contain large errors, as it was not developed to be accurate for the short time scale. However, for the long-term large angle TPW, it is not clear what the influence is of taking the quasi-fluid approximation on the TPW behaviour. Thus the accuracy of the non-linear method remains unclear since we are not aware of the existence of a non-linear method that contains the full visco-elastic response of a Maxwell body.
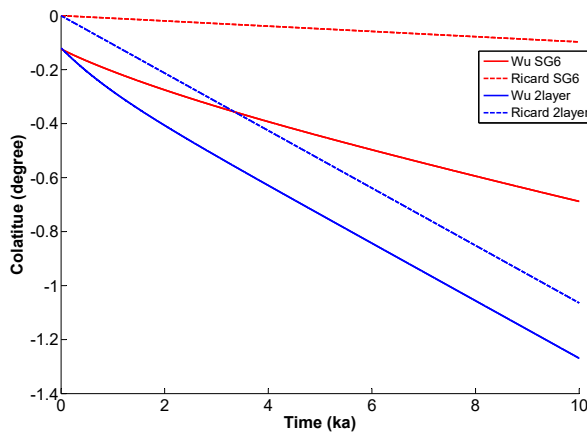

Figure 2.3: Polar wander in the x-z plane for two types of Earth models, two-layer and SG6 (Wu and Wang, 2006), triggered by a point mass of 2×10^{19} kg placed at $45°$ colatitude in the x-z plane, for both the linear (Wu and Peltier, 1984) and non-linear (Ricard et al., 1993) methods.

2.4. FLUID LIMIT METHOD

Both the linear and non-linear methods mentioned in the previous two sections can not be applied to bodies which are tidally deformed. The difficulty of obtaining a dynamic solution for reorientation of a tidally deformed body comes from two aspects. First there is an extra term in the MoI equation 2.12 due to the presence of the tidal bulge. Second, the reorientation of the body concerns both the rotational axis and the tidal axis.

In physical terms, the movement of the body consists of a forced nutation around the rotational axis where the tidal force applies a torque. Furthermore, as shown in section 2.1, for an incompressible body, the effect of the tidal force is the same as the centrifugal force, apart from the opposite direction of the force. So for the tidal axis, there is also a forced nutation where the centrifugal force applies extra torque. As a result, the complete mathematical description of the reorientation of a tidally deformed body consists of two Liouville equations besides the MoI equation. As seen in previous sections, even when only the centrifugal bulge is present, a (semi-)analytical solution requires approximation of either the Liouville equation 2.1 as in the linear method or approximation of the MoI equation 2.7 as in the non-linear method.

The orientation of a tidally locked rotating body is stable when the rotational axis coincides with the axis of the largest moment of inertia and the tidal bulge is pointing towards the source of the tidal potential. This state corresponds to the minimum total potential energy of the body when its viscoelastic part is fully relaxed. The deformation afterwards follows the minimum total potential energy principle. Perturbations such as mass redistribution, which change the body's MoI, will cause the body to reorient until a new minimal potential state is achieved. In other words, the rotational and tidal axes are aligned with the new axes of maximum and minimum MoI.

For the past decades (Willemann, 1984; Matsuyama et al., 2014), a different approach has been applied when the reorientation of a tidally deformed body is studied in which a static, instead of dynamic, solution is used. As shown in section 1.3.4, the presence of a lithosphere will prevent the equatorial and tidal bulge from fully readjusting. The non-lithospheric part of the body can sufficiently relax during the TPW. This part can achieve hydrostatic equilibrium in any orientation, therefore it does not determine the final orientation. Instead, the final orientation is controlled only by the MoI of the lithosphere and the mass anomaly. Consequently, if we are only interested in the end positions of the rotational and tidal axes without considering the process, the end state of a reorientation can be derived from the MoI equation which only contains the contribution from the lithosphere and the mass anomaly. The influence of the lithosphere on the reorientation was first studied by Willemann (1984). Mitrovica et al. (2005) introduced a method that uses the observed value of $C - A$ to correctly include the influence of the lithosphere in the linear scheme, where Cambiotti et al. (2010) discussed the differences between the influence of an elastic and a highly viscous lithosphere. Chan et al. (2014), Harada and Xiao (2015) and Moore et al. (2017) further extended the method of Ricard et al. (1993) and included the influence of the lithosphere in the non-linear scheme. For a tidally deformed body, the inertia tensor associated with the lithosphere and the mass anomaly can be written as (Matsuyama et al., 2014;

Matsuyama and Nimmo, 2007)

$$I_{i,j} = \frac{\Delta K \Omega^2 a^5}{3G}\left(e_i^R e_j^R - \frac{1}{3}\delta_{ij}\right) - \frac{\Delta K \Omega^2 a^5}{3G}\left(\frac{3M_C}{M+M_C}\right)\left(e_i^T e_j^T - \frac{1}{3}\delta_{ij}\right) + (1+k_f^L)C_{ij}$$

(2.42)

where the first term stands for the deformation due to the centrifugal force, the second term is the contribution from the tidal deformation and the last term stems from the mass anomaly. $\boldsymbol{e}^R$ and $\boldsymbol{e}^T$ are unit vectors giving the initial directions of the rotational and tidal axes in the body-fixed frame. Ω is the initial rotational speed and M and M_C are the mass of the body and its orbiting host, respectively. ΔK stands for either the modal strength in the Love number associated with the slower transient mode of the lithosphere (high viscous case) or the difference between the fluid tidal Love numbers of the body without and with the lithosphere (elastic case). For the highly viscous case, equation 2.42 is the infinite time limit of equation 2.12 and only the part that is associated with the lithosphere (ΔK instead of k^T) is retained. The new stable orientation, or the directions of the principle MoI, is obtained by diagonalizing the matrix $\boldsymbol{I}$. The eigenvectors of this matrix corresponding to the largest and smallest eigenvalues are the new orientation of the rotational and tidal axes.

Since the fluid limit method does not provide a time-dependent solution, for a time-invariant load this method can only provide the end position, and not the path and speed. Thus, most of previous studies concerning the reorientation of a tidally deformed body, simply did not consider the intermediate states. Some of them, e.g. (Rubincam, 2003), assumed that the rotational and tidal axes will move directly towards their end positions by the shortest path, which is incorrect in many cases as shown in figure 2.4. When a positive mass anomaly
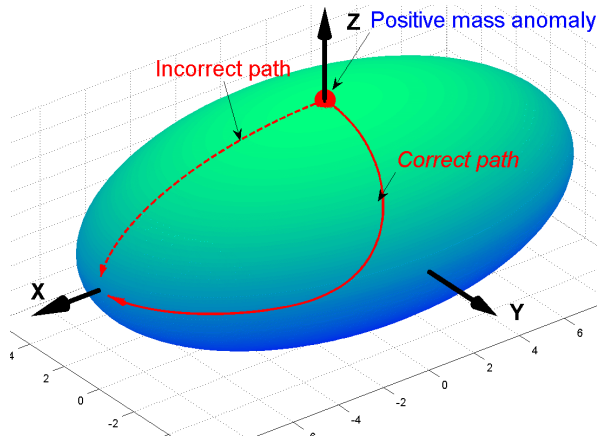
Figure 2.4: A typical misconception concerning the reorientation path of a tidally deformed body driven by a positive mass anomaly near the pole. The reorientation path is not directly targeting the end position by the shortest distance but the planet has a preference of rotating around the tidal axis where the resistance against reorientation is minimal.

is put in the neighbourhood of the north pole of a tidally deformed body, the orientation of the body is not stable. If the body is without lithosphere, or the magnitude or the mass

anomaly is large enough to almost completely nullify the resistance from the lithosphere, it will cause a reorientation of the body so that the mass anomaly eventually ends up at the sub-host or anti-host point. The question that remains is how will this reorientation be accomplished? As shown in figure 2.4, intuitively, one would probably assume that the mass anomaly will move towards the end position over a great circle arc of the body. However, as will be shown in chapters 3 and 5, this path is incorrect.

For a time-varying load, where C_{ij} in equation 2.42 becomes $C_{ij}(t)$, the fluid limit method can also obtain a time-dependent reorientation path. Then the question arises whether this path represents the real reorientation. Considering that the fluid method obtains results where the body is fully relaxed, it can be understood that if the reorientation is slow enough, the fluid limit method is accurate enough. Then the question becomes: how slow does the reorientation process need to be so that we can use the fluid-limit method? This is important to know so that we can better interpret conclusions drawn in previous studies concerning the direction, speed and path of a reorientation process based on the fluid-limit method. All these questions are to be answered in this thesis.

To sum up, the fluid limit method

- can calculate the reorientation of a tidally deformed body;

- does not provide the reorientation path for a time-invariant load;

- has unclear accuracy for a time-varying load.

2.5. DECOUPLING THE GOVERNING EQUATIONS AND NUMERICAL SOLUTIONS

As can be seen in previous sections, due to the difficulty of solving the Liouville equation 2.1 and MoI equation 2.7 analytically, previous studies took various assumptions to simplify either the Liouville equation (linear method) or the MoI equations (non-linear method). Consequently, the result is either an approximated solution or a solution with a limited applicable range. As a result, if we want to seek a more general and accurate method, a semi-analytical or numerical approach is needed.

The basic idea for developing a new method is to decouple the two governing equations 2.1 and 2.7. During the TPW, if we consider a point in time not too far away from a known state, the change in the rotational or tidal axis is small within this time span. Then such change in the rotational or tidal potential will cause a small deformation. This small change in the MoI leads to a small update in the rotational or tidal axis position. This process is illustrated in figure 2.5. Physically, TPW follows the minimal total potential energy principle, as discussed in (Goldreich and Toomre, 1969). The iteration shown in figure 2.5 is mathematically an optimization process to search for the new minimal energy position in each time step.

One advantage of decoupling the governing equations is that different types of approaches, numerical or analytical, can be applied to the Liouville or MoI equation independently. We
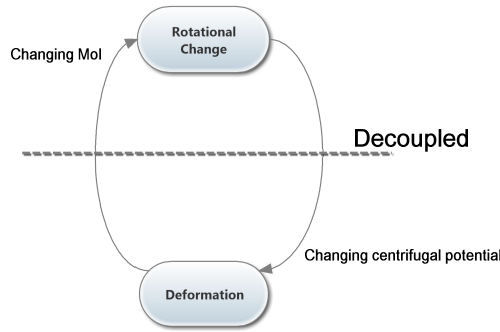
Figure 2.5: Flow chart of the iterative algorithm

can solve the MoI equation by either direct numerical integration of equation 2.7 or with finite element methods (FEM) and combine the result into iteration with a solution of the linearized or non-linear Liouville equation. If the numerical error of such an iterative procedure can be reduced, the obtained result is accurate. Moreover, the rheology and model for the planetary body can be much more general than for pure analytical methods. For example, non-linear rheology and laterally heterogeneous models can be dealt with much easier by FEM than by e.g. the normal mode method. However, the problem of using FEM to calculate deformation of planetary bodies is that two effects, the self-gravitation and the buoyancy force for internal density change, are usually not included in the stiffness equation of a general FEM software (Wu, 2004), e.g. ABAQUS or ANSYS. While the buoyancy force can be directly modelled in the FEM, the gravitational perturbation, since it depends on the deformation of the body itself, can only be included by an iterative procedure. Zhong et al. (2003); Wu (2004); Wu and Wang (2006) established such a method for using FEM to study deformation, sea level change and stress of planetary bodies. Applying the FEM in the study of TPW means that in each iteration, both the gravitational and rotational perturbation need to be calculated and fed back into the model, which is shown in figure 2.6.

One must realize that the original non-linear Liouville equation 2.1 and the linearized one
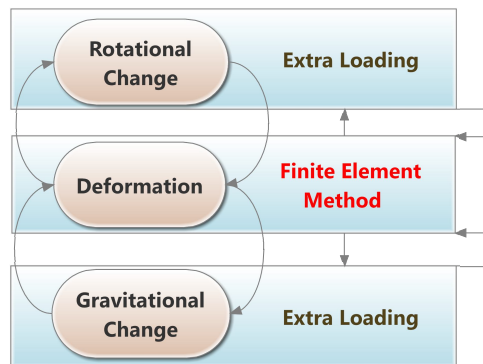
Figure 2.6: Flow chart of the iterative algorithm when finite element method is applied.

2.22 can not be used directly in such an iterative procedure because they are still differential equations which can not be directly solved by root finding procedures. Thus, the question that remains is how the rotational change should be calculated for large angle TPW. This issue will be further discussed and solved in section 3.3.

2.6. THESIS GOALS AND RESEARCH QUESTIONS

Based on the review in previous sections about the current methods for studying TPW of planetary bodies, the main goal of this PhD project can be stated as

*To establish a general numerical and semi-analytical approach to obtain accurate rotational variations of a planetary body which can have the following features:*

- *tidally deformed (co-rotating);*

- *undergoing large angle TPW;*

- *small equatorial bulge so that the Chandler wobble becomes dominant;*

- *containing complex rheology and lateral heterogeneity.*

With the established method, the following four major research questions, each of which contains several subquestions, concerning the applicability and accuracy of previous methods should be answered:

1. What is the applicable range of the linear method?

   - For the linear method, what is the effect of calculating the MoI of the mass anomaly in the body-fixed frame during the entire TPW?

   - What is the maximum degree for TPW that can be accurately calculated by the linear method if the MoI of the mass anomaly is calculated in this way?

2. What is the influence of the quasi-fluid approximation?

   - How accurate is the non-linear method based on the quasi-fluid approximation?

   - What is the influence of the approximation in the case of the Earth, Mars and Venus TPW?

3. How will a tidally deformed co-rotating body reorient?

   - How will a tidally deformed body reorient following a constant or changing load due to a positive or negative mass anomaly?

   - Does the TPW path obtained by the fluid limit method for a changing load represent the real path?

4. When or under which condition can we use the approximated solutions?

   - If the answers to the questions 2 and 3 are negative or conditional, then when can we use the quasi-fluid approximation or the fluid-limit method?

   - How can we properly evaluate conclusions drawn in previous studies that are based on these approximated solutions?

The following three chapters address the above mentioned questions:

- Chapter 3 establishes a numerical iterative procedure which can deal with a tidally deformed body without a lithosphere. The method is partially verified by both linear and non-linear methods and research question 1 is answered. Questions 2 and 3 are answered conditionally where the effect of the lithosphere was not considered. The content of this chapter is from on (Hu et al., 2017b) which is published as

  Hu, H., van der Wal, W., and Vermeersen, L. L. A. (2017b). A numerical method for reorientation of rotating tidally deformed viscoelastic bodies. *Journal of Geophysical Research: Planets*, 122(1):228–248.

- Chapter 4 establishes a semi-analytical approach which extends the numerical method to take into account the effect of a lithosphere. Research question 2 is answered and new insights for the TPW on Mars and Venus is provided. The content of this chapter is from (Hu et al., 2017a) which is published as

  Hu, H., van der Wal, W., and Vermeersen, L. L. A. (2017a). A full-maxwell approach for large angle polar wander of viscoelastic bodies. *Journal of Geophysical Research: Planets*, 122(12):2745- 2764.

- Chapter 5 establishes a semi-analytical method which meets the goal of this thesis. A criterion is established to judge whether the quasi-fluid and fluid limit approximation can be adopted for a given interior model and load. This chapter answers research questions 3 and 4.

- Chapter 6 summarizes the established new methods and answers to the research questions. It also shows the influence of applying the new method on calculating TPW of various planetary bodies in our solar system. Finally, suggestions for further development both in theory and applications are presented.

3

PAPER 1: A NUMERICAL METHOD FOR REORIENTATION OF ROTATING TIDALLY DEFORMED VISCO-ELASTIC BODIES

H.Hu,[1] W. van der Wal[1], L.L.A.Vermeersen[1]

Existing approaches for simulating the true polar wander (TPW) of a visco-elastic body can be divided into three categories: (i) a linear dynamic approach which uses the linearized Liouville equation (e.g. Wu and Peltier (1984); Mitrovica et al. (2005)); (ii) a non-linear dynamic approach which is based on the quasi-fluid approximation (e.g. Sabadini and Peltier (1981); Ricard et al. (1993); Cambiotti et al. (2011)); (iii) a long-term limit approach which only considers the fluid limit of a reorientation (e.g. Matsuyama and Nimmo (2007)). Several limitations of these approaches have not been studied: the range for which the linear approach is accurate, the validity of the quasi-fluid approximation, and the dynamic solution for TPW of a tidally deformed rotating body. We establish a numerical procedure which is able to determine the large angle reorientation of a visco-elastic celestial body that can be both centrifugally and tidally deformed. We show that the linear approach leads to significant errors for loadings near the poles or the equator. Secondly, we show that slow relaxation modes can have a significant effect on large angle TPW of Earth or other planets. Finally, we show that reorientation of a tidally deformed body driven by a positive mass anomaly near the poles has a preference for rotating around the tidal axis instead of towards it. At

---

[1] Delft University of Technology

a tidally deformed body which does not have a remnant bulge, positive mass anomalies are more likely to be found near the equator and the plane perpendicular to the tidal axis, while negative mass anomalies tend to be near the great circle with longitudes 0 and 180 degree.

3.1. INTRODUCTION

True polar wander (TPW), the non-periodical secular part of the displacement of the rotation axis with respect to surface topography or internal signatures, has been proposed to be the cause of many geologic features on various planets and moons (e.g, Mars (Schultz and Lutz, 1988), Venus (Malcuit, 2014), Enceladus (Nimmo and Pappalardo, 2006), Europa (Ojakangas and Stevenson, 1989)). The theoretical study of TPW can be dated back to Gold (1955) who introduced the modern concept and general mechanism of TPW. After the development of the normal mode method (Farrell, 1972), the Liouville equation could be solved semi-analytically (Sabadini and Peltier, 1981) for a visco-elastic multi-layer model to arrive at the dynamic solution of TPW. Early studies focused on the speed of present day TPW and small angular change, so a linear approach, which applies the linearised form of the Liouville equation (Munk and MacDonald, 1960), was adopted to calculate TPW when the rotational axis is not too far away from the initial position (Nakiboglu and Lambeck, 1980; Sabadini and Peltier, 1981; Wu and Peltier, 1984). In order to deal with the long-term rotational variation of Earth which may include large angular TPW, non-linear methods have been developed, but they adopt the quasi-fluid approximation which assumes that the variation of the driving force for TPW is much slower compared to the characteristic viscous relaxation. Mathematically, the quasi-fluid approximation is a first order approximation in the Taylor expansion of the tidal Love number (Spada et al., 1992a; Ricard et al., 1993; Cambiotti et al., 2011). Thus, these semi-analytical solutions have several limitations. Specifically, the approximations which have been adopted in the development of the methods have not been quantitatively tested. They will be discussed in the following.

Firstly, although some later studies solve the Liouville equation in different ways such as with a finite difference method (Nakada, 2002; Mitrovica et al., 2005), the linearised form of the Liouville equation is still used and there is a limit for the allowed range of TPW in order for the error to remain small. In order to show the limit of the linear method, Sabadini and Peltier (1981), within the frame of the quasi-fluid approximation, carried out a comparison between the non-linear scheme and the linear scheme, arriving at the conclusion that the linear method is valid for TPW about 10 degrees from the initial position of the rotation pole. The linearised form of the Liouville equation is derived in the body-fixed frame where the rotational axis coincides with the vertical axis in the beginning (Munk and MacDonald, 1960). Since the loading (the inertia tensor representing the geophysical process on the solid model) is also defined in the body-fixed fame, the linear theory actually also assumes that the relative location of the loading with respect to the rotational axis does not change during TPW. This assumption can lead to a large error for certain locations of the loading. For instance, when a point mass is located near the poles or equator, the effect of a change in colatitude of the point mass is relatively large. As a result, the linear methods should have a much smaller applicable range for loadings near the pole or equator. Currently, no study gives the expected error as a function of the angle of TPW and the position of the load when the linearised form of the Liouville equation is applied.

Secondly, the non-linear approach is currently the only general way to calculate large-angle TPW. As a result, the effect of the quasi-fluid approximation, which has been the fundamental assumption of many previous studies (Spada et al., 1992a, 1996; Ricard et al., 1993; Harada, 2012; Chan et al., 2014), has not been tested. So it is not clear what the effect is of taking the quasi-fluid approximation and ignoring the effects of the slow modes (such as the M1 and M2 modes for Earth) on the path of TPW.

Thirdly, a rotating tidally deformed body can be very difficult to deal with by current linear or non-linear rotation theory. As shown in figure 1.10, there are three different reorientations of a tidally deformed body while there is only one type of the reorientation when only a centrifugal force is applied. As a result, the complete description of the reorientation of a tidally deformed rotating body consists of the polar wander of both the rotational and tidal axes. We are not aware of other methods which solve the Liouville equation to give a time-dependent solution for the reorientation of a rotating tidally deformed visco-elastic body. Most studies concerning TPW of a tidally deformed body only focus on the fluid limit of the visco-elastic response which gives the final position of the rotational or tidal axis (Willemann, 1984; Matsuyama and Nimmo, 2007). In practice, it is difficult to know if the TPW or reorientation has already finished and the rotational or tidal axis are in their final position. This limits the application of methods which only calculate the final position and not the full reorientation path. More importantly, since these methods do not provide dynamic solutions, we do not have a clear insight on how the reorientation is accomplished. Studies which concern the direction of polar wander of tidally deformed bodies driven by either a positive mass anomaly such as ice caps on Triton (Rubincam, 2003) or a negative mass anomaly such as a diapirism induced low density area on Enceladus (Matsuyama and Nimmo, 2007; Nimmo and Pappalardo, 2006) suggest that the polar motion is directly targeting its end position. However, these suggestions are not tested in these papers because a theory for combined centrifugally and tidally induced TPW is lacking.

Considering all above mentioned problems and the difficulty of solving the Liouville equation analytically, we create a numerical model to tackle these problems. Another advantage of adopting a numerical approach is that the normal mode method, which is the foundation of all above mentioned dynamic rotation methods, can only be applied for a radially symmetric model, while many planets and moons can have considerable lateral heterogeneity, for example Mars (Šrámek and Zhong, 2012) or Enceladus (Nimmo and Pappalardo, 2006). The purpose of this paper is to establish a general numerical method which can determine the secular part of the rotational variation of a centrifugally and tidally deformed visco-elastic body. With the help of this method we aim to answer the following questions:

1. What is the effect of assuming that the load is stationary relative to the rotational axis in the linear method?

2. What is the effect of the quasi-fluid approximation for the TPW path of a planetary model?

3. How is the reorientation of a tidally deformed body driven by a certain mass anomaly accomplished?

It is important to note that we only consider pure visco-elastic bodies without a remnant bulge in this study. For some planets such as Earth, during the early stages of their formation, the outer layer cools down in an ellipsoidal shape and becomes fixed. The existence of such a bulge can have a significant effect on the behaviour of TPW. For the case of Earth and some other celestial bodies, this issue has been intensively studied during the past decades (Willemann, 1984; Mitrovica et al., 2005; Matsuyama and Nimmo, 2007; Cambiotti et al., 2010; Mitrovica and Wahr, 2011; Chan et al., 2014). The existence of a remnant bulge, would have two effects. Firstly, during the TPW, since the stress in the outer layer can not relax as the rest of the visco-elastic parts, the remaining stress in this layer would prevent the equa-

torial bulge to fully adjust into the vertical position to the rotational axis. Because of this, a positive anomaly, for instance, will not reach the equator as for the case of a pure visco-elastic body, as is demonstrated in figure 14 in Mitrovica et al. (2005). Secondly, when the TPW is finished or during the TPW, if the mass anomaly which causes the TPW is removed from the body, the stress in the outer layer would try to restore the shape of the body back into its initial form before the TPW starts, so the rotational axis would go back to its initial position. This is different from the case of a purely visco-elastic body in which the rotational axis is expected to retain its final position when the mass anomaly is removed. As a result, the study of TPW on models with such an elastic layer is significant. However, the numerical procedures and the validation of such models are beyond the scope and purpose of this paper. So in this paper, only models without a remnant bulge are considered.

The content is organized as follows: Section 3.2 shows how the change in the inertia tensor can be obtained by a finite element modelling (FEM). Section 3.3 presents a numerical method for solving the Liouville equation. After validating our numerical results with previous semi-analytical methods, we test the above mentioned assumptions. Finally, section 3.4 presents a method to calculate the reorientation of a tidally deformed rotating visco-elastic body and shows the cases of a body driven by a positive and negative mass anomaly respectively. This paper only focuses on the laterally homogeneous case, a follow-up paper will study the effects of lateral heterogeneity on TPW.

3.2. FINITE ELEMENT APPROACH FOR CALCULATING THE CHANGE IN THE MOMENT OF INERTIA

The Liouville equation gives the general dynamics of a rotational body that can deform. When no external torque is applied, it reads (Sabadini et al., 2016)

$$\frac{d}{dt}(\mathbf{I} \cdot \boldsymbol{\omega}) + \boldsymbol{\omega} \times \mathbf{I} \cdot \boldsymbol{\omega} = 0 \qquad (3.1)$$

where $\mathbf{I}$ is the inertia tensor and $\boldsymbol{\omega}$ is the rotational vector. Both values are defined in a body-fixed coordinate system. In order to solve this equation, information about the change in the inertia tensor must be given. When the moments of inertia are perturbed by a geophysical process for a centrifugally deformed body without tidal deformation, the rotational axis shifts, and the resulting change in the centrifugal force also deforms the body. Analytically, given a rotational vector as $\boldsymbol{\omega} = \Omega(\omega_1, \omega_2, \omega_3)^T$, where Ω is the angular speed of the rotation and $(\omega_1, \omega_2, \omega_3)^T$ is a unit vector which represents the direction of the rotation, the total moment of inertia attributable to such process is given by (similar to equation 2 in Ricard et al. (1993))

$$I_{ij}(t) = I\delta_{ij} + \frac{k^T(t)a^5}{3G} * (\Omega^2[\omega_i(t)\omega_j(t) - \frac{1}{3}\delta_{ij}])$$
$$+ [\delta(t) + k^L(t)] * C_{ij}(t) \qquad (3.2)$$

where I is the principle moment of inertia of the unloaded laterally homogeneous spherical body, G and a are the gravitational constant and the radius of the planet, respectively. $k^T(t)$ and $k^L(t)$ are the degree 2 tidal Love number and load Love number respectively. The $*$ denotes convolution in the time-domain. C_{ij} represents the change in the moments and products of inertia without considering the dynamic deformation. These values trigger the polar wander. The second and third term in Equation 3.2 represent the changes which derive from the perturbed centrifugal force and from the mass redistribution induced by the original load respectively. The use of Love numbers limits the simulation to the case of a laterally homogeneous model and thus we also seek a numerical method as an alternative for equation 3.2 to calculate the change in the inertia tensor. This will be the foundation for dealing with heterogeneous cases in our second paper.

In order to obtain the change in the inertia tensor, we need to know the deformation of the body for which we can use FEM. This part is mainly based on the method of Wu (2004). One of the problems of applying FEM to calculate the visco-elastic response of a 3-D celestial body is the effect of self-gravitation which is dependent on the deformation itself. In Wu (2004), the deformation is first determined by assuming the perturbed potential is zero, and the result from FEM is used to calculate the perturbed potential. The potential is applied to the model again and iteration continues until the result converges. We develop a finite-element (FE) model with the commercial package Abaqus version 6.13 in which the average grid size for the Earth model is chosen to be around 400 km and linear brick elements are used. With the information of the deformation the change in the inertia tensor is also calculated numerically after the result from FEM converges. In the FE model, the Poisson ratio of the planet model can be set to that of a compressible material, but the effects of a change in density on gravity and inertia are not taken into account. Hence our method does not include the full effect of compressibility but only material compressibility (similar to e.g. Wang et al. (2008)). Since we ignore the density changes, when the deformation is
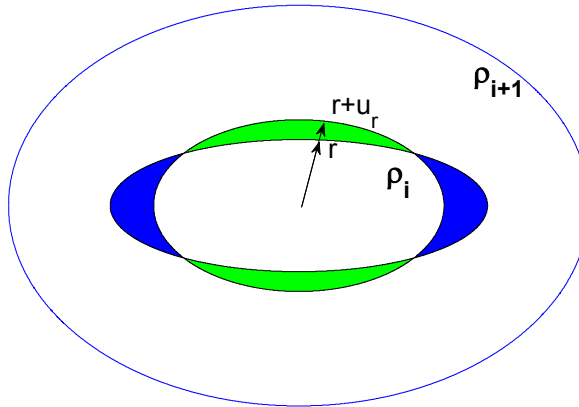
Figure 3.1: Deformation of a boundary layer whose radius changes from r to $r + u_r$. The densities inside and outside of the layer are ρ_i and ρ_{i+1}, respectively.

small, only the radial displacement for each layer is required for calculating the change in the moment of inertia, which is shown in the following method. As we can see in figure 3.1, the deformation changes the shapes of the boundaries which switches the density of cer-

tain parts: for the shaded area in figure 3.1, the density of the green parts changes from ρ_{i+1} to ρ_i and the density of blue parts from ρ_i to ρ_{i+1}. As a result, for a model which contains N layers, at the pth internal boundary, the change in the inertia tensor is calculated as:

$$
\begin{aligned}
\Delta I_{ij,p} &= \int_{\Delta V} (\rho_{p+1} - \rho_p)(r_k r_k \delta_{ij} - r_i r_j) dV \\
&\simeq \int_S (\rho_{p+1} - \rho_p)(r_k r_k \delta_{ij} - r_i r_j) u_r dS, \quad p = 0, 1, 2 \ldots N - 1
\end{aligned}
$$

and at the surface:

$$
\Delta I_{ij,N} = \int_S (\rho_N)(r_k r_k \delta_{ij} - r_i r_j) u_r dS \tag{3.3}
$$

Here ΔV is the perturbed volume which contains the above mentioned density switch and S is the complete interface or the surface. The complete change of the inertial tensor is given by the sum of the changes at all interfaces and at the surface:

$$
\Delta I_{ij} = \sum_{p=0}^{N} \Delta I_{ij,p} \tag{3.4}
$$

We validate our FE model by calculating the change in the inertia tensor of a two-layer Earth model (table 3.1) which is forced by a varying centrifugal force.

Table 3.1: Properties of the two-layer Earth model

Layer	Outer Radius (km)	Density (kg m^{-3})	Shear Modulus (Pa)	Viscosity (Pa s)
Mantle	6371	4448	1.7364×10^{11}	1×10^{21}
Core	3480	10977	0	0

We apply the centrifugal force to an initially unloaded model, and let the rotational axis move towards the equator with a constant speed of 45 degree in 5000 years. The change in the moment of inertia for this case can be calculated by equation 3.2 with $C_{ij}(t) = 0$. The comparison between the semi-analytical and FEM results is given in Figure 3.2. For the non-zero components I_{11}, I_{22}, I_{33}, and I_{13}, the numerical results show very good agreement with the semi-analytical results. FEM results of I_{12} and I_{23} are also non-zero while they should be theoretically zero. However, the numerical results of these two values are about four orders of magnitude smaller than the other four components in the inertia tensor. Thus, these values result in a numerical error which is around 0.1% for our configuration of a mesh with an average grid size of 400 km for the Earth model.

As will be shown in the next section in the linearised Liouville equation and algorithm 2, the accuracy of the TPW is controlled by four terms which are combinations of components of the inertia tensor and the angular speed in a coordinate system whose z-axis coincides with the rotational axis: $\frac{\Delta I_{13}(t)}{C-A}, \frac{\Delta I_{23}(t)}{C-B}$ and $\frac{C \Delta \dot{I}_{13}(t)}{\Omega(C-A)(C-B)}, \frac{C \Delta \dot{I}_{23}(t)}{\Omega(C-A)(C-B)}$. In order to show that
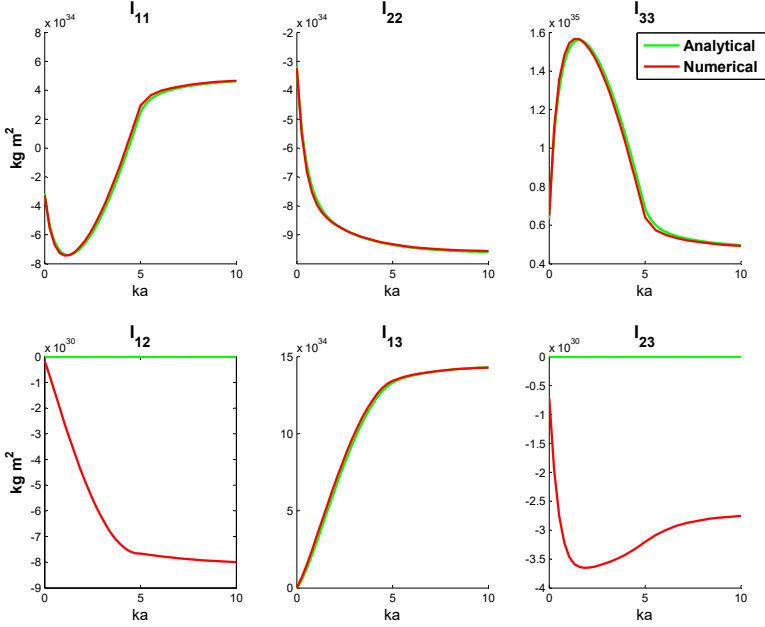
Figure 3.2: Change in the moment of inertia for a two-layer Earth model with the rotation axis linearly drifting from 0 to 45 degree colatitude in the x-z plane in 5000 years.

the change in the moment of inertia obtained from FEM is accurate enough for calculating TPW, we compare both the analytical and numerical values of these four terms for a given TPW history. As shown in figure 3.3, the theoretical non-zero terms $\frac{\Delta I_{13}(t)}{C-A}$ and $\frac{C\Delta \dot{I}_{13}(t)}{\Omega(C-A)(C-B)}$ show very good agreement. For a grid size of 300 km, $\frac{\Delta I_{13}(t)}{C-A}$ and $\frac{C\Delta \dot{I}_{13}(t)}{\Omega(C-A)(C-B)}$ terms have less than 0.5% error level. We see again that two theoretical zero components are at least 4 orders of magnitude smaller than the non-zero components. It was found that, in order to get results close to the analytic result which is based on Maxwell rheology, in Abaqus, a "Viscoelastic" option need to be used. "Viscoelastic" setting in Abaqus uses the Prony series which is a general scheme that encompasses a simple Maxwell rheology. We show this issue in Appendix I.

3.3. NUMERICAL SOLUTIONS OF LIOUVILLE EQUATION

With the information about the change in the inertia tensor obtained either by equation 3.2 or FEM, the Liouville equation can be solved numerically. Cases with small angular change, to which linear theory can be directly applied, and large angular change will be dealt with separately. We validate our numerical methods by comparing the results with semi-analytical linear (Wu and Peltier, 1984) and non-linear (Ricard et al., 1993) methods with the same assumptions. After that, we test the validity of the assumptions made in these methods.
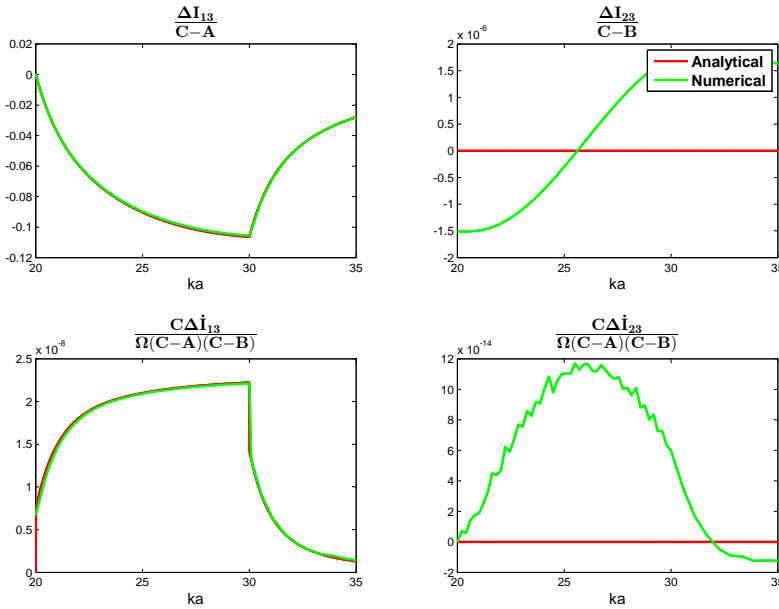
Figure 3.3: Values of four terms for a SG6 Earth model with the rotation axis linearly drifting from 0 to 45 degree colatitude in the x-z plane in 10 thousand years after the centrifugal force is applied to the spherical model for 20 thousand years.

3.3.1. SMALL-ANGLE POLAR WANDER

Considering that we want to deal with lateral heterogeneity in paper II and tidally deformed bodies, we first need to derive a more general form of the linearised Liouville equation. The procedure is similar to that given on page 104 of (Sabadini et al., 2016).
In equation 3.1, when assuming that changes in **I** are small, the perturbed inertia tensor can be written as

$$\mathbf{I} = \begin{pmatrix} A + \Delta I_{11} & \Delta I_{12} & \Delta I_{13} \\ \Delta I_{21} & B + \Delta I_{22} & \Delta I_{23} \\ \Delta I_{31} & \Delta I_{32} & C + \Delta I_{33} \end{pmatrix} \tag{3.5}$$

Here A, B and C denote the moments of inertia of the rotational body for the equatorial principal axes and polar principal axis. We do not assume $A = B$ as in (Sabadini et al., 2016). We define the perturbed vector of the rotation as

$$\boldsymbol{\omega} = \Omega(m_1, m_2, 1 + m_3)^T \tag{3.6}$$

where Ω is the angular speed of the rotation and $m_i, i = 1, 2, 3$ are small values with m_1 and

m_2 representing the TPW and m_3 the change in the length of the day (LOD). By omitting the products of the small quantities m_i and ΔI_{ij}, we have:

$$\mathbf{I} \cdot \boldsymbol{\omega} \approx \begin{pmatrix} A\Omega m_1 + \Omega \Delta I_{13} \\ B\Omega m_2 + \Omega \Delta I_{23} \\ C\Omega + Cm_3\Omega + \Delta I_{33}\Omega \end{pmatrix} \tag{3.7}$$

$$\boldsymbol{\omega} \times (\mathbf{I} \cdot \boldsymbol{\omega}) \approx \begin{pmatrix} -Bm_2\Omega^2 + Cm_2\Omega^2 - \Delta I_{23}\Omega^2 \\ Am_1\Omega^2 - Cm_1\Omega^2 + \Delta I_{13}\Omega^2 \\ 0 \end{pmatrix} \tag{3.8}$$

Substituting equation 3.7 and 3.8 into 3.1 we have:

$$\dot{m}_1 = -\frac{C-B}{A}\Omega m_2 + \frac{\Omega}{A}\Delta I_{23} - \frac{\Delta \dot{I}_{13}}{A} \tag{3.9a}$$

$$\dot{m}_2 = \frac{C-A}{B}\Omega m_1 - \frac{\Omega}{B}\Delta I_{13} - \frac{\Delta \dot{I}_{23}}{B} \tag{3.9b}$$

$$\dot{m}_3 = -\frac{\Delta \dot{I}_{33}}{C} \tag{3.9c}$$

Note that now we can not define the Eulerian free precession frequency as $\sigma_r = \frac{C-A}{A}\Omega$ to further combine these equations. Equation 3.9 gives the rotational dynamics of a triaxial body for a small perturbation which has been previously studied by Hinderer et al. (1982); Matsuyama et al. (2010) for the case of Earth. Matsuyama et al. (2010) made the assumptions that the time scale of the loading is much longer than both the period of rotation and the Euler wobble periods. Based on these assumptions, the derivatives on both side of the equation 3.9 are ignored. The same procedure is also used in (Sabadini et al., 2016). These assumptions might be true for Earth but not for some slow rotating bodies like Venus. In order to establish a more general method, we can not directly ignore these derivative terms. Instead, we take advantage of the fact that numerically the TPW is calculated stepwise and deal with equation 3.9 as follows: In each step of the numerical integration, we assume that the size of the step is small enough so that the change in the inertia tensor can be treated as linear, which gives

$$\Delta I_{13}(t) = a_1 + b_1 t \tag{3.10a}$$

$$\Delta I_{23}(t) = a_2 + b_2 t \tag{3.10b}$$

After substituting (3.10) into (3.9), m_1, m_2 can be solved analytically. The results contain both secular terms and periodic terms, which represent the TPW and the Chandler wobble respectively. We ignore the periodical terms and obtain

$$m_1(t) = \frac{\Delta I_{13}(t)}{C-A} + \frac{C\Delta \dot{I}_{23}(t)}{\Omega(C-A)(C-B)} \quad (3.11a)$$

$$m_2(t) = \frac{\Delta I_{23}(t)}{C-B} - \frac{C\Delta \dot{I}_{13}(t)}{\Omega(C-A)(C-B)} \quad (3.11b)$$

$$m_3(t) = -\frac{\Delta I_{33}}{C} \quad (3.11c)$$

Besides the A and B terms, the equations also contain the derivatives of the elements of the inertia tensor. When only the centrifugal force is considered for a laterally homogeneous model, $(C-A)/C = (C-B)/C$ represents the flattening of the model and the magnitude of $(C-A)/C$ is proportional to the square of the rotational rate Ω^2. As a result, the magnitudes of the second terms on the right side become significantly larger for slowly rotating bodies such as Venus. When the magnitude of the second terms on the right side becomes comparable to that of the first terms, it results in the phenomenon of the so-called mega wobble (Spada et al., 1996; Sabadini et al., 2016) as shown on the right figure 3.4(a). For most of the bodies in the solar system including Earth, long-term TPW acts as in figure 3.4(b). In this case the part which contains the derivatives of the changes in the inertia tensor is small and the path of TPW driven by a point mass is almost along the great circle of the body. So if we place a point mass load in the x-z plane, the TPW can be almost completely described by the value m_1.

Since we study the TPW of the bodies in the hydrostatic state, the centrifugal force needs to
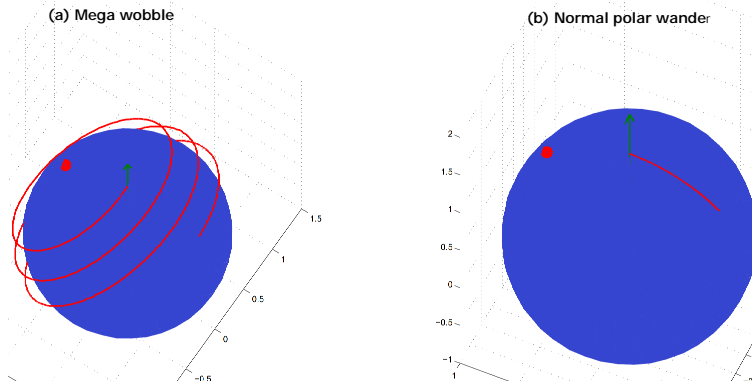
Figure 3.4: Two types of polar wander path. The green arrow is the initial position of the rotational axis and the red dot is the point mass load.

be applied for a certain length of time T_0 until the model can be considered to have reached its equilibrium. For laterally homogeneous models, the choice of T_0 can be derived from the time history of the tidal Love number. We choose T_0 to be the time at which the tidal Love number reaches more than 99.95% of the fluid tidal Love number:

$$k^T(T_0) > 99.95\% \, k_f^T \quad (3.12)$$

Here k_f^T is the fluid tidal love number. For the two-layer Earth model of table 1 it follows that $T_0 = 15$ ka. In the FE model, we apply a centrifugal force at its original rotational axis

for T_0 before we start to apply the algorithm to calculate the path of TPW. If equation 3.2 is used, then we have

$$\boldsymbol{\omega}(t) = (0, 0, \Omega) \quad \text{for} \quad 0 \le t \le T_0 \tag{3.13}$$

where Ω is the angular velocity of the body. For a centrifugally deformed body triggered by a mass anomaly with inertia tensor $\Delta \mathbf{I}_L$, the algorithm for calculating the small-angle polar wander and LOD $m = (m_1, m_2, m_3)$ is given as follows.

Algorithm 1

1. Assume that the step i starts at time t_i with the rotational axis being located at $\boldsymbol{\omega}^i = \Omega^i(m_1^i, m_2^i, 1 + m_3^i)$ and ends at time t_{i+1} with the rotational axis at $\boldsymbol{\omega}^{i+1}$. For the first iteration we assume that the rotation axis does not change: $\boldsymbol{\omega}^{i+1} = \boldsymbol{\omega}^i$.

2. For a laterally homogeneous model we use equation 3.2 for calculating the change in the inertia tensor. In equation 3.2, set $C_{ij}(t) = \Delta I_{L\_ij}$ and let

$$\boldsymbol{\omega}(t) = \boldsymbol{\omega}^i + \frac{t_i - t}{t_i - t_{i+1}} \boldsymbol{\omega}^{i+1} \quad \text{for} \quad t_i \le t \le t_{i+1} \tag{3.14}$$

then the result of equation 3.2 can directly give the total change in the inertia tensor $\Delta \mathbf{I}$ and its derivative $\Delta \dot{\mathbf{I}}$.

For a laterally heterogeneous model we use FEM to obtain the inertia tensor. Change the centrifugal potential from its initial direction along $\boldsymbol{\omega}^i$ at t_i linearly to its new direction of $\boldsymbol{\omega}^{i+1}$ at t_{i+1} in the FEM and calculate the change in the inertia tensor $\Delta \mathbf{I}_D$ and its derivative $\Delta \dot{\mathbf{I}}_D$ due to centrifugal deformation and surface load by equation 3.4. The total change in the inertia tensor is the sum of that due to the deformation and the tensor of the initial load: $\Delta \mathbf{I} = \Delta \mathbf{I}_D + \Delta \mathbf{I}_L$, $\Delta \dot{\mathbf{I}} = \Delta \dot{\mathbf{I}}_D + \Delta \dot{\mathbf{I}}_L$.

3. Substitute $\Delta \mathbf{I}$ and $\Delta \dot{\mathbf{I}}$ into equation 3.11 and obtain the updated $\boldsymbol{\omega}^{i+1}$. This value is fed back into step 2 until the result converges.

The small angle numerical results are compared with results from the linear semi-analytical method of Wu and Peltier (1984). In that paper, the Chandler wobble is filtered out by assuming that all rotational modes have a much longer relaxation time than the Chandler wobble. By taking $|s| << \sigma_0$, where s and σ_0 are the Laplace frequency and Eulerian free precession frequency respectively, the imaginary, harmonic part of the fundamental mantle mode (M0) which contains the most influence on the Chandler wobble, is omitted. It has been proven that the elastic term of equation 79 in Wu and Peltier (1984) is a highly accurate approximation of the effect on TPW of the real part of the M0 mode (Vermeersen and Sabadini, 1996; Peltier and Jiang, 1996). So for small angular motion, since the method stated in (Wu and Peltier, 1984) contains the effects of all modes, we expect that it gives an accurate prediction of the TPW on a layered visco-elastic model against which our method can be benchmarked. We test our method both with the two-layer Earth model (table 3.1) and the six-layer Earth model SG6 as defined in table 3.2. We calculate the corresponding Love number of this model by setting the viscosity of the lithosphere to an extremely high value but exclude the slowest mode generated by this layer. This scenario corresponds

to the situation where the elastic layer exists before the centrifugal potential is applied to the spherical Earth, as demonstrated in figure 14 of (Mitrovica et al., 2005) as case B. Of course this situation does not correspond to the real Earth (case C and D in the same figure) which has a remnant bulge. However, as mentioned in the introduction, the purpose here is method development and validation, and we leave the effect of a remnant bulge in our method to future work. The models are driven by a constant point mass of 2×10^{19} kg which is attached to the surface at 45 degree colatitude. We assume that the point mass is stationary at the surface, so in equation 3.2 $k_L = 0$. For the SG6 model, the initial time T_0 for which the centrifugal force needs to be applied is chosen to be 4 million years according to equation 3.12. The numerical results for both models agree very well with the prediction of Wu and Peltier (1984), see figure 3.5. From this figure, we can also see the effect of the delayed viscous adjustment of the rotational bulge. This stabilization is larger for layers with higher viscosity and this is why TPW of SG6 model driven by the same anomaly is slower.

Table 3.2: Properties of the viscoelastic Earth model SG6

Layer	Outer Radius (km)	Density (kg m^{-3})	Shear Modulus (Pa)	Viscosity (Pa s)
Lithosphere	6371	4120	0.73×10^{11}	∞
Upper mantle	6271	4120	0.95×10^{11}	0.6×10^{21}
Transition zone	5950	4220	1.10×10^{11}	0.6×10^{21}
Shallow lower mantle	5700	4508	2.00×10^{11}	1.6×10^{21}
Deeper lower mantle	5040	4508	2.00×10^{11}	3×10^{21}
Core	3480	10925	0	0
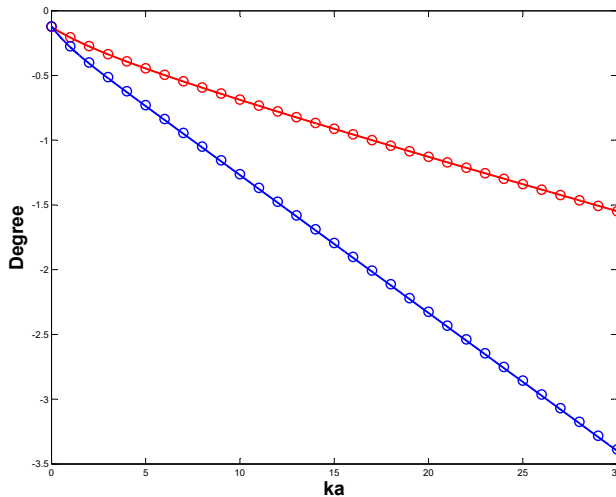
Figure 3.5: The polar wander path in the x-z plane of the two-layer (blue) and SG6 (red) Earth models triggered by a mass anomaly of 2×10^{19} kg attached at 45 degree colatitude in the x-z plane. Lines show the results with semi-analytical method of Wu and Peltier (1984) and circles represent our numerical ones.

Usually 7-8 iterations in each step are necessary for the use of equation 3.2 and 9-10 for FEM with equation 3.4 are required to achieve an accuracy of 0.1%. The required number of iterations is reduced for smaller step sizes.

The agreement of our numerical method and the method from Wu and Peltier (1984) shows

the validity of the assumption $|s| << \sigma_0$. However, as mentioned in the introduction, there is one problem with the method in (Wu and Peltier, 1984): the loading itself is assumed to be stationary relative to the rotational axis and is not updated by the polar motion. For the case of TPW due to a mass anomaly which is shown in figure 3.5, during the polar wander, the mass anomaly is calculated in the body-fixed coordinates, which means it is treated as being always located at 45 degree colatitude. However, when the rotation axis drifts away from the mass anomaly by 1 degree, in that instantaneous moment, the mass anomaly is actually placed at 46 degree colatitude. Of course, when only very small angle TPW is considered, the difference can be small but the exact effect has not been studied. We will show the magnitude of the error in the next subsection with a new method for calculating large angle TPW.

3.3.2. LARGE-ANGLE POLAR WANDER

The limitation of the method in Wu and Peltier (1984) and the numerical method presented in the previous section is that they are based on the Liouville equation which is linearised at the position where the z-axis of the coordinate system is the rotational axis and the equatorial bulge is perpendicular to this axis. As a result, this method can not deal with large-angle TPW when the rotation axis drifts away from this position. However, if we assume that during the process of polar wander the equatorial readjustment is fast enough (or the polar wander is slow enough) so that the equatorial bulge is always nearly (but not necessarily exactly) perpendicular to the rotational axis, then we can define a new reference frame in which the new z-axis coincides with the current rotational axis and we can linearise the Liouville equation in the new coordinate system. Physically, the process of TPW is the process of the rotational axis moving towards the axis of the maximum moment of inertia while the axis of the maximum moment of inertia is being pushed further away by the visco-elastic relaxation of the body and the displacement of the mass anomaly. What we assume is that the angle between these two axes is small enough so that the linearisation of the Liouville equation is valid. This assumptions is fundamentally different from assuming that during the TPW the rotational axis and the principle axis of the moment of inertia coincide (Jurdy, 1978; Rouby et al., 2010; Steinberger and O'Connell, 1997). The validity of this assumption is studied and discussed in detail in the study of Cambiotti et al. (2011) which develops, within the frame of a non-linear approach for TPW induced by internal mass anomalies, a linear scheme of the Liouville equation in the system of the principal moments of inertia reference frame of the mass anomaly. Apparently, this assumption can be violated by a situation where the TPW is triggered by a very large mass anomaly which corresponds to an inertia tensor that is comparable in magnitude to the inertia tensor of the rotational body itself. In this case, the angle between the largest moment of inertia (the sum of the inertia tensors of both rotating body and the mass anomaly) and the rotational axis would be too large to apply the linearised Liouville equation. One advantage of our numerical method is that during the calculation, we can constantly monitor the validity of this assumption as will be shown by the end of this section. Generally, we can do a coordinate transformation in each step and apply the method we used for small angular change in the new coordinate system so that the local angular change in each step remains small enough.

We define the vector of the rotation as $\boldsymbol{\omega} = \Omega(\omega_1, \omega_2, \omega_3)^T$, where $(\omega_1, \omega_2, \omega_3)$ is a unit vector. For an arbitrary $\boldsymbol{\omega}$, the TPW which starts from this vector needs to be calculated in the

frame whose Z-axis coincides with $\boldsymbol{\omega}$. So we need to transform the original body-fixed coordinates into this new frame . The coordinate transformation matrix of a rotation from the vector $(0,0,1)$ to the unit vector $\boldsymbol{\omega}$ can be obtained from a general rotation matrix (Arvo, 1992) in which the third column of the matrix is $(\omega_1, \omega_2, \omega_3)^T$.

$$\mathbf{Q} = \begin{pmatrix} \omega_3 + \frac{\omega_2^2}{1+\omega_3} & -\frac{\omega_1\omega_2}{1+\omega_3} & \omega_1 \\ -\frac{\omega_1\omega_2}{1+\omega_3} & 1 - \frac{\omega_2^2}{1+\omega_3} & \omega_2 \\ -\omega_1 & -\omega_2 & \omega_3 \end{pmatrix} \tag{3.15}$$

For a centrifugally deformed body triggered by a mass anomaly which corresponds to the inertia tensor $\Delta\mathbf{I}_L$, the algorithm for calculating the large-angle TPW is as follows:

Algorithm 2

1. Assume that the step i starts at time t_i with the vector of the rotation being $\boldsymbol{\omega}^i = \Omega^i(\omega_1^i, \omega_2^i, \omega_3^i)$. and ends at time t_{i+1} with the vector of the rotation $\boldsymbol{\omega}^{i+1}$. For the first iteration, we assume that the vector of the rotation does not change: $\boldsymbol{\omega}^{i+1} = \boldsymbol{\omega}^i$.

2. Obtain $\Delta\mathbf{I}$ and its derivative $\Delta\dot{\mathbf{I}}$ from FEM or using equation 3.2 in the same way as step 2 in algorithm 1. With $\mathbf{Q}$ as defined in equation 3.15 being the coordinate transformation matrix from the body-fixed coordinates to the local coordinates where the Z-axis aligns with the direction of the rotation, the inertia tensors in the transformed coordinates are obtained by $\Delta\mathbf{I}_1 = \mathbf{Q}^T\Delta\mathbf{I}\mathbf{Q}$ and $\Delta\dot{\mathbf{I}}_1 = \mathbf{Q}^T\Delta\dot{\mathbf{I}}\mathbf{Q}$.

3. Substitute $\Delta\mathbf{I}_1$ and $\Delta\dot{\mathbf{I}}_1$ into equation 3.11 and obtain $\boldsymbol{\omega}' = \Omega^i(m_1, m_2, 1 + m_3)^T$. We normalize this vector as $\boldsymbol{\omega}' = \Omega^{i+1}\bar{\boldsymbol{\omega}}'$ where $\bar{\boldsymbol{\omega}}'$ is the direction of the perturbed rotational axis in the local coordinate system and needs to be transformed back into the body-fixed frame to obtain $\boldsymbol{\omega}^{i+1} = \Omega^{i+1}\mathbf{Q}\bar{\boldsymbol{\omega}}'$ where Ω^{i+1} is the same as in the previous equation.

4. Substitute $\boldsymbol{\omega}^{i+1}$ into step 2 until the result converges.

There are two major differences between algorithm 1 and 2. First, in algorithm 2, the rotational perturbation is calculated in a transformed coordinate system instead of the original body-fixed frame in each step. Secondly, the initial load $\Delta\mathbf{I}_L$ is also updated in each step in response to the change of the rotational axis. As we can see in step 2 in algorithm 2, since $\Delta\mathbf{I}$ contains both the change in the moment of inertia due to deformation $\Delta\mathbf{I}_D$ and the initial load $\Delta\mathbf{I}_L$, we have $\mathbf{Q}^T\Delta\mathbf{I}\mathbf{Q} = \mathbf{Q}^T\Delta\mathbf{I}_D\mathbf{Q} + \mathbf{Q}^T\Delta\mathbf{I}_L\mathbf{Q}$. So $\mathbf{Q}^T\Delta\mathbf{I}_L\mathbf{Q}$ instead of $\Delta\mathbf{I}_L$ is used as the input for the driving factor of the TPW. In this way we lift the assumption of a stationary load as in Wu and Peltier (1984) and algorithm 1.

For validation purposes, we test if algorithm 2 can produce the same result as algorithm 1 for a small angle when we disable the updating of $\Delta\mathbf{I}_L$. This means in step 2 of algorithm 2, we only do a coordinate transform for the inertia tensor due to deformation but keep the one for the loading the same, so the total change for the inertia tensor is calculated as $\Delta\mathbf{I}_1 = \mathbf{Q}^T\Delta\mathbf{I}_D\mathbf{Q} + \Delta\mathbf{I}_L$ instead of $\Delta\mathbf{I}_1 = \mathbf{Q}^T(\Delta\mathbf{I}_D + \Delta\mathbf{I}_L)\mathbf{Q}$. Then the condition is the same as in Wu and Peltier (1984) and algorithm 1. To show the effect of the assumption of a stationary load, we also calculate the result with the original algorithm 2 ($\Delta\mathbf{I}_L$ is updated). The

comparison of the semi-analytical result from Wu, our numerical result without updating the loading and the numerical result with updated loading is shown in figure 3.6. When
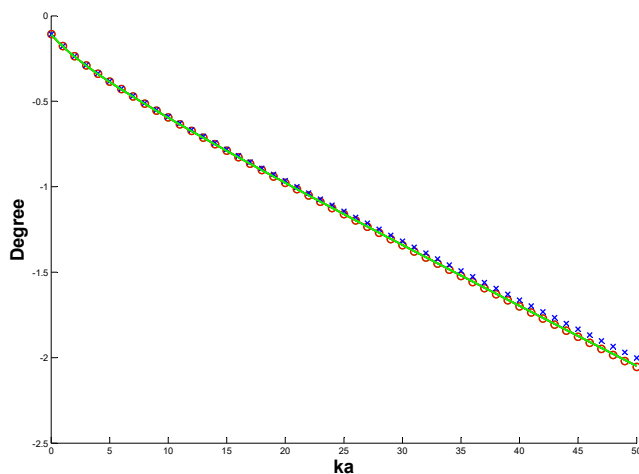

Figure 3.6: Polar wander in the x-z plane for the SG6 Earth model triggered by a point mass of 2×10^{19} kg attached at the surface at $60°$ colatitude. The line, red circles and blue crosses represent the semi-analytical result from Wu and Peltier (1984), our numerical result without updating loading, and the numerical result with updated loading, respectively.

the loading is not updated in each step, the numerical and the normal-mode results show perfect agreement. This validates algorithm 2 as well as the assumption that the equatorial readjustment in this case is fast enough to catch up the polar wander. On the other hand, when the loading is updated in each step, as we can see in figure 3.6, the normal-mode result overestimates the TPW by about 2.5% for 2 degrees of TPW. This is understandable, as the mass anomaly has its largest loading effect when it is at 45 degree (or 135 degree) colatitude. When the positive mass anomaly is attached at the surface at 60 degree colatitude, as the TPW proceeds, the mass anomaly moves towards the equator and the loading effect decreases. As a result, the speed of TPW slows down. Thus, with the method of Wu and Peltier (1984), depending on whether or not the TPW is displacing the mass anomaly towards or away from 45 degree latitude, the result can be either underestimated or overestimated, respectively. The bias becomes much larger if the mass anomaly is close to 0, 90 and 180 degree colatitude: If we place the same mass anomaly at 10 degree colatitude, after a polar wander of 2 degrees the error can be up to 12 % with the stationary loading assumption. Consequently, the applicable range of the linear method becomes even smaller when the loading is close to poles or the equator. The comparison between the result from Wu and Peltier (1984) and the updated linear method (algorithm 2), is similar to that in the figure 3 of Sabadini and Peltier (1981) which compares the TPW path on a homogeneous visco-elastic sphere from both a linear and non-linear scheme. One apparent difference is the lack of an elastic response in the results of Sabadini and Peltier (1981). Figure 3.7 shows how large the TPW can be as a function of colatitude in order to keep the error below 1.5%. As can be derived from figure 3.7, for the situation when the initial load is close to the pole or equator, the applicable range of the linear theory is quite limited. As a consequence, re-
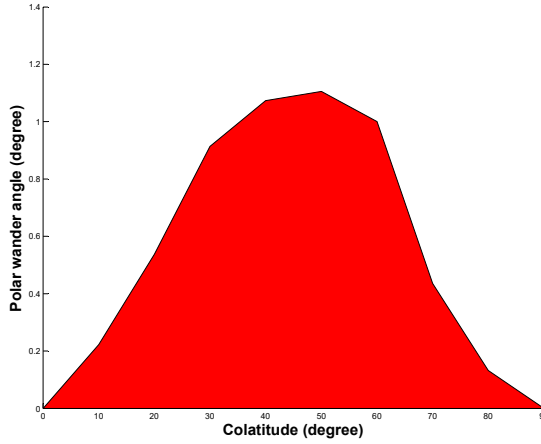
Figure 3.7: The allowed range of polar wander in order to obtain less than 1.5% error as a function of the colatitude of the loading.

sults obtained from linear rotation theory may need to be reconsidered for studies such as TPW on Earth driven by ice loss from Greenland or Antarctica, since these areas are close to the poles.

Next we test the behaviour of our numerical method for large-angle polar wander and compare the result with the method of Ricard et al. (1993). Ricard et al. assume that the Earth model has no internal non-adiabatic density gradients (no M1 or M2 modes) and with $|s| << |s_i|$, the tidal Love number is approximated as

$$
\begin{aligned}
k^T(s) = \ & k_e^T + \sum_{i=1}^{M} \frac{k_i^T}{s - s_i} \\
\approx \ & k_e^T - \sum_{i=1}^{M} \frac{k_i^T}{s_i} \\
= \ & k_f^T (1 - T_1 s)
\end{aligned}
\tag{3.16}
$$

where k_e^T is the elastic Love number, k_i^T are the residues of each mode and s_i are the inverse relaxation times. The time constant T_1 is

$$
T_1 = \frac{1}{k_f^T} \sum_{i=1}^{M} \frac{k_i^T}{s_i^2}
\tag{3.17}
$$

This assumption, which is called the quasi-fluid approximation, is actually the first order approximation of the tidal Love number. It assumes that the relaxation time of every mode

is much shorter than the time span for long-term polar wander. With this approximation, the non-linear equation 3.1 can be simplified into a first order differential equation for $\omega(t)$ and solved numerically. We first validate the accuracy of our numerical method by calculating TPW for the two-layer Earth model (Table 3.1). This is because a two-layer Earth model, which is a visco-elastic layer over a fluid core, does not contain the relatively slow modes (M1 and M2 modes). So the quasi-fluid approximation is reliable in this case and the TPW calculated by the method in Ricard et al. (1993) can be expected to be accurate. The comparison of our numerical and the semi-analytical results for a two-layer model is shown in figure 3.8(a) . As we can see, the two methods have very good agreement. Except for the first few points, where the difference is due to the elastic response that is missing in Ricard et al's results, the differences are below 0.5%.

Then we use both methods to calculate TPW for the 6-layer SG6 model. This model approx-
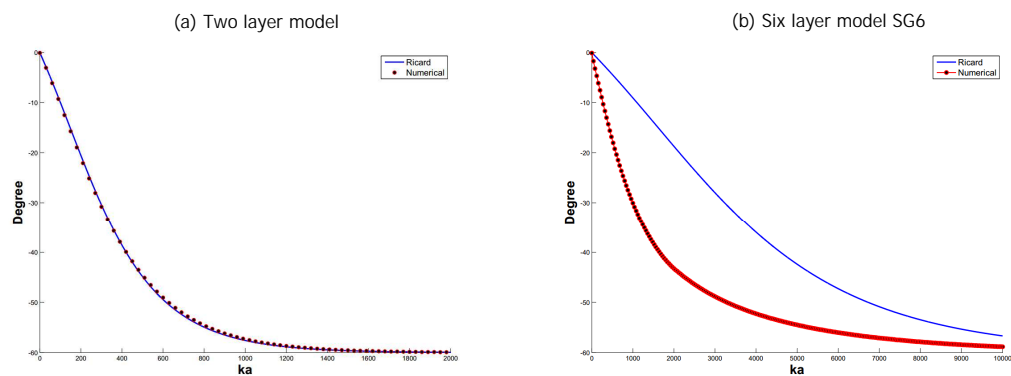
Figure 3.8: The polar wander in x-z plane of the two Earth models triggered by a point mass of 2×10^{19} kg placed at 30° colatitude in the x-z plane. Lines show the semi-analytical results from Ricard et al. (1993) and symbols represent our numerical results (only half of the data points for the two-layer model and 1/10 of the SG6 data points are shown in the figures).

imates the real Earth better and also contains the slow M1 and M2 modes, which allows us to test the quasi-fluid approximation. The results are shown in figure 3.8(b) . It is clear that for the SG6 model, the two methods show large differences and the polar wander given by Ricard et al. (1993) is much slower due to the lack of the relaxation from the M1 and M2 modes. To further validate our results and rule out the cause of numerical error, we also compare the semi-analytical results from both Wu and Peltier (1984) and Ricard et al. (1993) for short-angle changes. As shown in figure 2.3, we see again that in the two-layer model, despite the lack of the elastic response which gives the initial jump in Ricard et al's results, both results stay almost parallel. However, for the SG6 model, Ricard et al's results, which lacks the contribution from M1 and M2 modes, lags behind from the beginning.

After long enough time results from Ricard et al. (1993) will converge to the same end position as the numerical one, but the large difference in transient behaviour suggests that the quasi-fluid approximation is not a good choice for obtaining a time-dependent solution. The numerical method we developed in this section is very general since the only assumption we take is that the equatorial readjustment is fast enough that the equatorial bulge is

almost always perpendicular to the rotational axis. This means that the largest principle axis for the moment of inertia must nearly coincide with the rotational axis, so the inertia tensor in the coordinate system where the Z-axis is the direction of the rotation is close to a diagonal matrix. We can check if this condition is satisfied during the numerical calculation by comparing the diagonal elements in the inertial tensor with the non-diagonal ones: in the transformed coordinate system, the condition $\Delta I'_{ij}, i \neq j << \Delta I'_{ii}$ must be satisfied. Tests show that for TPW on two-layer Earth model with magnitudes of the mass anomalies below 2×10^{22} kg (this amount is about 100 times that of the ice sheets melted during the last deglaciation (Ricard et al., 1993)), this condition is satisfied. Only when the model is driven by an even larger mass anomaly, this condition fails by a significant amount and the linear and non-linear methods do not agree any more like in figure 3.8(a).

3.4. REORIENTATION OF A ROTATING TIDALLY DEFORMED VISCO-ELASTIC BODY

As mentioned in the introduction, Willemann (1984) and Matsuyama and Nimmo (2007) presented a solution which only calculates the final position of the reorientation. We are not aware of a general dynamic solution for the reorientation of a tidally deformed body. Two major difficulties prevent applying the existing rotation theory, linear or non-linear, to a tidally deformed body. First, the principle inertia moments A and B are not equal in this case. Secondly, it is difficult to combine the effects of the centrifugal and tidal potential so that the deformed body and load can achieve the minimal potential state throughout the reorientation process. In the previous section we have already solved the first problem by deriving a more general linearised form of the Liouville equation (equation 3.11). The main focus for the development of the method in this section is on how the tidal potential is treated and how the centrifugal and tidal potential can be combined.

When the reorientation of a tidally deformed body is studied, it is necessary that not only the rotational axis is considered but also the direction of the tidal axis which is the vector pointing to the central body. In this paper, we only consider the situation in which the rotational body is tidally locked in a circular orbit so the body is co-rotating with its central body and the direction of the tidal axis is always perpendicular to the rotational axis (the obliquity or axial tilt is zero).

For an incompressible model, the effective centrifugal potential is (Murray and Dermott, 2000)

$$\Phi_c = \frac{1}{3}\Omega^2 r^2 P_2^0(\cos\theta) \tag{3.18}$$

with θ being the colatitude and P_2^0 the associated Legendre function of degree 2, order 0. The tidal potential due to the central body at the same point can be written as (Murray and Dermott, 2000)

$$\Phi_t = -\frac{GM}{a^3} r^2 P_2^0(\cos\psi) \tag{3.19}$$

Here G, M and a are the gravitational constant, the mass of the central body and the radius of the orbit, respectively. ψ is the angle between the radius vector and the direction of the tidal bulge. Generally if we define the equivalent angular speed of the tidal potential as:

$$\Omega' = \sqrt{\frac{3GM}{a^3}} \tag{3.20}$$

then the form of the tidal potential becomes the same as the centrifugal potential except for the negative sign. When the rotational body is tidally locked in a circular orbit, then the rotational period is the same as the orbital period which is $T = 2\pi\sqrt{a^3/GM}$, from which it is easy to see that the magnitude of the tidal potential is always three times the magnitude of the centrifugal potential.

Because of the negative sign, the effect of applying a tidal potential to a certain object is the same as applying the centrifugal potential of the same magnitude but with opposite direction of the force. As a result, a positive mass anomaly driven by a centrifugal potential acts exactly like a negative mass anomaly driven by a tidal potential and vice versa. A centrifugal force always tries to relocate a positive mass anomaly to the equator and a negative mass anomaly to the poles to minimize the total potential, while a tidal potential tries to relocate the positive mass anomaly to the sub-host point (the closest point on the body to the central body) or its antipodal and a negative mass anomaly to the great circle which is perpendicular to the direction of the tidal bulge. In order to calculate the change of the inertia tensor due to both the rotational and tidal potential, in FEM we need to add the tidal force to the model and apply equation 3.4. If equation 3.2 is used instead of the FE model, then we need to add an extra term for the contribution of the tidal potential. Since the effect of the tidal potential is exactly the same as the centrifugal potential except the direction, similar to the rotational vector, we can define a tidal vector which describes the strength and direction of the tidal force as $\mathbf{X} = \Omega'(\omega'_1, \omega'_2, \omega'_3)^T$, where Ω' is equivalent angular speed and $(\omega_1, \omega_2, \omega_3)^T$ is a unit vector. We have the perturbed inertia tensor due to tidal potential as

$$\Delta I_{T\_ij}(t) = -\frac{k^T(t)a^5}{3G} * (\Omega'^2[\omega'_i(t)\omega'_j(t) - \frac{1}{3}\delta_{ij}]) \tag{3.21}$$

This term needs to be added to the right side of the equation 3.2. Notice the negative sign because in the case of the tidal potential, the direction of the force to the body is opposite to the centrifugal potential, so the perturbed inertia tensor is also negative.

In previous sections, the assumption was stated that the centrifugal potential is applied along the Z-axis. Since the centrifugal force flattens the body, we have $C > A, B$. On the other hand, if we treat the tidal potential in the same way and apply it along the Z-axis, the tidal force would elongate the body and we have $C < A, B$. For equation 3.11 to be valid, the conditions $C \neq A$ and $C \neq B$ are required. So we can use equation 3.11 to calculate the perturbation of both rotational and tidal axes. We define a moving bulge-fixed coordinate

system in which the Z-axis aligns with the direction of rotation and the X-axis with the tidal bulge, as shown in figure 3.9. In order to use equation 3.11, the direction of the tidal potential needs to be along the third axis of the coordinates (just as the rotation axis is along the Z-axis of (X, Y, Z) frame). So the "polar" wander of the tidal axis is calculated in the coordinate system (X', Y, Z') where X' and Z' align with the negative Z- and X- axes, see figure 3.9. The transformation matrix from (X, Y, Z) to (X', Y, Z') is written as

$$\mathbf{S} = \begin{pmatrix} 0 & 0 & -1 \\ 0 & 1 & 0 \\ 1 & 0 & 0 \end{pmatrix} \tag{3.22}$$

If the inertia tensor for both the triggering load and the deformation and its derivative are obtained in the (X, Y, Z) frame as $\Delta\mathbf{I}$ and $\Delta\dot{\mathbf{I}}$, these values are to be used to calculate the rotational axis change. Then the corresponding values for the tidal axis change are

$$\Delta\mathbf{I}_T = -\mathbf{S}^T\Delta\mathbf{I}\mathbf{S} \tag{3.23}$$

$$\Delta\dot{\mathbf{I}}_T = -\mathbf{S}^T\Delta\dot{\mathbf{I}}\mathbf{S} \tag{3.24}$$

$\Delta\mathbf{I}_T$ and $\Delta\dot{\mathbf{I}}_T$ are substituted into equation 3.11 to determine the local change of the tidal axis. When both the centrifugal and tidal potential are applied to the body perturbed by a
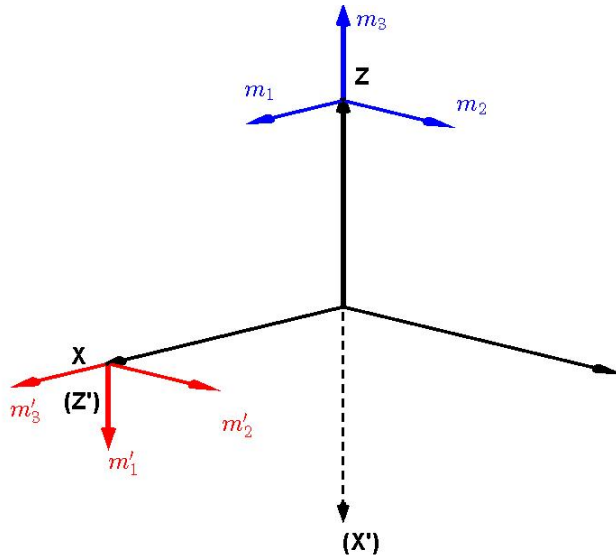
Figure 3.9: Bulge-fixed coordinate system where the X and Z axes are aligned with the direction of the tidal axis and the rotational axis respectively. m_1, m_2 and m_3 correspond to the perturbation of the rotational axis. m'_1, m'_2 and m'_3 correspond to the perturbation of the tidal axis.

certain load, as can be seen from figure 3.9, the centrifugal force tries to relocate the rotational axis from $\mathbf{Z} = (0, 0, \Omega)^T$ to

$$\mathbf{Z}' = \Omega(m_1, m_2, 1 + m_3)^T \tag{3.25}$$

and the tidal force tries to push the tidal axis from $\mathbf{X} = (\Omega', 0, 0)$ to

$$\mathbf{X}' = \Omega'(1 + m'_3, m'_2, -m'_1)^T \tag{3.26}$$

Here Ω' is the equivalent angular speed defined by equation 3.20. The problem here is that these two conditions can not be simultaneously satisfied since the new X- and Z-axes should also be perpendicular to each other because the feature of the tidal axis being orthogonal to the rotation axis does not change due to the reorientation. Considering that the X-Z plane is the one which constrains the directions of both rotational and tidal axes, this plane has to satisfy both conditions. So we have to make a compromise of the conditions: we let one of the axes, either X- or Z-, to be relocated at the exact desired location of equation 3.26 or 3.25 but the other one only lies within the new X-Z plane defined by vector $\mathbf{X}'$ and $\mathbf{Z}'$. Let $\bar{\mathbf{X}}'$ and $\bar{\mathbf{Z}}'$ be the normalised vectors of $\mathbf{X}'$ and $\mathbf{Z}'$, then we can calculate the new Y-axis which is perpendicular to the X-Z plane as

$$\bar{\mathbf{Y}}' = \bar{\mathbf{Z}}' \times \bar{\mathbf{X}}' \tag{3.27}$$

Here $\times$ is the cross product. If we put the X-axis at x, then the new Z-axis which lies in the $X - Z$ plane is determined as

$$\bar{\mathbf{Z}}'' = \bar{\mathbf{X}}' \times \bar{\mathbf{Y}}' \tag{3.28}$$

and the coordinate transformation matrix from the frame (X,Y,Z) to the frame (x_0, y_0, z_0') is given by

$$\mathbf{V} = [\bar{\mathbf{X}}', \bar{\mathbf{Y}}', \bar{\mathbf{Z}}''] \tag{3.29}$$

Physically, the relocation of X and Z axis minimizes the total potential of the body and the initial mass anomaly related to the tidal and centrifugal force respectively. Our method first achieves the minimization of the potential corresponding to one of the forces, then the other. When the relocation of X-axis converges, then the change of the X-axis becomes nearly 0, namely $\bar{\mathbf{X}}' \approx (1,0,0)$. As a result, from equation 3.28 and 3.29, we have $\bar{\mathbf{Z}}'' \approx \bar{\mathbf{Z}}'$. So eventually, the minimal potential state associated with both the centrifugal and tidal force is found. This is similar to multiple-objective optimization (Miettinen, 1999). Of course we can also first put the Z-axis at $\mathbf{Z}'$ and then we calculate the new X-axis as $\bar{\mathbf{X}}'' = \bar{\mathbf{Y}}' \times \bar{\mathbf{Z}}'$ and obtain the coordinate transform matrix $\mathbf{V} = [\bar{\mathbf{X}}'', \bar{\mathbf{Y}}', \bar{\mathbf{Z}}']$. Tests show that in either way, the results converge to the same final position of both rotational and tidal axes in each step.

For a tidally deformed body triggered by a certain mass anomaly which corresponds to inertia tensor $\Delta \mathbf{I}_L$, the complete algorithm for calculating the reorientation is given as follows:

Algorithm 3

1. Assume that the step i, from time t_i to t_{i+1}, starts with the direction of the rotational axis given by $\boldsymbol{\omega_r^i} = \Omega_r^i (\omega_1^i, \omega_2^i, \omega_3^i)^T$ and the direction of the tidal axis by $\boldsymbol{\omega_t^i} = \Omega_t^i (\omega_4^i, \omega_5^i, \omega_6^i)^T$ in which $(\omega_1^i, \omega_2^i, \omega_3^i)^T$ and $(\omega_4^i, \omega_5^i, \omega_6^i)^T$ are unit column vectors which satisfy $\omega_1^i \omega_4^i + \omega_2^i \omega_5^i + \omega_3^i \omega_6^i = 0$. Ω_t^i is the equivalent angular speed of the tidal potential calculated from equation 3.20. For the first iteration, we assume that the rotation and tidal axes in this step do not change: $\boldsymbol{\omega_r^{i+1}} = \boldsymbol{\omega_r^i}$ and $\boldsymbol{\omega_t^{i+1}} = \boldsymbol{\omega_t^i}$.

2. Apply both the centrifugal and tidal potential to the model in the same way as stated in step 2 in Algorithm 1 to either FE model (equation 3.4) or use equation 3.2 and add the term from equation 3.21. Obtain the total change in the inertia tensor and its derivative as $\Delta \mathbf{I}$ and $\Delta \dot{\mathbf{I}}$. The coordinate transformation matrix from the body-fixed to the bulge-fixed coordinate system is given by

$$\mathbf{U} = [\boldsymbol{\omega}_t^{i+1}, \boldsymbol{\omega}_r^{i+1} \times \boldsymbol{\omega}_t^{i+1}, \boldsymbol{\omega}_r^{i+1}] \tag{3.30}$$

The local values of the inertia tensor for the centrifugal part are obtained by $\Delta \mathbf{I}_1 = \mathbf{U}^T \Delta \mathbf{I} \mathbf{U}$ and $\Delta \dot{\mathbf{I}}_1 = \mathbf{U}^T \Delta \dot{\mathbf{I}} \mathbf{U}$. The corresponding inertia tensors for calculating tidal perturbation are $\Delta \mathbf{I}_2 = -\mathbf{S}^T \Delta \mathbf{I}_1 \mathbf{S}$ and $\Delta \dot{\mathbf{I}}_2 = -\mathbf{S}^T \Delta \dot{\mathbf{I}}_1 \mathbf{S}$

3. Apply equation 3.11 to $\Delta \mathbf{I}_1$ and $\Delta \dot{\mathbf{I}}_1$ and obtain the perturbation for the rotational axis as $\Omega_1(m_1, m_2, m_3)$. Apply equation 3.11 to $\Delta \mathbf{I}_2$ and $\Delta \dot{\mathbf{I}}_2$ and obtain the perturbation for the tidal axis as $\Omega_2(m_1', m_2', m_3')$. Then we have the perturbed Z- and X-axis as $\mathbf{Z}' = \Omega_1(m_1, m_2, 1 + m_3)^T$ and $\mathbf{X}' = \Omega_2(1 + m_3', m_2', -m_1')^T$. We normalize these vectors as $\mathbf{Z}' = \Omega_r^{i+1} \bar{\mathbf{Z}}'$ and $\mathbf{X}' = \Omega_t^{i+1} \bar{\mathbf{X}}'$. The local coordinate transformation matrix from the bulge-fixed frame at time t_i to the new frame at time t_{i+1} is obtained as $\mathbf{V} = [\bar{\mathbf{X}}', \bar{\mathbf{Z}}' \times \bar{\mathbf{X}}', \bar{\mathbf{X}}' \times (\bar{\mathbf{Z}}' \times \bar{\mathbf{X}}')]$. The updated direction of the rotational and tidal axes in the original body-fixed coordinates are obtained as

$$\boldsymbol{\omega}_r^{i+1} = \Omega_r^{i+1} \mathbf{U} \mathbf{V}[0, 0, 1]^T \tag{3.31a}$$
$$\boldsymbol{\omega}_t^{i+1} = \Omega_t^{i+1} \mathbf{U} \mathbf{V}[1, 0, 0]^T \tag{3.31b}$$

4. Substitute $\boldsymbol{\omega}_r^{i+1}$ and $\boldsymbol{\omega}_t^{i+1}$ in step 2 until the results converge.

In order to show how the reorientation of a tidally deformed rotating body is accomplished, we choose a model of Triton, the largest moon of Neptune. Triton is an icy moon and tidally locked. It has zero obliquity and small orbital eccentricity which is about 1.6×10^{-5} and can be ignored, so it fits the situation of our assumption. The interior structure is chosen according to the empirical model presented in Spohn et al. (2014) which fits observations of Triton's mass and moment of inertia. Depending on the amount of internal heating, there can be an ocean between the high pressure and low pressure ice (Spohn et al., 2014). For simplicity, the effect of a possible ocean is ignored. The physical properties of the model are shown in Table 5.1.

Table 3.3: Properties of Triton

Layer	Outer Radius (km)	Density (kg m^{-3})	Shear Modulus (Pa)	Viscosity (Pa s)
Ice I	1352	937	3.6×10^9	1×10^{21}
Ice II	1100	1193	6.2×10^9	1×10^{21}
Mantle	950	3500	65×10^9	1×10^{19}
Core	600	5844.8	0	0

To trigger the reorientation, a surface mass anomaly with a magnitude of 3.6×10^{17} kg, either positive of negative, is chosen. This amount is approximately the accumulation of nitrogen

snow during 10,000 years which is sublimated from the equatorial area, then moves to the polar areas where it is deposited (Rubincam, 2003). We simulate the polar wander of Triton for two cases: 1. a positive mass anomaly at high latitude (20 degree colatitude). 2. a negative mass anomaly at low latitude (60 degree colatitude). In each case, the mass anomaly is placed at three different longitudes: -15, -45 and -75 degree. Due to the symmetry, only situations in one quadrant are considered. The initial loading time T_0 and the time span for the TPW are both chosen to be 4 million years at which, from normal mode method, the time history of the tidal Love number reaches about 99.75% of its fluid Love number, following equation 3.12. With this range of time, the reorientation should be close to its equilibrium position. In order to better describe the three types of the reorientation as shown in figure 1.10, in the bulge-fixed frame we define the reorientation of the tidal deformed rotating body around the Z, X and Y axes as the Z-reorientation, X-reorientation and Y-reorientation respectively. The results for the cases of positive mass anomalies are shown in figure 3.10 and 3.11.

Figure 3.10: Reorientation caused by positive mass anomalies placed at 20 degree colatitude, -15, -45 and -75 longitudes. Figure (a) shows the traces (lines) of the positive mass anomalies (filled circles) in the bulge-fixed frame where the sub-Neptune point is at 0 degree longitude. Figure (b) shows the traces of the north pole of Triton (lines) and sub-Neptune point (dashed lines) in the body-fixed frame.

Figure 3.10(a) gives the paths of the mass anomalies in the bulge-fixed coordinates. We can see that when the positive mass anomaly is placed at high colatitude, the reorientation first pushes the mass anomalies towards the equator with an X-reorientation. When the mass anomaly is close to the equator, a Z-reorientation follows and eventually the mass anomaly tries to reach the sub-Neptune point. Due to the Z-reorientation, in the body-fixed coordinates as shown in figure 3.10(b), the pole does not drift away from the mass anomalies in a straight line; instead it moves closely along the great circle which is perpendicular to the tidal axis. This is different compared to the case of polar wander on a centrifugally deformed body such as Earth. From figure 3.11(a) and 3.11(b), by comparing the speed of the pole in colatitude direction and that of the sub-host point in longitudinal direction, we can see that the X-reorientation is much faster than the Z-reorientation. This indicates that it is much easier to reorient the tidal bulge around the tidal axis than the rotational axis. So the direction of the polar wander due to unbalanced ice-caps on Triton is more likely to go around the tidal axis instead of going towards it. As a result, the suggestion that the direction of the

Figure 3.11: Reorientation caused by positive mass anomalies placed at 20 degree colatitude, -15, -45 and -75 degree longitudes. Figure (a) shows the time history for the colatitudes (solid lines) and longitudes (dashed lines) of the north pole. Figure (b) shows the time history for the colatitudes (solid lines) and longitudes (dashed lines) of the sub-Neptune point.

polar wander for the visco-elastic case of Triton would be towards the sub-Neptune point when the reorientation starts (Rubincam, 2003), does not seem to be correct.
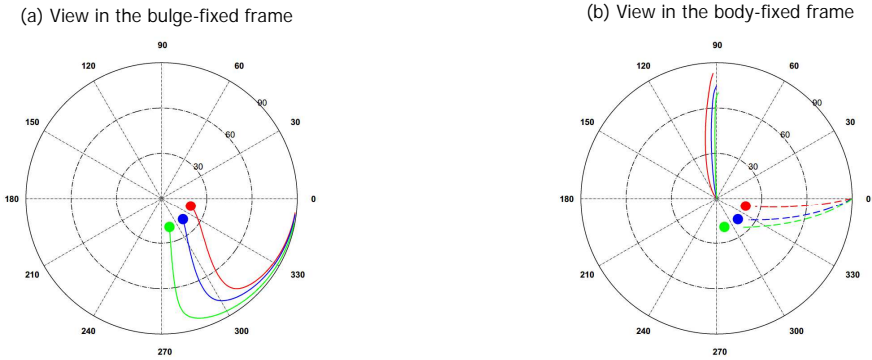

Figure 3.12: Reorientation cased by negative mass anomalies placed at 60 degree colatitude, -15, -45 and -75 longitudes. Figure (a) shows the traces (lines) of the negative mass anomalies (filled circles) in the bulge-fixed frame where the sub-Neptune point is at 0 degree longitude. Figure (b) shows the traces of the north pole (lines) in the body-fixed frame.

Cases of negative anomalies are shown in figure 3.12 and 3.13. These cases apply to situations like the south polar terrain of Enceladus, in which (Nimmo and Pappalardo, 2006) suggests that the diapirism of the lower-density material creates a negative mass anomaly which is relocated to the south pole due to the reorientation of Enceladus. In contrast with the case of positive mass anomaly, we see in figure 3.12(a) that the reorientation has a slight preference to first push the mass anomaly to the great circle where both tidal and rotational axes are located or to the 0 and 180 longitude circle. This indicates that the Z-reorientation is slightly faster than the Y-reorientation, so the direction of both rotational and tidal axes are still not directly targeting their end positions. Figure 3.13(a) and 3.13(b) shows that, except for the case where the negative mass anomaly is close to the ±90 longitude (case with
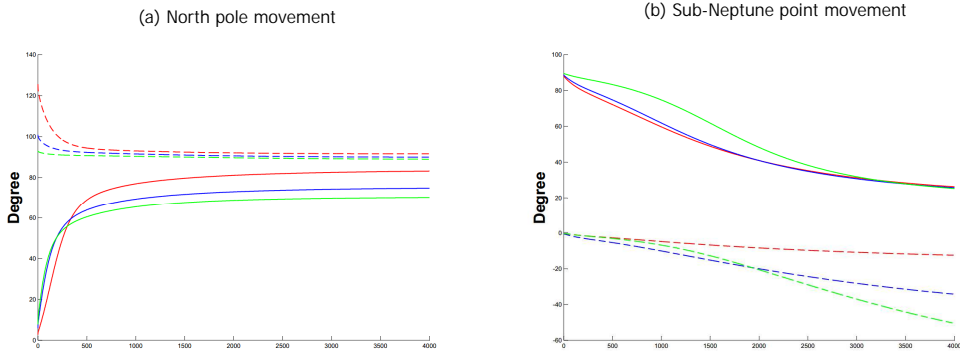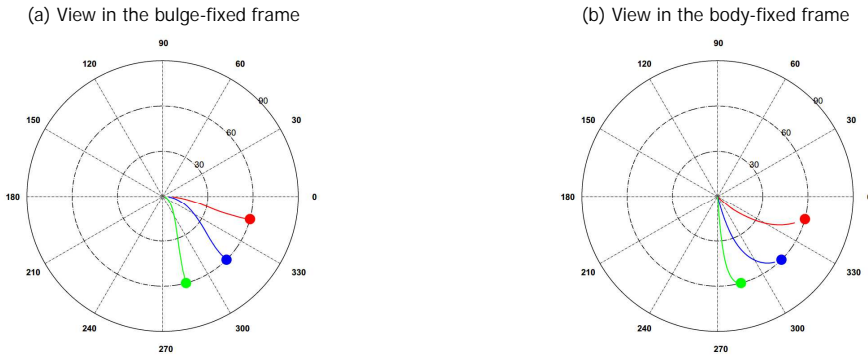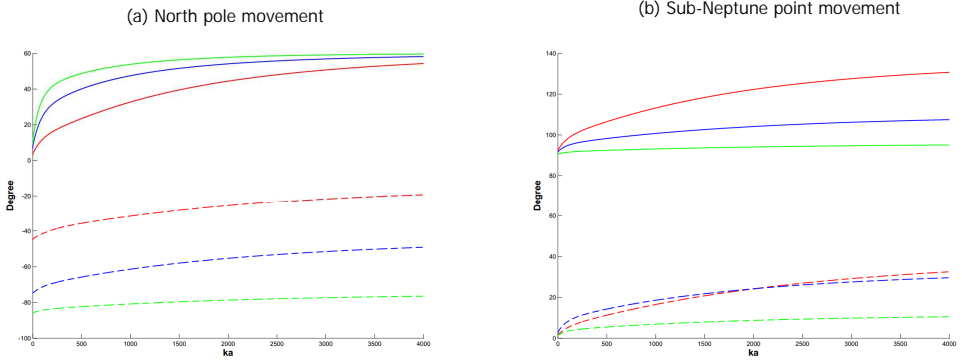
Figure 3.13: Reorientation cased by negative mass anomalies placed at 60 degree colatitude, -15, -45 and -75 degree longitudes. Figure (a) shows the time history for the colatitudes (solid lines) and longitudes (dashed lines) of the north pole and figure (b) shows the time history for the colatitudes (solid lines) and longitudes (dashed lines) of the sub-Neptune point.

the green color), there is no drastic speed change. This is quite different compared to cases with positive anomalies which always begin with a relatively fast X-reorientation.

From both cases of positive and negative anomalies, we see that for a tidally deformed rotating body, the X-reorientation is much faster than the Z-reorientation while the Z-reorientation is slightly faster than the Y-reorientation. Such preference for the direction of the reorientation can be explained in the following way. Since the tidal potential is larger than the centrifugal potential, diagonal elements of the inertia tensor in the bulge-fixed frame satisfies $A < B < C$ and $C - B < B - A$. The rotation of the same small angle around X-,Y- and Z-axes changes the diagonal inertia tensor $\mathbf{I}$ into $\mathbf{Q}_i^T \mathbf{I} \mathbf{Q}_i$, where $\mathbf{Q}_i$, i=1,2,3, are the transformation matrices for rotations around X-, Y- and Z-axes. These transformations produce non-diagonal elements with magnitude $\Delta I_{23}, \Delta I_{13}$ and ΔI_{12} respectively and it is easy to prove that they have the relation: $\Delta I_{23} < \Delta I_{12} < \Delta I_{13}$. These cross products represent the resistance of the bulge, either rotational or tidal, against the polar (tidal) wander, so the reorientation around the X-axis is the fastest while that around the Y-axis is the slowest. From the track of both positive and negative mass anomaly in various positions shown in figure 3.10 and 3.12, we can also conclude that except for the six dead zones where both centrifugal and tidal force are either very small or in equilibrium (the areas around the poles, the sub-host point and its antipode and the two points facing the orbit), positive mass anomalies are more likely to be found around the equator and the great circle perpendicular to the tidal axis while negative mass anomalies tend to be around the 0 and 180 degree longitude great circle in the bulge-fixed frame.

It is also worth to mention that our method can be extended to situations where the obliquity or orbit eccentricity is non-zero. In these cases, we need to change the transformation matrix $\mathbf{S}$ given by equation 3.22, which would become time-dependent and needs to be updated according to the position of the body in the orbit and the relative location of the rotational and tidal axes in each step of the numerical calculation.

3.5. CONCLUSIONS

Numerical methods for calculating both small and large angle reorientation of a centrifugally and tidally deformed visco-elastic body are established. The methods are validated by comparing with existing normal-mode methods which were developed for both small-angle and large-angle TPW. With the help of the developed numerical methods, the following conclusions can be drawn:

- Linear rotation theory leads to a bias which can be very large when the initial position of the mass anomaly causing the true polar wander (TPW) is close to the poles or equator. This significantly limits the applicable range of the linear method if loads are close to poles or equator.

- The time-dependent result of TPW obtained by taking the first order approximation of the tidal love number, namely the quasi-fluid approximation, gives large errors for the transient behaviour and only when the model is close to its final orientation, results taking quasi-fluid approximation give reliable prediction. This makes quasi-fluid approximation not a good choice for studying transient visco-elastic readjustment of Earth or other planets which contain significant slow relaxation modes.

- A tidally deformed body has a preference of the reorientation around the tidal axis over that around the rotational axis. Rotational axis driven by a positive mass anomaly near the poles tends to first rotate around the tidal axis instead of towards it. For tidally locked bodies which do not have a remnant bulge, positive mass anomalies are more likely to be found around the equator and the great circle perpendicular to the tidal axis, while negative mass anomalies tend to be around the great circle that contains the tidal and rotational axes.

APPENDIX I

Since the results from the FEM are validated by comparing with the analytical results obtained from a normal mode method which is based on Maxwell rheology, the material properties need to be defined in FEM such that the visco-elastic response of the material is equivalent to that of a Maxwell material. In the ABAQUS FEM package, the visco-elastic property of the material is defined in the following way: (1) the initial elasticity is defined separately by giving the Young's modulus in the option "Elasticity". (2) the normalized visco-elastic behaviour can be defined either with the "Creep" option which uses power law strain-hardening or a "Viscoelastic" option which uses the Prony series which is a general scheme that encompasses a simple Maxwell rheology. In Abaqus, Prony series expansion is defined by the dimensionless relaxation modulus g_R as:

$$g_R(t) = 1 - \sum_{i=1}^{N} g_i^P (1 - e^{-t/\tau_i^G}) \tag{3.32}$$

where N, g_i^P and τ_i^G are material constants. As the equivalence of Maxwell rheology, we have $N = 1$, $g_1^P = 1 - 1^{-10}$ (Abaqus requires that $g_i^P < 1$, so a value very close to 1 is chosen)

and $\tau_1^G = \mu/E$ where μ and E are material viscosity and elasticity.

Both options give similar results with the same accuracy for the time history of the tidal Love number or the individual components of the inertia tensor (figure 3.2). However, when the terms which determine the TPW (like in figure 3.3) are calculated, which are the combinations of the components of the inertia tensor, the results obtained with the "Creep" option, as can be seen in figure 3.14, show a much larger error compared to those obtained with the option "Viscoelastic" as shown in figure 3.3. This demonstrates that the "Viscoelastic" option in Abaqus is a better choice to represent a Maxwell material. This suggests that also comparisons between results from ABAQUS and spectral models (Wu and van der Wal, 2003; van der Wal et al., 2015) might be improved.
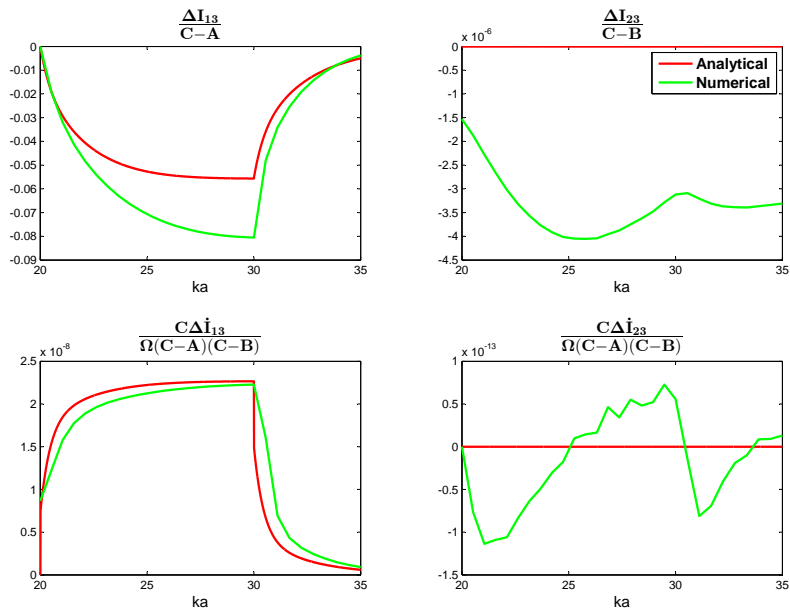
Figure 3.14: Result of the same test as that in figure 3.3 with the viscous deformation being defined with the option "Creep" in Abaqus.

4

PAPER 2: A FULL-MAXWELL APPROACH FOR LARGE ANGLE POLAR WANDER OF VISCOELASTIC BODIES

H.Hu,[1] W. van der Wal[1], L.L.A.Vermeersen[1]

For large-angle long-term true polar wander (TPW) there are currently two types of non-linear methods which give approximated solutions: those assuming that the rotational axis coincides with the axis of maximum moment of inertia (MoI), e.g. Nakada (2007), which simplifies the Liouville equation and those based on the quasi-fluid approximation (e.g. Ricard et al. (1993)) which approximates the Love number. Recent studies show that both can have a significant bias for certain models (Cambiotti et al., 2011; Hu et al., 2017b). Therefore, we still lack an (semi-)analytical method which can give exact solutions for large-angle TPW for a model based on Maxwell rheology. This paper provides a method which analytically solves the moment of inertia equation and adopts an extended iterative procedure introduced in Hu et al. (2017b) to obtain a time-dependent solution. The new method can be used to simulate the effect of a remnant bulge or models in different hydrostatic states. We show the effect of the viscosity of the lithosphere on long-term, large-angle TPW. We also simulate models without hydrostatic equilibrium and show that the choice of the initial stress-free shape for the elastic (or highly-viscous) lithosphere of a given model is as important as its thickness for obtaining a correct TPW behaviour. The initial shape of the lithosphere can be an alternative explanation to mantle convection for the difference between the observed and model predicted flattening. Finally, it is concluded that, based on the quasi-fluid approximation, TPW speed on Earth and Mars is underestimated while the speed of the rotational axis approaching the end

---

[1] Delft University of Technology

position on Venus is overestimated.

4.1. INTRODUCTION

Concerning the study of large angle true polar wander (TPW) on a visco-elastic body such as terrestrial planets like the Earth, Mars and Venus, there are currently two types of non-linear approaches to obtain a time-dependent solution. One of them is from Nakada (2007) which applies an iterative scheme but simplifies the Liouville equation by ignoring the time derivative of the MoI term. This approximation is equivalent to assuming that the rotation axis coincides with the axis of the maximum moment of inertia during the process of TPW. The validity of this assumption was discussed in detail in Cambiotti et al. (2011) who showed that even for the Earth this assumption is not always appropriate. Another approach which is more commonly applied in recent studies was formulated originally by Sabadini and Peltier (1981) and further developed by Sabadini et al. (1982), Spada et al. (1992a) and Ricard et al. (1993) which is based on the quasi-fluid approximation. Mathematically, this approximation is the first order Taylor expansion of the Love number in the Laplace domain. The consequence of adopting the quasi-fluid approximation is that the elastic response of a Maxwell model is missing, and it also simplifies the individual viscous relaxation of different modes. Hu et al. (2017b) tested the validity of the quasi-fluid approximation and showed that it can lead to a large error in the transient behavior of TPW for a model whose strong modes have very different relaxation times. This could lead to erroneous conclusions when the model predicted TPW speed is compared with the speed that is observed or inferred from surface features (e.g. on Mars (Bouley et al., 2016)). The method developed by Hu et al. (2017b) is a numerical approach which requires that the change in the inertia tensor is calculated either by convolution or by a finite-element package. Both the numerical convolution and the finite-element package are not suitable for studies of models containing layers with very different viscosities since the large contrast in viscosity results in a large increase in computational time for numerical methods. The increase in the computational time is caused by the fact that the total integration time has to be long to account for the long relaxation time while the integration step-size must be small to accurately simulate the layers with short relaxation time.

Another issue which is intensively studied in recent years is the effect of an elastic or highly viscous layer on TPW (Willemann, 1984; Mitrovica et al., 2005; Cambiotti et al., 2010; Harada, 2012; Chan et al., 2014; Harada and Xiao, 2015; Moore et al., 2017). The existence of such a layer can create a delayed readjustment of the equatorial bulge (often called remnant bulge) which significantly changes the behavior of TPW as discussed by Willemann (1984) and Mitrovica et al. (2005). Mitrovica et al. (2005) show the importance of a correct choice for the initial hydrostatic state when the TPW is estimated. They used the fluid tidal Love number which corresponds to the observed flattening instead of the model predicted flattening. Recent studies often assume that this extra flattening comes from mantle convection (Mitrovica et al., 2005; Cambiotti et al., 2010). Alternatively, if we do not assume that the model is in hydrostatic equilibrium, this difference can also come from the elastic lithosphere which has its background shape corresponding to a faster rotational speed. As far as we know, this issue has not been discussed yet. Recent studies concerning the time-dependent solution of long-term large-angle TPW with an elastic or highly viscous lithosphere (Harada, 2012; Chan et al., 2014; Moore et al., 2017) are all based on the method developed by Ricard et al. (1993) and adopt the quasi-fluid approximation.

Compared with the linear approach (e.g. Wu and Peltier (1984)), which can only simulate TPW for small-angle changes, the method from Ricard et al. (1993) enables the study of

issues such as the coupling of the rotational perturbation in the X and Y directions. This means that in the body-fixed frame, a mass distribution imbalance in the X-Z plane would cause a rotational perturbation not only in the X-Z plane but also in the Y-Z plane. This coupling effect increases as the rotational speed of the object decreases and can turn TPW into a mega-wobble for some objects like Venus which rotates very slowly (Spada et al., 1996). The phenomenon of the mega-wobble is caused by the increase of the contribution from the mass anomaly itself compared to that of the equatorial bulge readjustment. When the contribution from the equatorial bulge readjustment is dominant, the periodic behaviour, often called Chandler wobble, damps out quickly and its secular effect on the long-term TPW can be ignored. However, when the rotational speed decreases which causes the equatorial bulge to decrease, the change in the inertia tensor becomes dominated by the mass anomaly itself. As a result, the rotational behaviour resembles the free nutation of a rigid body (Lambeck, 2005). This coupling effect, or periodic behaviour, is almost always neglected in the linear scheme for the study of the Earth (e.g. Wu and Peltier, 1984; Cambiotti et al., 2010).

To conclude, a semi-analytical approach which can accurately calculate TPW of a Maxwell model in different hydrostatic states is missing. It is the main purpose of this paper to develop such a method and show how more accurate solutions are obtained. We also show if the difference in results between the methods has a significant impact on planetary studies (e.g. observation, modelling) in the following cases:

- TPW for slowly rotating objects: mega-wobble of Venus.

- Effect of a remnant bulge caused by an elastic or highly viscous lithosphere on large-angle TPW.

- TPW on a body that is not in hydrostatic equilibrium.

In section 4.2, the influence of the quasi-fluid approximation is discussed in more detail and our new method will be presented. Sections 4.3, 4.4 and 4.5 will cover the above listed issues. Section 3 and 4 contain a case study of Venus and Mars, respectively, which compares the results obtained in previous studies and that from our new method.

4.2. METHOD

The governing equation for the rotation of a rigid body in the body-fixed rotating reference frame is the well-known Euler's equation. As the body becomes deformable, it is often referred to as the Liouville equation. For a torque-free case, it reads (Sabadini et al., 2016)

$$\frac{d}{dt}(\mathbf{I} \cdot \boldsymbol{\omega}) + \boldsymbol{\omega} \times \mathbf{I} \cdot \boldsymbol{\omega} = 0 \tag{4.1}$$

where $\mathbf{I}$ is the inertia tensor and $\boldsymbol{\omega}$ is the rotational vector whose magnitude is the rotating speed. Both values are defined in a body-fixed coordinate system. When the moment

of inertia of the body is perturbed by a geophysical process which causes mass redistribution, the rotational axis shifts, and consequently the equatorial bulge readjusts. Analytically, given a rotational vector as $\boldsymbol{\omega} = (\omega_1, \omega_2, \omega_3)^T = \Omega(\bar{\omega}_1, \bar{\omega}_2, \bar{\omega}_3)^T$, where Ω is the angular speed of the rotation and $(\bar{\omega}_1, \bar{\omega}_2, \bar{\omega}_3)^T$ is a unit vector which represents the direction of the rotation, the total moment of inertia attributable to such a process is given by (Ricard et al., 1993)

$$
\begin{aligned}
I_{i,j}(t) = I\delta_{ij} + \frac{k^T(t)a^5}{3G} &* [\omega_i(t)\omega_j(t) - \frac{1}{3}\Omega(t)^2\delta_{ij}] \\
&+ [\delta(t) + k^L(t)] * C_{i,j}(t)
\end{aligned}
\tag{4.2}
$$

where I is the principle moment of inertia of the spherical body in hydrostatic equilibrium, G is the gravitational constant and a is the radius of the planet. $k^T(t)$ and $k^L(t)$ are the degree 2 potential tidal Love number and load Love number, respectively. Love numbers are obtained by the normal mode method and based on the Maxwell rheology (Farrell, 1972). The $*$ denotes convolution in the time-domain. $C_{i,j}$ represents the change in the moments and products of inertia without considering the deformation and this is the triggering load for the TPW. The most difficult part of solving equations 3.1 and 4.2 is the convolution of the tidal Love number and the centrifugal potential, in particular the part $k^T(t) * \omega_i(t)\omega_j(t)$. In the following subsection, we first show how this problem is tackled by adopting the quasi-fluid approximation and the influence of this approximation on calculation of the inertia tensor. Following this subsection a new approach is presented to calculate the MoI equation analytically. Section 4.3 demonstrates how to use the developed algorithm and provides initial results from our method.

4.2.1. CONVENTIONAL APPROACH BASED ON THE QUASI-FLUID APPROXIMATION

The tidal Love number in the Laplace domain for a given harmonic degree is expressed as (Peltier, 1974):

$$
k^T(s) = k^T_e + \sum_{i=1}^{m} \frac{k^T_i}{s - s_i}
\tag{4.3}
$$

where k^T_e is the elastic Love number, k^T_i are the residues of each mode, and s_i are the inverse relaxation times. This form of the Love number contains all the information about how a multi-layered Maxwell body deforms: an instantaneous elastic response characterized by k^T_e followed by viscous relaxation of separate modes characterized by their different inverse relaxation time s_i and mode strength $-k_i/s_i$. We call this form of the Love number the full-Maxwell rheology scheme, as opposed to the quasi-fluid approximation introduced below.

In order to solve equation 4.2, Ricard et al. (1993) took the quasi-fluid approximation which approximates the tidal Love number with its first order Taylor expansion:

$$
\begin{aligned}
k^T(s) &\approx k_e^T - \sum_{i=1}^{m} \left(\frac{k_i^T}{s_i} + \frac{k_i^T s}{s_i^2} \right) \\
&= k_f^T(1 - T_1 s)
\end{aligned}
\tag{4.4}
$$

where k_f^T is the fluid Love number which is the sum of the mode strength:

$$
k_f^T = k_e - \sum_{i=1}^{m} \frac{k_i^T}{s_i}
\tag{4.5}
$$

The time constant T_1 is

$$
T_1 = \frac{1}{k_f^T} \sum_{i=1}^{m} \frac{k_i^T}{s_i^2}
\tag{4.6}
$$

Thus, by taking the quasi-fluid approximation, all information for a viscoelastic layered model is combined into one constant T_1. Because of the k_i/s_i^2 term, this constant is dominated by the slowest modes. Thus applying the quasi-fluid approximation on a physical model which contains modes with both very long and short relaxation times will result in a large bias. It can also be seen that with this approximation, the elastic response as well as the viscous relaxation characterized by the function $1/(s - s_i)$ in the Laplace domain ($e^{s_i t}$ in the time domain) are missing (as will be shown in equation 4.7), therefore, the ongoing deformation does not agree with the complete Maxwell rheology scheme. The convolution of equation 4.4 with a linear load function $F(t) = a + bt$, where a, b are constants, results in a time domain response of the form:

$$
R(t) = k_f^T F(t) - F'(t) k_f^T T_1
\tag{4.7}
$$

where the derivative $F'(t) = b$ and $R(t)$ is the response function. This response demonstrates the effect of the quasi-fluid approximation: for a near constant load ($F'(t) \approx 0$), the response reaches its fluid-limit $k_f^T F(t)$ immediately without the time-dependent viscous behaviour. This means that when the speed of TPW is very slow compared to the characteristic relaxation speed of the body, the results based on the quasi-fluid approximation approach those which are obtained from the fluid-limit method which diagonalizes equation 4.2, such as in (Matsuyama and Nimmo, 2007). For other loads which change linearly in time, the instantaneous fluid-limit response $k_f^T F(t)$ is shifted by a value which is proportional to the speed of the change of the load, as given by the second term of the equation 4.7.

For the complete Maxwell rheology scheme, the original form of the Love number (equation 4.3) needs to be convoluted with the loading function, resulting in damping of this part with a function of e^{-At} where A is a positive constant. As a result, compared to the original Maxwell rheology, the response of a Heaviside or fast changing load based on the quasi-fluid approximation will likely result in a very different TPW path. For example, the change in the inertia tensor due to an impact crater which appears instantly and is preserved afterwards is a Heaviside load to the planet.

Next, we quantitatively show that adopting quasi-fluid approximation can either underestimate or overestimate the equatorial readjustment for certain components of the inertia tensor in the normal polar wander case and in the mega-wobble case. Substituting equation 4.4 into 4.2 gives the change in the moment of inertia as (Ricard et al., 1993)

$$\Delta I_{i,j}(t) = \frac{k_f^T a^5}{3G} [\omega_i(t)\omega_j(t) - \frac{1}{3}\Omega(t)^2\delta_{ij}]$$
$$- \frac{k_f^T a^5}{3G} T_1 [\dot{\omega}_i(t)\omega_j(t) + \omega_i(t)\dot{\omega}_j(t) - \frac{2}{3}\omega_l(t)\omega_l(t)\delta_{ij}] + E_{ij} \tag{4.8}$$

where $E_{i,j}(t)$ and $\dot{E}_{i,j}(t)$ are obtained by convolving $C_{i,j}(t)$ and $\dot{C}_{i,j}(t)$ with $\delta_{i,j} + k^L(t)$. We compare the change in the moment of inertia calculated by equation 4.8 and equation 4.2 to show the influence of adopting the quasi-fluid approximation. The latter is obtained by numerical calculation of the convolution. As a representative of terrestrial planets, we use a SG6 Earth model (which represents a multi-layered model with interior density, rigidity and viscosity change) and let the rotational axis move in two ways:

- The rotational axis drifts with a constant speed along the X-Z plane in the body-fixed coordinates for 90 degrees. This is to simulate the normal polar wander case for fast-rotating planets such as the Earth and Mars.

- The rotational axis initially stays at 30 degree colatitude and 0 degree longitude in the X-Z plane and moves longitudinally with a constant speed along the 30 degree colatitude circle for 720 degrees. This is to simulate the mega wobble for very slowly rotating objects such as Venus.

In the first case, the drift speed of the rotational axis is chosen to be fast enough to view the effect of the quasi-fluid approximation. We define a bulge-fixed frame whose Z'-axis coincides with the instantaneous rotational axis and whose X'-axis lies within the Z-Z' plane as shown in figure 4.1. So a pure rotation (around Y'-axis) can transform the body-fixed frame into the bulge-fixed frame.

Figure 4.2 gives the change in the six components of the MoI tensor in the bulge-fixed frame. In this figure, the differences in I_{11}, I_{22}, I_{33} are small, but the most important component I_{13} calculated with the quasi-fluid approximation is significantly larger than the accurate value. The magnitude of I_{13} in the bulge-fixed frame determines how fast the equatorial bulge readjusts. A larger value of I_{13} suggests a slower readjustment (if the readjustment is complete, then the rotational axis coincides with the new principle axis and I_{13} would be zero). So adopting the quasi-fluid approximation in the normal polar case causes an large underestimation for the speed of the equatorial bulge readjustment.
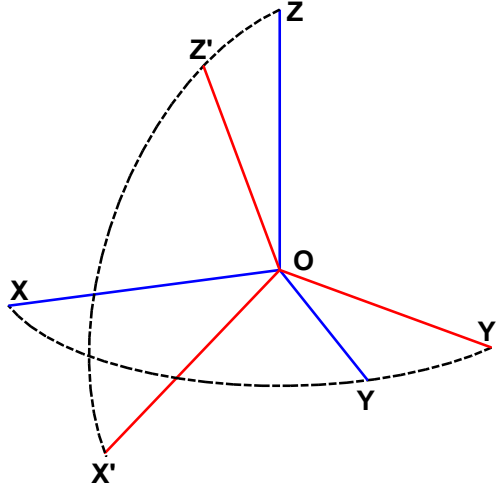
Figure 4.1: O-XYZ is the body-fixed frame where the Z-axis is the original rotational axis. O-X'Y'Z' is the bulge fixed frame where the Z'-axis is the instantaneous rotational axis and the X'-axis lies within the Z-Z' plane.

For the second case where the rotational axis tends to wobble around a fixed point, in the bulge-fixed frame, I_{23} implies the readjustment in the direction along the track of the rotational axis (called along track direction in the following) and I_{13} gives the readjustment in the direction which is perpendicular to the plane that contains the along track direction and the rotational axis (called normal direction in the following). The results are shown in figure 4.3. For components I_{11}, I_{22}, I_{33}, the quasi-fluid approximation misses the small oscillations but the differences are still very small between the two methods, thus for these three components the error introduced by the approximation can be ignored. However, the magnitude of the along-track component I_{23}, is largely underestimated just like the I_{13} component in figure 4.2 (I_{13} is the along-track component for the normal polar wander case). On the other hand, the normal directional component I_{13} in figure 4.3 is underestimated by the quasi-fluid approximation which suggests an overestimation of the equatorial bulge readjustment in this direction.

The key information obtained in this subsection is that by adopting the quasi-fluid approximation, the speed for equatorial readjustment can be, depending on the model and load, largely underestimated in the along-track direction but overestimated for the mega wobble case in the normal direction. These are the main reasons for the difference of the TPW path calculated by different methods which will be discussed in section 4.3 and 4.4.

4.2.2. A NEW APPROACH

In order to eliminate the convolution in the part $k^T(t) * \omega_i(t)\omega_j(t)$ while staying consistent with the fundamental rheology of the system, we adopt the strategy of approximating the load term $\omega_i(t)\omega_j(t)$ instead. Within the considered time period T_n, at time $t = T_p, p = 0, 1, ... n$, values of $\omega_i(t), i = 1, 2, 3$ are known, then we have $\omega_i(T_p) = W_{i,p}$. Assuming that
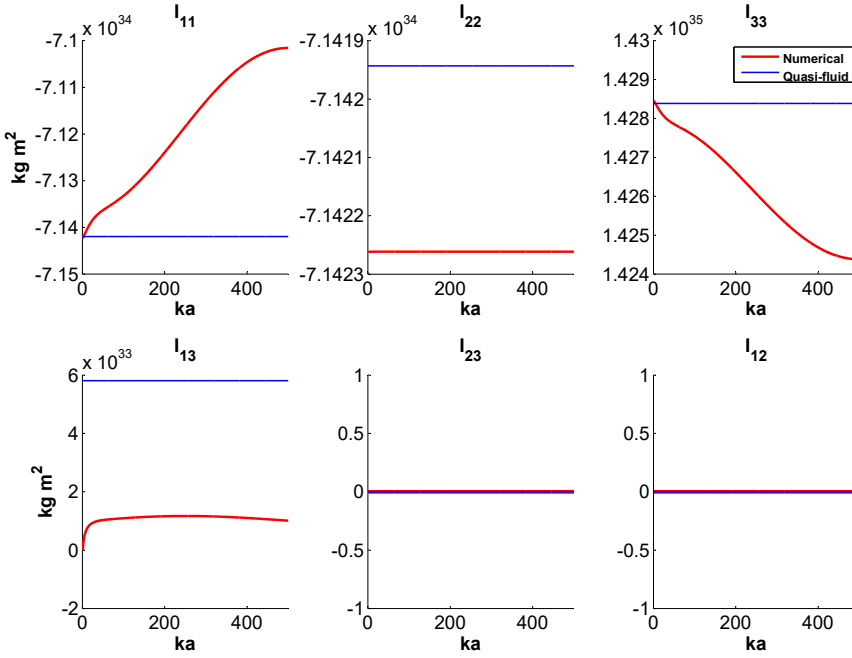
Figure 4.2: Normal polar wander case: Change in the six components of the MoI tensor when the rotational axis initially stays at 30 degree colatitude and 0 degree longitude in the X-Z plane and precesses with a constant speed along the 30 degree colatitude circle for 720 degrees in 500 ka. Red lines are the accurate results and blue lines are from the quasi-fluid approximation.

$\omega_i(t), i = 1, 2, 3$ changes linearly between each time step, $\omega_i(t)$ can be written as a piecewise linear function:

$$\omega_i(t) = \sum_{p=1}^{n} \omega_{i,p} \tag{4.9}$$

$$\tag{4.10}$$

where

$$\omega_{i,p} = \left(W_{i,p-1} + \frac{W_{i,p} - W_{i,p-1}}{T_p - T_{p-1}} (t - T_{p-1}) \right) H(t - T_{p-1}) H(T_p - t) \tag{4.11}$$

and $H(t)$ is the Heaviside step function. With this form, $k(t) * \omega_i(t)\omega_j(t)$ and its derivative can be expressed analytically by applying the Laplace transformation

$$k^T(t) * \omega_i(t)\omega_j(t) = \mathscr{L}^{-1}[\mathscr{L}[k^T(t) * \omega_i(t)\omega_j(t)]] \tag{4.12}$$
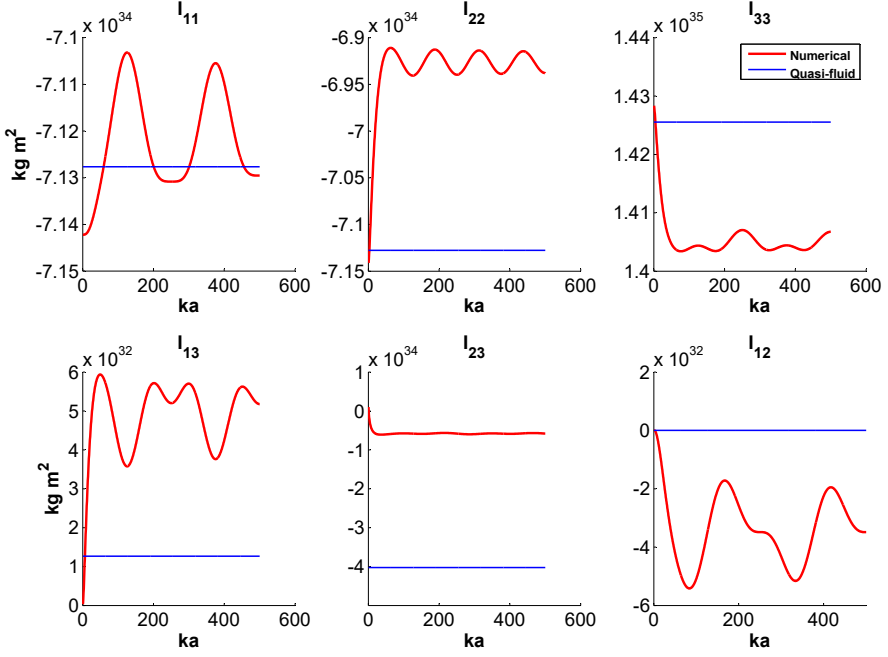
Figure 4.3: Mega wobble case: Change in the six components of the MoI tensor. The rotational axis initially stays at 30 degree colatitude and 0 degree longitude in the X-Z plane and precesses longitudinally with a constant speed along the 30 degree colatitude circle for 720 degrees in 600 ka. Red lines are the accurate results and blue lines are from the quasi-fluid approximation.

where $\mathscr{L}$ and $\mathscr{L}^{-1}$ stand for the Laplace and inverse Laplace transformation, respectively. The explicit expression of equation 4.12 can be found in appendix I as equation 4.30. Substituting equation 4.30 into equation 4.2, the inertia tensor and its derivative at time $t = T_n$ can be expressed analytically as

$$I_{i,j}(T_n) = I\delta_{i,j} + \frac{a^5}{3G}[(A_{i,j}(T_n) + B_{i,j}) - \frac{1}{3}\sum_{k=1}^{3}(A_{k,k}(T_n) + B_{k,k})] + E_{i,j}(T_n) \qquad (4.13a)$$

$$\dot{I}_{i,j}(T_n) = \frac{a^5}{3G}[(C_{i,j}(T_n) + D_{i,j}) - \frac{1}{3}\sum_{k=1}^{3}(C_{k,k}(T_n) + D_{k,k})] + \dot{E}_{i,j}(T_n) \qquad (4.13b)$$

where expressions for $A_{i,j}(t)$, $B_{i,j}(t)$, $C_{i,j}(t)$ and $D_{i,j}(t)$ can be found in appendix I. When $t = T_p$ with $p = 0, 1, ...n$ and $\omega_i(T_p) = W_{i,p}$ with $p = 0, 1, 2...n - 1$ are given, equations 4.13 expresses the moments and products of inertia and its derivative as a function of $W_{i,n}$. Then $W_{i,n}$ can be solved by equation 3.1. To this end, it helps to see the problem as a global optimization problem: we seek the value of $W_{i,n}$ in the neighbourhood of $W_{i,n-1}$ so that the value of $|\frac{d}{dt}(\mathbf{I} \cdot \boldsymbol{\omega}) + \boldsymbol{\omega} \times \mathbf{I} \cdot \boldsymbol{\omega}|$ is minimized. As a result, the method which is introduced in Hu et al. (2017b) as *algorithm 2* (page 10) can be applied. This method applies the linearised form of the Liouville equation and an iteration procedure to obtain $W_{i,n}$. It will be briefly

explained in the following and outlined in appendix II. We define the perturbed rotational vector as

$$\boldsymbol{\omega}' = \Omega(m_1, m_2, 1 + m_3)^T \tag{4.14}$$

where m_1, m_2 and m_3 are small real numbers. The Liouville equation can be linearised to obtain the form (Hu et al., 2017b):

$$m_1(t) = \frac{\Delta I_{13}(t)}{C - A} + \frac{C\Delta \dot{I}_{23}(t)}{\Omega(C - A)(C - B)} \tag{4.15a}$$

$$m_2(t) = \frac{\Delta I_{23}(t)}{C - B} - \frac{C\Delta \dot{I}_{13}(t)}{\Omega(C - A)(C - B)} \tag{4.15b}$$

$$m_3(t) = -\frac{\Delta I_{33}}{C} \tag{4.15c}$$

In equation 4.15, the terms of the inertia tensor, A, B, C and $I_{13}, I_{23}, \dot{I}_{13}, \dot{I}_{23}$ are not in the body-fixed frame but in the bulge-fixed frame. The transformation matrix from the body-fixed frame to the bulge-fixed frame by a pure rotation can be obtained as

$$\mathbf{Q} = \begin{pmatrix} \omega_3 + \frac{\omega_2^2}{1+\omega_3} & -\frac{\omega_1\omega_2}{1+\omega_3} & \omega_1 \\ -\frac{\omega_1\omega_2}{1+\omega_3} & 1 - \frac{\omega_2^2}{1+\omega_3} & \omega_2 \\ -\omega_1 & -\omega_2 & \omega_3 \end{pmatrix} \tag{4.16}$$

A coordinate transformation is required before we can substitute the value of the inertia tensor calculated from equation 4.13. The detailed procedure of algorithm 2 in Hu et al. (2017b) is given in Appendix II.

In general, the only assumptions we make in the entire calculation are two linear approximations: the changes in the rotational vector and the inertia tensor (see equation 10 in Hu et al. (2017b)) are small in each step and can be treated as linear. This is valid when the step-sizes ($\Delta t_p = T_p - T_{p-1}, p = 2, 3, ..n$) are small enough. Since we do not approximate Love numbers, our method gives the TPW path for a viscoelastic body which is consistent with the complete scheme of Maxwell rheology. We will label our method in the following as full-Maxwell method.

4.2.3. INITIAL SETTING AND VALIDATION

One of the major factors that controls the TPW behaviour is the shape of the equatorial bulge (and the tidal bulge which is discussed in Hu et al. (2017b)). When the interior model and rotational speed is given, this shape is controlled by the hydrostatic state of the model. Due to the limitation of the method, previous studies based on either linear (Sabadini et al.,

1982; Wu and Peltier, 1984) or non-linear (Ricard et al., 1993; Chan et al., 2014; Moore et al., 2017) approaches can only simulate TPW on a model which is assumed to be in hydrostatic equilibrium. However, as will be shown in section 4.5, the choice of the hydrostatic state can have a significant impact on the TPW behaviour. With our method, we can choose the hydrostatic state of the model at which the TPW starts.

To simulate the TPW of a body at a certain hydrostatic state, we need to apply a centrifugal force to the model for a certain length of time. If the rotational vector at the start of the simulation is given by $\boldsymbol{\omega}_0 = \Omega(0, 0, 1)^T$, applying centrifugal force to the model for a duration of T_h is expressed in our scheme as

$$T_0 \quad = \quad 0 \tag{4.17a}$$

$$T_1 \quad = \quad T_h \tag{4.17b}$$

$$(W_{1,0}, W_{2,0}, W_{3,0})^T \quad = \quad (W_{1,1}, W_{2,1}, W_{3,1})^T = \boldsymbol{\omega}_0 \tag{4.17c}$$

The triggering load $E_{i,j}(t)$ needs to be applied at $t = T_h$ to start the TPW. To simulate a model in hydrostatic equilibrium, T_h needs to be large enough so that all modes of the model are sufficiently relaxed. In order to achieve this we can choose a T_h so that the slowest mode is relaxed more than 99.999%. Assuming s_1 is the slowest mode,

$$1 - e^{s_1 T_h} > 0.99999 \tag{4.18}$$

translates into

$$T_h > \frac{-11.513}{s_1} \tag{4.19}$$

This choice is similar to that in Hu et al. (2017b), which sets T_h so that $k^T(T_h) > 99.95\% \, k_f^T$, but much more strict. If the model contains a very slow and strong mode, we can obtain a very large value of T_h and this will cause an extremely long calculation time for a pure numerical method (Hu et al., 2017b). By expressing the inertia tensor analytically, a very large T_h can be dealt with. Eventually, there is no limit for the choice of T_h as well as the initial loading $\boldsymbol{\omega}_0$ as long as numerical errors (e.g. truncation error) are avoided. As a result, TPW for a body in a different hydrostatic state can be obtained. This makes our method suitable to study the effect of a remnant bulge or TPW on a model without hydrostatic equilibrium as will be shown and discussed in detail in sections 4.4 and 4.5.

The algorithm, as shown in appendix II, was developed in (Hu et al., 2017b). The main idea is to decouple the two governing equations. The MoI equation was solved by either direct convolution or from a finite element method and the result is fed back into the linearized Liouville equation and solved by an iterative procedure. Such algorithm has been validated by both comparing to the linear (Wu and Peltier, 1984) and non-linear method (Ricard et al.,

1993) in figure 6 and 9 of (Hu et al., 2017b). The difference between the method in this paper and that of (Hu et al., 2017b) is that here the MoI equation is solved analytically with the assumption that the rotational vector changes linearly during each time step of TPW. If the step size is set to be much smaller than the relaxation time of the dominant modes, which is the same requirement for calculating TPW, the analytical solution of the MoI equation with the linear assumption will be sufficiently equivalent to the result from direct convolution. Therefore, the TPW solution generated in this paper can approach that from (Hu et al., 2017b) for a small enough step size. We first demonstrate the result of TPW calculated with T_h = 2000 ka, which is the choice in Hu et al. (2017b) for a six-layer incompressible Earth model SG6 (table 2 in the same paper), and a much higher value ($T_h = 10^6$ ka) for which the model can be considered in hydrostatic equilibrium (equation 4.19 holds). We place a stationary ($k^L(t) = 0$) mass anomaly, which means that the mass anomaly does not "sink" into the body, at the surface at 30 degree colatitude. Here we do not consider the effect of the remnant bulge (which will be discussed in detail in section 4.4), so we ignore the slowest mode generated by the lithosphere (its viscosity is set to 10^{31} Pa s to calculate the Love numbers). We also include the result obtained by the quasi-fluid approximation according to Ricard et al. (1993).
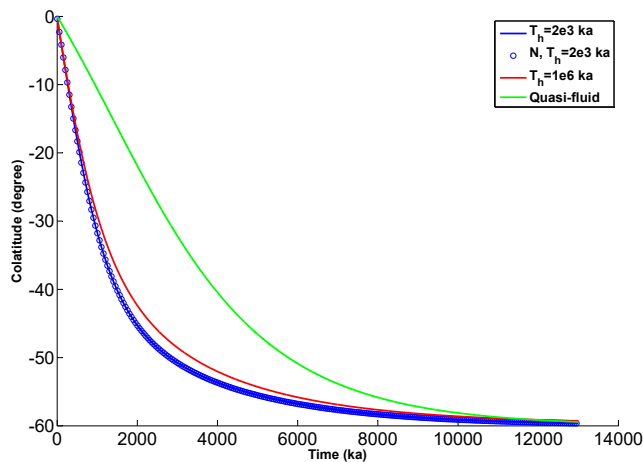
Figure 4.4: Polar wander in the X-Z plane for the SG6 Earth model triggered by a point mass of 2×10^{19} kg attached at the surface at 30 degree colatitude.

The result obtained for T_h = 2000 ka by the full-Maxwell method is within less than 0.05% from the result of the numerical method, as given in figure 9 in (Hu et al., 2017b), for a step-size of 5ka. As we can also see from figure 4.4, choosing T_h = 2000 ka still shows a TPW path that is different from that of a body which can be considered to be in hydrostatic equilibrium ($T_h = 10^6$ ka). This suggests the sensitivity of the TPW to a small deviation from its hydrostatic equilibrium. So choosing T_h large enough is the first guarantee that the correct TPW path for models with hydrostatic equilibrium is obtained.

The computational cost of our method depends on three factors: (1) the complexity of the layered model, or more precisely, the number of the modes in the Love numbers. (2) the

number of iteration necessary to obtain a convergent result in each step. (3) the number of time steps. The computational time increases roughly linearly with these factors. For the results shown in figure 4.4, which is for a SG6 Earth model that contains 12 modes, the number of time steps is 2600 (each step is 5 ka) and every step requires 50 (first step) to 18 (last step) iterations. The program is written in *Matlab* and the total computational time on our desktop computer is about 3 minutes. Compared with the numerical computation (Hu et al., 2017b) which is about several hours, the speed from the semi-analytical approach is much faster.

Based on the analysis in the last section 2.1, the largely underestimated TPW speed by adopting the quasi-fluid approximation is caused by the underestimation of the speed of the equatorial readjustment for the case of Earth and Mars. For the mega-wobble case in Venus, the situation can be quite different as will be discussed in the following section.

4.3. MEGA-WOBBLE: TPW ON VENUS

The linearized Liouville equation (equation 4.15) is obtained by two fundamental assumptions. First, during the TPW, the components of the inertia tensor satisfy $I_{33}(C) > I_{11}(A)$ and $I_{33}(C) > I_{22}(B)$. Secondly, the periodic terms which represent the Chandler wobble can be ignored. While these assumptions are true for cases like Mars and the Earth, it can be invalid for some slowly rotating objects such as Venus. Since the rotational speed of Venus is so slow that its equatorial bulge is also extremely small, the difference of the two principle moment of inertia: $C - A$, which can be calculated by

$$C - A = \frac{k_f^T a^5 \Omega^2}{3G} \tag{4.20}$$

for Venus is less than 1.5×10^{-5} of that for Earth. For magnitudes of a mass anomaly of 10^{-5} or 10^{-6} of the total mass of the planet considered in Spada et al. (1996), depending on the depth and position, the moment around the rotational axis may not be the largest of the diagonal components anymore ($C > A, B$ are not satisfied). Furthermore, the period of the wobble, which can be estimated as $\frac{2\pi}{\Omega} \sqrt{\frac{AB}{(C-A)(C-B)}}$ (see equation 4.22) when $C > A, B$, is about 4 months (depending on the interior model) on Earth or Mars, but can be, depending on the interior model, over 10 million years on Venus. Because of such low frequency, the periodic terms will have a secular effect for TPW on Venus and can not be ignored as for the Earth and Mars. Therefore, in order to study TPW on Venus, it is necessary to first derive a new set of linearized Liouville equations suitable for a body with a very long wobble period. The linearized Liouville equation for a triaxial body reads (Sabadini et al., 2016)

$$\dot{m}_1 = -\frac{C-B}{A}\Omega m_2 + \frac{\Omega}{A}\Delta I_{23} - \frac{\Delta \dot{I}_{13}}{A} \tag{4.21a}$$

$$\dot{m}_2 = \frac{C-A}{B}\Omega m_1 - \frac{\Omega}{B}\Delta I_{13} - \frac{\Delta \dot{I}_{23}}{B} \tag{4.21b}$$

$$\dot{m}_3 = -\frac{\Delta \dot{I}_{33}}{C} \tag{4.21c}$$

We first deal with the cases of $C > A, C > B$ and $C < A, C < B$. By assuming that the change in the moment of inertia is linear, equation 4.21 can be solved analytically. The result contains the non-periodic terms in equation 4.15 and periodic terms

$$\bar{m}_1(t) = \sqrt{\frac{B}{A(C-A)^3(C-B)\Omega^2}} \sin\left(\sqrt{\frac{(C-A)(C-B)}{AB}}\Omega\Delta t\right)\left((A-C)\Delta I_{23}(t) + C\Delta \dot{I}_{13}(t)\right)$$

$$- \cos\left(\sqrt{\frac{(C-A)(C-B)}{AB}}\Omega\Delta t\right)\left(\frac{\Delta I_{13}(t)}{C-A} + \frac{C\Delta \dot{I}_{23}(t)}{\Omega(C-A)(C-B)}\right) \tag{4.22}$$

$$\bar{m}_2(t) = \sqrt{\frac{A}{B(C-A)(C-B)^3\Omega^2}} \sin\left(\sqrt{\frac{(C-A)(C-B)}{AB}}\Omega\Delta t\right)\left((C-B)\Delta I_{13}(t) + C\Delta \dot{I}_{23}(t)\right)$$

$$- \cos\left(\sqrt{\frac{(C-A)(C-B)}{AB}}\Omega\Delta t\right)\left(\frac{\Delta I_{23}(t)}{C-B} + \frac{C\Delta \dot{I}_{13}(t)}{\Omega(C-A)(C-B)}\right) \tag{4.23}$$

When the period of the wobble becomes very long and the step size Δt is small enough, the magnitude of $\sqrt{\frac{(C-A)(C-B)}{AB}}\Omega\Delta t$ in the trigonometric functions is very small, and we can apply $\sin(\theta) \approx \theta$ and $\cos(\theta) \approx 1 - \theta^2/2$. Applying these approximations, combining equation 4.15, 4.22 and 4.23 and ignoring the derivative terms of the inertia tensor gives

$$m_1(t) = \frac{(C-B)\Omega^2\Delta I_{13}(t)\Delta t^2 + 2B\Omega\Delta I_{23}(t)\Delta t}{2AB} \tag{4.24a}$$

$$m_2(t) = \frac{(C-A)\Omega^2\Delta I_{23}(t)\Delta t^2 - 2A\Omega\Delta I_{13}(t)\Delta t}{2AB} \tag{4.24b}$$

$$m_3(t) = -\frac{\Delta I_{33}}{C} \tag{4.24c}$$

The derivation for other situations such as $B < C < A$ or $B > C > A$ are shown in Appendix III. Note that in equation 4.24, as well as in equation 4.44 and 4.45, we do not have the $C - A$ or $C - B$ terms in the denominator, thus these expressions have no singularity problem for $C = B$ or $C = A$. When TPW on a very slowly rotating object like Venus is calculated, equation 4.24 instead of equation 4.15 should be applied. Basically, equation 4.15 and equation 4.24 give two extreme situations for calculating the rotational perturbation. When the step size of the calculation Δt can be set to much larger than the Chandler period, equation 4.15 should be used to give the secular behaviour. When the step size Δt is chosen to be much smaller than the period of the Chandler wobble, equation 4.24 can give the periodic "short"-term behaviour which leads to the mega-wobble on Venus or, when the step size is set to days, the Chandler wobble on Earth or Mars.

Next, we apply our method to a model of Venus and test some results obtained in Spada et al. (1996) who apply the quasi-fluid approximation. We create a five-layer Venus model

which approximates the density and rigidity profile used in Armann and Tackley (2012) and the viscosities are chosen similar to those of Earth. The interior properties are shown in table 4.1. The effect of a remnant bulge is not included here and will be discussed in the next section.

Table 4.1: Venus model

Outer Radius (km)	Density (kg m^{-3})	Shear Modulus (Pa)	Viscosity (Pa s)
6052	2900	0.36×10^{11}	∞
6002	3350	0.68×10^{11}	0.6×10^{21}
5500	3725	0.93×10^{11}	1.6×10^{21}
5200	4900	2.07×10^{11}	6.4×10^{21}
3250	10560	0	0

For this model, the period $\frac{2\pi}{\Omega} \sqrt{\frac{AB}{(C-A)(C-B)}}$ is about 11.45 million years. The step size needs to be much smaller than this value, therefore, a value of less than 5 thousand years is sufficient to obtain an accurate solution. One way to test if the chosen step size is indeed small enough is to recalculate the TPW with half of the step size. If the chosen step size is indeed sufficiently small, the result will not change significantly. We first simulate the TPW on Venus driven by a negative mass anomaly of magnitude 5×10^{18} kg (which is about the maximum value simulated by Spada et al. (1996)) which is attached at the surface at 45 degree colatitude. We decompose the displacement of the rotational axis in the direction which lies in the plane that contains the mass anomaly (normal direction) and the along-track direction. The result is shown in figure 4.5. As we can see, for the along-track displacement which describes the long-term wobble of the rotational axis around the mass anomaly, the results from the two methods differ less than 1%. However, for the displacement in the normal direction, representing the movement of the rotational axis towards the negative mass anomaly, the result obtained based on the quasi-fluid approximation overestimates the speed. The agreement in the along track direction displacement and a disagreement in the normal direction displacement between the two methods can be explained by the small contribution of the equatorial bulge readjustment to the rotational perturbation for Venus. As pointed out by Spada et al. (1996), for Venus, the rotational behaviour is largely dominated by the long-term wobble which resembles the free nutation of a rigid body. The long-term wobble is mainly caused by the mass anomaly itself while the equatorial readjustment contributes very little. Based on the discussion of figure 4.3, the component I_{23} also contributes to the along track speed of the wobble. This component is largely overestimated by the quasi-fluid approximation, but since its magnitude is much smaller than the contribution from the mass anomaly itself (less than 1% in this case), the difference between the two methods can be ignored. However, the damping of the oscillatory motion, or the displacement of the rotational axis in the normal direction, is solely controlled by the viscous relaxation of the body, specifically the component I_{13} in figure 4.3. Since this component is underestimated by the quasi-fluid approximation, the rotational behaviour on Venus obtained by adopting the approximation results in too much damping.

In the study of terrestrial planets whose tidal bulge can be ignored, like Earth, Mars, Venus and Mercury, we may see certain geographic features (e.g. the supercontinent Pangaea on the Earth or the Tharsis plateau on Mars) which have the potential to cause (or have caused)
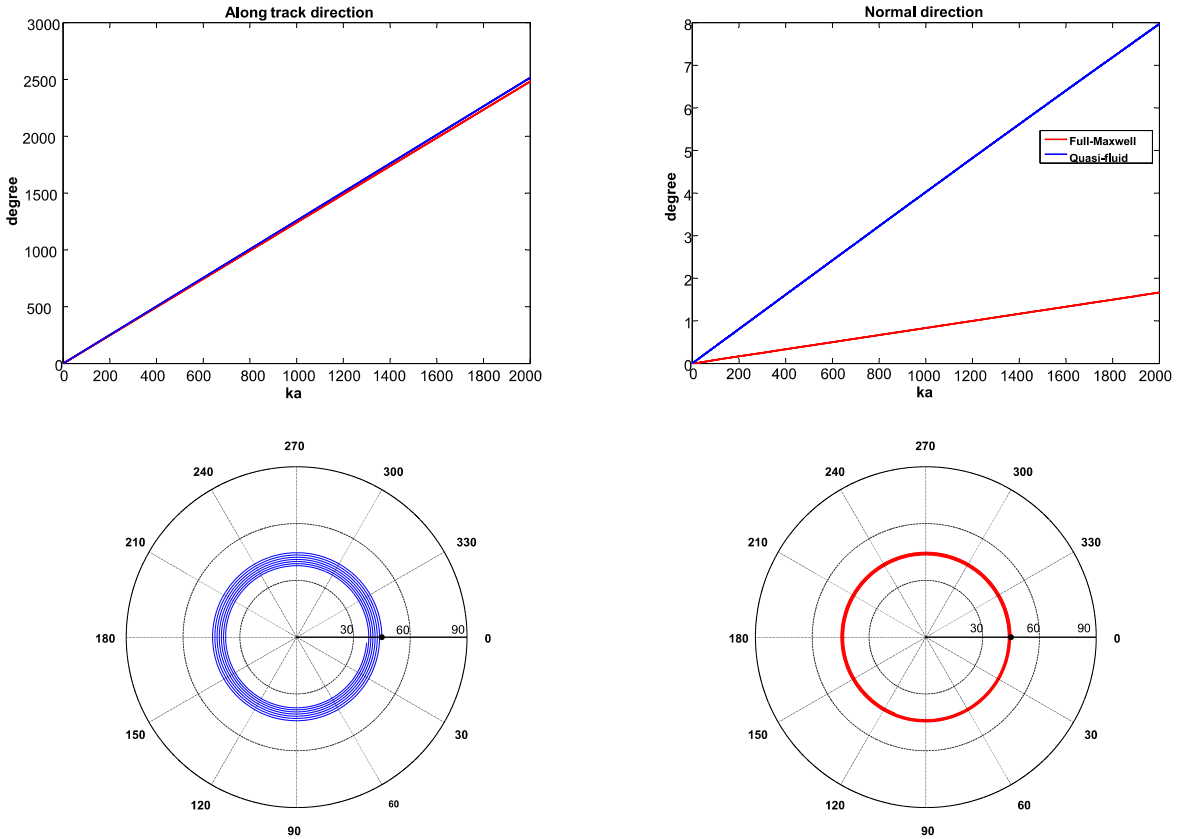
Figure 4.5: A point mass of -5×10^{18} kg is attached at the surface at 45 degrees colatitude. The top figures show the displacement of the rotational axis in the along track and normal direction. The bottom figures show the movement of the mass anomaly in the bulge-fixed frame where the rotational axis is always pointing upwards at the centre. Blue lines are obtained by applying the quasi-fluid approximation and red lines are from the full-Maxwell method. The black dots are the original locations of the mass anomalies in the bulge-fixed frame.

polar wander. Based on an interior model and TPW history, we can estimate the age of the feature or the history of its relocation by its (estimated) former and current latitude since we know that positive mass anomaly tends to relocate towards equator and negative one towards the pole. The latitudinal information in many situations is much more important than the longitudinal one if the body is not tidally locked. As a result, correctly estimating the TPW speed in the latitudinal (normal) direction is crucial for a better understanding of the planet reorientation. In the following the same Venus model is used and several different magnitudes of mass anomaly are tested. We compare the difference in speed as a function of colatitude of the mass anomaly in the normal direction between the two methods. Magnitudes of mass anomaly 1×10^{16}, 1×10^{17}, 1×10^{18} and 5×10^{18} kg are chosen, which covers 10^{-5} to 10^{-6} times of the total mass of Venus, similar to the values chosen in (Spada et al., 1996). The results are shown in figure 4.6. Generally methods based on the quasi-fluid approximation overestimate the normal-directional speed by a factor of 3 to 5.

Spada et al. (1996) state that for the same mass anomaly, the instantaneous velocity of rotational pole on Venus is about 30 times larger than that of Earth and Mars. But they compared the complete rotational behaviour of Venus whose largest part is the wobble with the secular rotational behaviour of Earth and Mars in which the Chandler wobble has been filtered out. A more proper comparison would be either between the speed of Chandler wobble on Earth or Mars with the mega-wobble on Venus, or between the secular speed of rotational variation on Earth or Mars and the normal-directional speed of the rotational axis on Venus. In the latter case, for an Earth, Mars and Venus model with the same average viscosity (ranging from 10^{20} to 10^{22} Pa s), it can be shown that TPW on Earth and Mars is 10 to 15 times larger than the normal-directional speed of Venus' axis for the mass anomalies considered in this study. This means that for the same scale of mass anomaly, it will take much longer on Venus than on Earth or Mars before it can reach the pole or equator. The knowledge of Venusian viscosity is very limited, if the observed normal-directional change of Venus" axis is out of this range (1/10 to 1/15 times of the Earth's TPW), then the average viscosity of Venus must be lower or higher than that of the Earth.

The results we obtained in this section (e.g. the speed in figure 4.5 and 4.6) are, of course, dependent on the interior model of Venus. With different viscosities (10^{19} Pa s to 10^{22} Pa s), the TPW speed can be very different but adopting the quasi-fluid approximation always largely overestimates the normal-directional speed.

4.4. EFFECT OF A REMNANT BULGE ON TPW AND A STUDY OF MARS

For a viscoelastic model which can be sufficiently relaxed, a positive mass anomaly with any magnitude will end up at the equator while a negative mass anomaly will eventually reach the poles. However, most of the observed geophysical features which are thought to have triggered a reorientation, such as the Tharsis plateau on Mars (Bouley et al., 2016) or Sputnik Planitia on Pluto (Keane et al., 2016), are not located exactly at the equator. A common explanation is that certain parts of the planet, usually the lithosphere which is considered to be elastic or to have a very high viscosity, have not yet relaxed, preventing the mass anomaly from being relocated further. The effect of such elastic or highly viscous lithosphere on TPW has been studied for the linear scheme, e.g. (Mitrovica et al., 2005; Cambiotti et al., 2010), and the non-linear scheme with the quasi-fluid approximation, e.g. (Harada, 2012; Chan et al., 2014; Moore et al., 2017). Here we demonstrate the effect of a remnant bulge on the large-angle TPW with the full-Maxwell method.

First, the origin of the remnant bulge is shown using the normal mode method. This has also been discussed by Moore et al. (2017). The remnant bulge, either formed by an elastic layer or a highly viscous layer, appears because of a certain mode(s) which has a much longer (or infinite) relaxation time compared to other dominant relaxation modes of the model. We demonstrate this with simple two/three-layer Earth models with and without a lithosphere of varying viscosity. In table 4.2, the physical properties of the models are shown. Model M1 has a lithosphere viscosity of 10^{21} Pa s which is the same as the mantle, thus this is actually
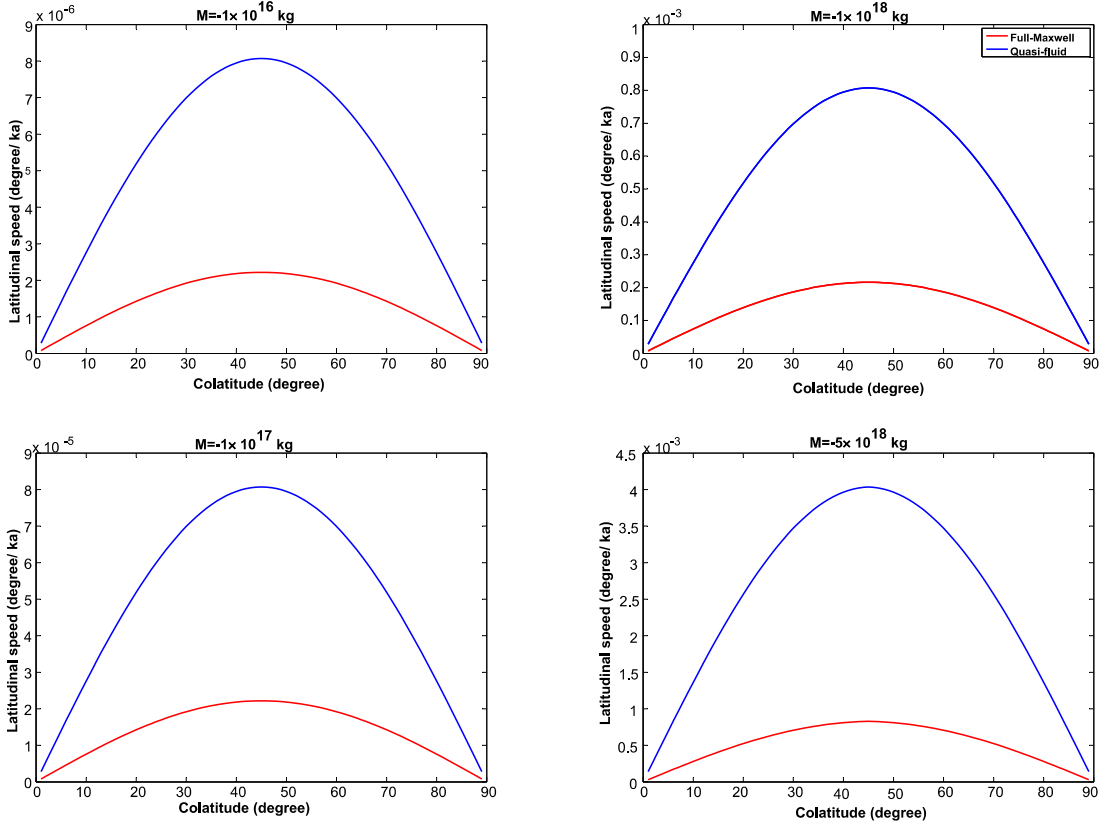
Figure 4.6: Normal directional speed of the rotational axis towards the mass anomaly as a function of the colatitude.

a two-layer model without lithosphere. The lithosphere of models M2-M5 have viscosities of $10^{24}, 10^{26}, 10^{29}$ and ∞ Pa s, respectively.

Table 4.2: Properties of the two/three-layer Earth models (M1-M5)

Layer	Outer Radius (km)	Density (kg m^{-3})	Shear Modulus (Pa)	Viscosity (Pa s)
Lithosphere	6371	4448	1.7×10^{11}	$1 \times 10^{21,24,26,29}, \infty$
Mantle	6361	4448	1.7×10^{11}	1×10^{21}
Core	3480	10977	0	0

The degree 2 potential tidal Love numbers of models M1-M5 are shown in table 4.3, where the inverse relaxation time s_i has unit 1/ka. Following Sabadini et al. (2016), we can see that the two layer model M1 only contains two relaxation modes, C_0 corresponding to the core-mantle boundary and M_0 corresponding to the surface. When a viscoelastic layer with the same density is added to the model (M2-M5), two additional transition modes, $\bar{T}_1$ and $\bar{T}_2$, are triggered if the Maxwell time on either side of the boundary is different. In the case

of model M2, these two additional modes have relaxation times not too different from the dominant modes (C_0 and M_0 in this case). Consequently, the delayed relaxation of both $\bar{T}_1$ and $\bar{T}_2$ is not large enough to cause a remnant bulge. However, in the case of M3 and M4, as the viscosity of the lithosphere increases, the relaxation time for one of the $\bar{T}$ modes increases with the same order as the viscosity. It is this $\bar{T}$ mode that determines if the remnant bulge is present. As the viscosity of the lithosphere increases further and eventually approaches infinity, as is the case in model M5, the $\bar{T}_1$ mode disappears and its mode strength $-k_1/s_1$ becomes absent in the fluid Love number k_f. It can be seen that the difference in the fluid Love number between M5 and M4 is almost the same as the mode strength of $\bar{T}_1$ in M4: $k_f^{M4} - k_f^{M5} \approx (k_1/s_1)^{M4}$. The remnant bulge is dealt with in previous studies by either those dealing with an elastic lithosphere Mitrovica et al. (2005); Cambiotti et al. (2010); Harada (2012); Chan et al. (2014) or viscoelastic lithosphere (Cambiotti et al., 2010; Moore et al., 2017) by isolating this part of the Love number and formulating the influence of it separately.

Table 4.3: Potential tidal Love number of models M1-M4

Modes	M1 (10^{21} Pa s)		M2 (10^{24} Pa s)		M3 (10^{26} Pa s)		M4 (10^{29} Pa s)		M5 (∞ Pa s)	
	s_i	$-k_i/s_i$	s_i	$-k_i/s_i$	s_i	$-k_i/s_i$	s_i	$-k_i/s_i$	s_i	$-k_i/s_i$
k_e		0.3449		0.3449		0.3449		0.3449		0.3449
T_1			-0.5341e-1	0.4731e-2	-0.5343e-3	0.4204e-2	-0.5343e-6	0.4200e-2		
T_2			-0.7886e-1	0.3045e-2	-0.2764e-1	0.2035e-2	-0.2713e-1	0.2027e-2	-0.2712e-1	0.2027e-2
C_0	-0.4086	0.2376	-0.4208	0.2337	-0.4193	0.2351	-0.4193	0.2352	-0.4193	0.2352
M_0	2.225	0.4591	-2.2344	0.4552	-2.2343	0.4553	-2.2343	0.4553	-2.2343	0.4553
k_f		1.0416		1.0416		1.0416		1.0416		1.0374

One of the advantages of the full-Maxwell method is that we can choose any value for the initial loading time T_h. This enables us to simulate the influence of the remnant bulge without any extra formulation. To include such a bulge caused by a very slow relaxation mode, we only need to set the initial loading time T_h to a value large enough so that this slow mode is fully relaxed to the centrifugal force, according to the condition in equation 4.19. For instance, for the model M4 in table 4.3, we can set $T_h = 1 \times 10^9$ ka which guarantees that the $\bar{T}_1$ mode is relaxed. In practice, we do not need to simulate the case with a fully elastic layer. Instead, we can always set the viscosity of the layer high enough to guarantee that its relaxation within the considered time can be ignored. In that case, the lithosphere is effectively elastic.

Now we demonstrate the effect of a remnant bulge with the full-Maxwell method and compare the results with those obtained by applying the quasi-fluid approximation. A more realistic SG6 model is used, in contrast with those shown in figure 4.4 where the slowest mode is ignored. Three cases with different thickness of the lithosphere are considered and the viscosity of this layer is set to 10^{31} Pa s so that within the considered time span (10 million years), the relaxation of the slowest mode can be ignored. We compare our results with those obtained by using the method of Chan et al. (2014) which is based on the quasi-fluid approximation. The results are shown in figure 4.7. While predicting the same end position of TPW, the quasi-fluid approximation gives a much slower transient response.

Next we show the effect of a viscoelastic lithosphere whose viscosity has a relaxation time which is comparable with the considered time span. This issue is important because whether or not the lithosphere can relax during the considered period can affect the TPW behaviour
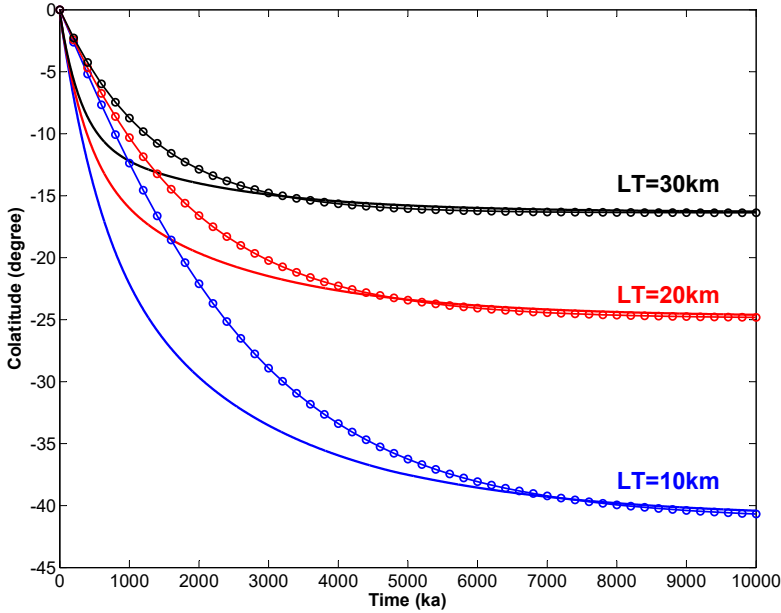
Figure 4.7: Polar wander in the X-Z plane for the Earth models with different lithosphere thickness triggered by a point mass of 2×10^{19} kg attached at the surface at 20 degrees colatitude. Solid lines show results obtained with the full-Maxwell method from this paper, the line-dots are calculated with the method by Chan et al. (2014) which is based on the quasi-fluid approximation.

both in the short term (e.g. the speed) and the long term. The comparison between the effect of an effectively-elastic and a viscoelastic lithosphere on small-range TPW (less than 2 degrees) has been done by Cambiotti et al. (2010) using a linear scheme. Here we show the effect when large angle TPW is considered. For this issue Moore et al. (2017) extend the theory in Chan et al. (2014) and consider the slowest mode(s) separately while applying the quasi-fluid approximation to the rest of the modes. Apart from the bias introduced by the quasi-fluid approximation as shown in figure 4.7, another problem of this approach is that for a complex multi-layered model like the SG6 Earth model with its lithosphere viscosity smaller than a certain value (e.g. 10^{28} Pa s for SG6 model), the slowest mode might not be the $\bar{T}_1$ mode from the lithosphere but one of the M modes ($M2, M3...$) which is generated by a density difference of the inner layers. Moreover, there might not be a large difference in the relaxation time between two modes (such as cases M3 and M4 in table 4.3), as a result, it is not clear which modes need to be modelled separately. Our approach does not have this limitation. Similar to the case of an effectively-elastic lithosphere, we only need to choose a large enough value for T_h. Here the SG6 model with lithospheric thicknesses of 0, 10 and 20 km and with viscosities of 10^{27} and 10^{31} Pa s is used. A mass anomaly of 2×10^{19} kg is placed at 30 degree colatitude for 10 million years, then removed. Within the considered time span of 20 million years, the lithosphere with viscosity of 10^{31} Pa s can be considered as effectively elastic while that with a viscosity of 10^{27} Pa s is partially relaxed. The result is shown in figure 4.8. We see that the behaviour of the TPW is very sensitive to the thick-

ness of the lithosphere. A thicker lithosphere gives stronger resistance against TPW as well as a faster rebounding of the rotational axis when the triggering load is removed. Due to the partial relaxation of the $\bar{T}_1$ mode, which allows the equatorial bulge to adjust faster for the high viscosity lithosphere, the TPW for models with a low viscosity lithosphere is larger and the rotational axis can not go back to its original position after the mass anomaly is removed.
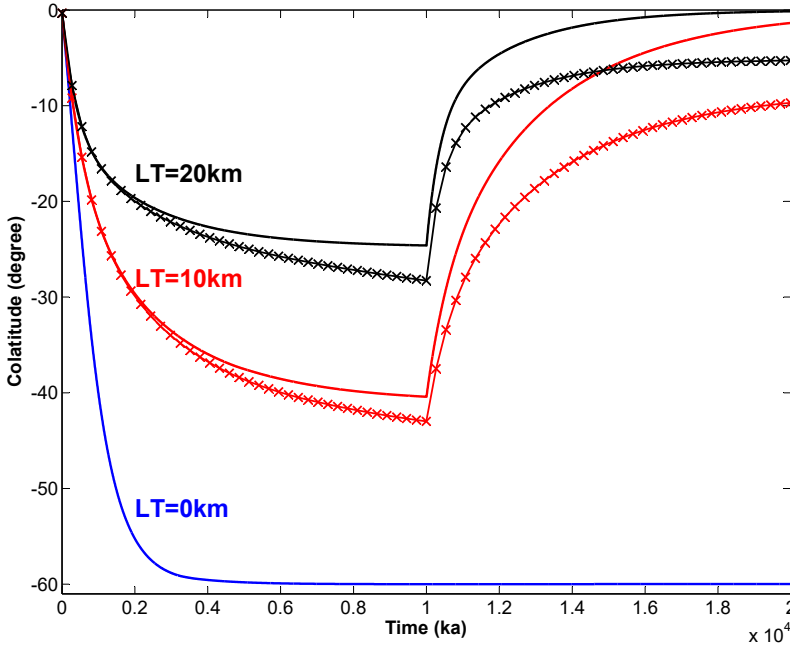
Figure 4.8: A point mass of 2×10^{19} kg attached at the surface at 30 degree colatitude and removed after 10 million years. Lines are for models with viscosity of 10^{31} Pa s and line-crosses are for models with viscosity of 10^{27} Pa s.

We also apply our method to a model of Mars to compare the speed of TPW on Mars calculated by the two methods. We establish a 5 layer model whose density and rigidity approximates the model in Zharkov and Gudkova (2005) which contains a 50 km lithosphere. The viscosity of the model is divided into an effectively elastic lithosphere and a uniform mantle of viscosities 10^{19} Pa s, 10^{20} Pa s, 10^{21} Pa s and 10^{22} Pa s which covers the value used in most recent studies (Hauck and Phillips, 2002; Breuer and Spohn, 2006). We load the model with a surface mass anomaly of magnitude 3.5×10^{19} kg (which is about the magnitude for Q=1 for the normalized load parameter Q defined in Willemann (1984) and used by Matsuyama and Nimmo (2007); Chan et al. (2014)) placed at 45 degree latitude. The results are shown in figure 4.9. Similar to the Earth model, the quasi-fluid approximation has a large underestimation of the speed for most of the duration of the TPW. The instantaneous speed from the full-Maxwell method is, for all four viscosities, about 4.6 times as large as those obtained based on the quasi-fluid approximation. The reason for this is, as mentioned before, the underestimation of the equatorial bulge readjustment when the approximation is adopted. When the rotational axis approaches its end position, the speed of TPW obtained from the full-Maxwell method drops faster than for the quasi-fluid approximation which results in

the end position being reached later. Generally, the method based on the quasi-fluid approximation underestimates the time it takes for a mass anomaly to reach its end position by about half, compared to the full-Maxwell method.
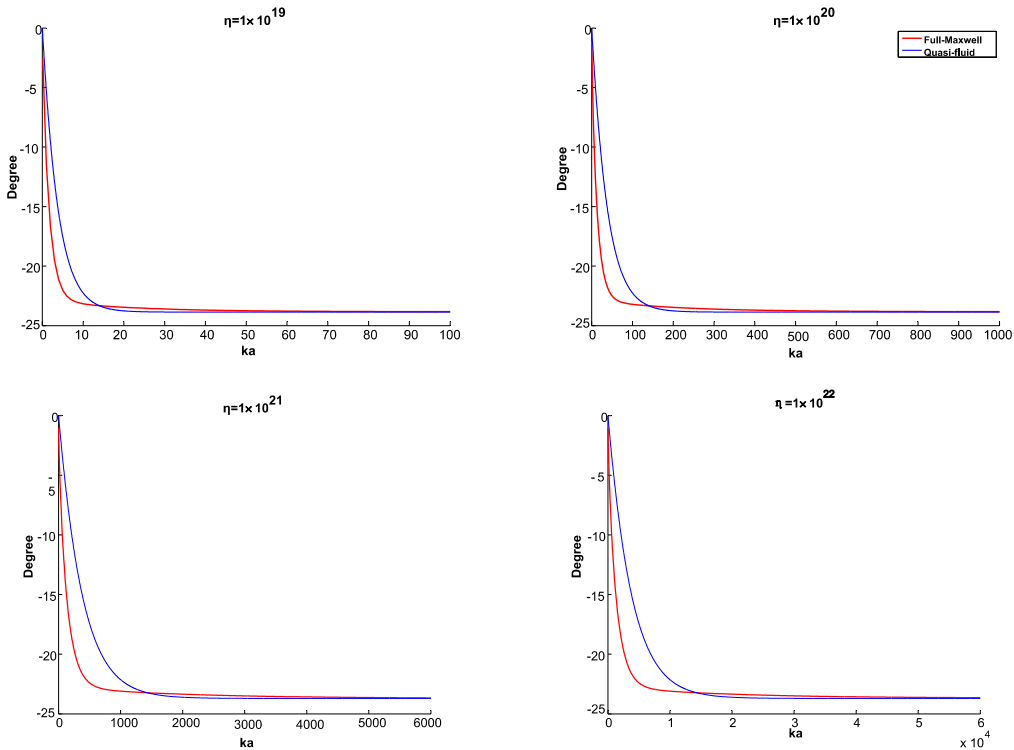
Figure 4.9: TPW on Mars triggered by a mass anomaly of 3.5×10^{19} kg which is attached at the surface at 45 degree latitude for four different values of mantle viscosity. This magnitude is about the same as for Q=1 of the normalized load parameter Q defined in Willemann (1984).

4.5. TPW ON A MODEL WITHOUT HYDROSTATIC EQUILIBRIUM

In practice, a physical model (consisting of layers with given density, rigidity and viscosity) can be derived from a geochemical model and the density profile matches the total mass and/or gravitational data. However, it can happen that the predicted tidal fluid Love number based on the physical model does not match the observed value for the present-day rotational speed Ω. By assuming that the model is in hydrostatic equilibrium, the fluid Love number can be estimated from the observed difference in the polar and equatorial moments of inertia $C - A$ (Mound et al., 2003):

$$k_f^{obs} = \frac{3G}{a^5 \Omega^2} (C - A)_{obs} \tag{4.25}$$

For the Earth, this issue appears to have been studied first by Mitrovica et al. (2005) who introduced the β correction term to the tidal fluid Love number when the present-day TPW speed is estimated. Usually it is considered that this extra non-hydrostatic contribution stems from mantle convection. Here we simulate another possible cause for this contribution and its effect on TPW. Before the TPW starts, the lithosphere is not in hydrostatic equilibrium, or more specifically, the permanent shape of the elastic lithosphere does not match the present-day rotational speed. The stress-free flattening of the elastic layer can be either larger or smaller because the rotational speed during the formation of the planet (or moon) was either faster or slower than the present-day value, e.g. for the Moon (Garrick-Bethell et al., 2006; Matsuyama, 2013). We demonstrate here the influence on the TPW of a lithosphere with the same thickness but in different hydrostatic state.

Since the influence of each relaxation mode s_i is formulated separately in terms $a_{i,j,p,q}(t)$ and $c_{i,j,p,q}(t)$ in equation 4.30 in Appendix I of this chapter, we can set both the initial loading potential characterized by $\omega_i(t)$ and the loading period differently for each relaxation mode to simulate the model being in a different hydrostatic state. For each relaxation mode s_i, we set the initial loading period as T_{i_h} and the rotational speed as $\boldsymbol{\omega}_{i_0}$. In contrast to equation 4.17, we now have

$$T_{0,i} = 0 \tag{4.26a}$$
$$T_{1,i} = T_{i_h} \tag{4.26b}$$
$$(W_{1,0}, W_{2,0}, W_{3,0})_i = (W_{1,1}, W_{2,1}, W_{3,1})_i = \boldsymbol{\omega}_{i_0} \tag{4.26c}$$

In the following, we show that the choice of the hydrostatic state is as important as the choice of the model. We demonstrate this concept using SG6 models with a thin (10 km) and thick (20 km) lithosphere. As shown in figure 4.8, when the models are in hydrostatic equilibrium, different lithospheric thicknesses result in significantly different TPW behaviour. This SG6 model is put into two categories which results in four scenarios in total.

Category **I**:
I. a A thin-lithosphere model in hydrostatic equilibrium with the present-day rotational speed.
I. b A thick-lithosphere model whose slowest mode has relaxed so that its mode strength is equal to that of the thin lithosphere model:

$$(\frac{k_1}{s_1})^{\text{thick}} \times (1 - e^{s_1 T_{h_1}}) = (\frac{k_1}{s_1})^{\text{thin}} \tag{4.27}$$

Since other modes are much faster than the slowest mode, this T_{h_1} is set for all the modes. In this way, all other modes except the slowest one are fully relaxed. The partial relaxation of the slowest mode of the thick-lithosphere model has the same strength as the slowest mode of the thin-lithosphere model. Scenario **I. b** is created to simulate that the rotational speed during the formation of the lithosphere was slower than present-day.

Category **II**:

II. a A thick-lithosphere model in hydrostatic equilibrium with the present-day rotational speed.

II. b A thin-lithosphere model whose slowest mode has fully relaxed for a faster rotational speed of:

$$\boldsymbol{\omega}_{1_0}^{\text{Thin}} = \sqrt{\frac{(k_1/s_1)^{\text{Thick}}}{(k_1/s_1)^{\text{Thin}}}} \boldsymbol{\omega}_0 \qquad (4.28)$$

where $\boldsymbol{\omega}_0$ is the present-day rotational speed. $(k_1/s_1)^{\text{Thick}}$ and $(k_1/s_1)^{\text{Thin}}$ are the mode strengths of the slowest modes of the thick and thin lithosphere model, respectively. Scenario **II. b** corresponds to the situation that the rotational speed during the formation of the lithosphere is faster than the present-day value. With equations 4.27 and 4.28, we configure the scenarios of models without hydrostatic equilibrium, **I. b** and **II. b**, such that the influence of the slowest mode has the same contribution to the inertia tensor of the entire model at the start of the simulation in each category. We test the model with an effectively elastic lithosphere (viscosity 10^{31} Pa s) with the same loading as those in figure 4.8. The results are shown in figure 4.10.
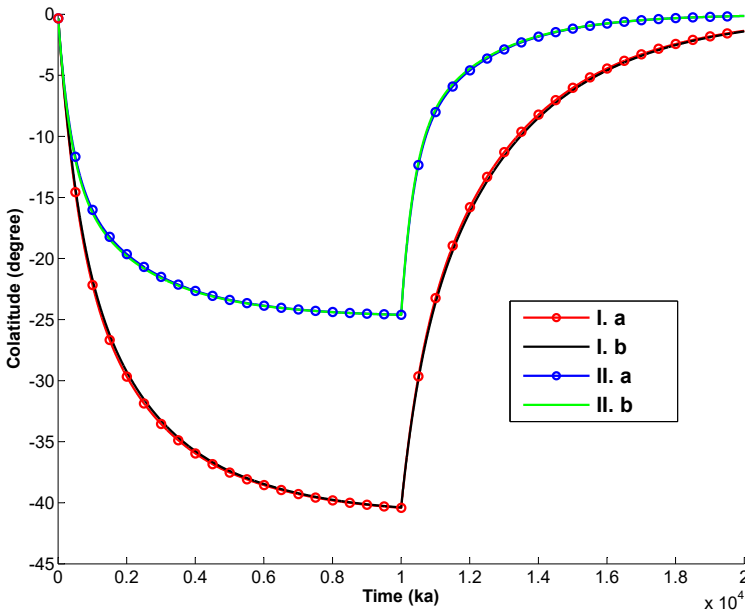
Figure 4.10: TPW for a point mass of 2×10^{19} kg attached at the surface at 30 degree colatitude and removed after 10 million years. Red and blue lines are models with an effectively-elastic (viscosity 10^{31} Pa s) lithosphere with thickness of 10 km and 20 km, respectively, which are in hydrostatic equilibrium. Green and black lines represent models with a lithosphere thickness of 10 km and 20 km, respectively and their lithospheres initially contribute the same to the moment of inertia as the models in hydrostatic equilibrium.

As we can see in figure 4.10, although the models in each category have different thicknesses of the lithosphere and hydrostatic states, the performance of TPW is almost identical. This

can be understood as follows: when the lithosphere is thin enough (e.g. less than 100 km for the Earth's case), the influence of changing the properties of this layer (thickness, rigidity, viscosity) is very small on modes other than $\bar{T}_1$ and $\bar{T}_2$ generated from the non-lithosphere part of the model. Its largest effect is, as shown in figure 4.4, a remnant bulge which resists the readjustment of the equatorial bulge. Once we choose a proper hydrostatic state so that the same contribution to the inertia tensor is guaranteed from the lithosphere of a different model, the path of TPW will also be almost the same. As for the issue concerning the difference between the observed and model predicted flattening, it can be seen from equation 4.28 that if the elastic layer generates a mode with strength $-k_1/s_1$ and the rotational speed during its formation is Ω_0, and Ω_c at present-day, then this elastic layer would cause an extra flattening represented in the observed fluid Love number as:

$$\Delta k_f^{obs} = -\frac{k_1}{s_1}\left[(\frac{\Omega_0}{\Omega_c})^2 - 1\right] \tag{4.29}$$

For the Earth model, for instance, considering that 6 million years ago the rotational speed of Earth was about 15% faster (Zahnle and Walker, 1987), the rotational speed during the formation of the lithosphere would be even higher considering that tidal dissipation started when the Earth-moon system formed about 4.5 billion years ago. An elastic lithosphere of 80 km with a rotational speed during formation that is 30% faster than the present-day speed would cause the observed fluid Love number to increase by about 0.01.

We conclude that for the study of TPW for a model with a lithosphere, it is necessary to know both the initial stress-free shape of the lithosphere as well as its thickness before a correct TPW behaviour can be predicted. This can be significant for the study of TPW on Mars since it has less tectonic activity compared to Earth to release the stress in its lithosphere, which results in a higher chance that Mars is not in hydrostatic equilibrium.

4.6. CONCLUSION

We have established a new semi-analytical method for calculating large-angle true polar wander (TPW) which is consistent with the complete scheme of Maxwell rheology, meaning that both fast and slow modes are correctly taken into account, in contrast with previous studies which adopt the quasi-fluid approximation that approximate the Love number. We extend the scheme of the linearized Liouville equation in Hu et al. (2017b) which can also be used to simulate the mega-wobble on Venus. The influence of the delayed relaxation of elastic or highly viscous layers as well as models in different hydrostatic states (e.g. not in hydrostatic equilibrium) has been studied. With the help of our model, the following conclusions can be drawn:

- The quasi-fluid approximation can introduce a large error in the transient response for a time-dependent solution. The TPW speed on Earth and Mars based on the quasi-fluid approximation can be underestimated while the speed of the rotational axis approaching the end position on Venus is overestimated.

- Depending on the considered period, the TPW for a model with a viscoelastic lithosphere can have a larger displacement and a weaker restoring response compared to a model with an (effectively) elastic lithosphere. Due to the sensitivity of TPW to the shape of the lithosphere, the viscosity of the lithosphere needs to be taken into account when the studied period is not much shorter than the relaxation time of the lithosphere.

- The permanent shape of the elastic lithosphere can have a large effect on the TPW and this can be an additional explanation for the difference between the observed and model-predicted flattening of a rotating body.

Thus, studies involving TPW can benefit from our method to achieve better accuracy in the pole path, especially while taking into account a viscous lithosphere or non-hydrostatic background. Our method can also be extended to tidally deformed models. In this paper we applied algorithm 2 of Hu et al. (2017b) to calculate the rotational perturbation. In the same paper, a new iterative procedure was also presented to combine both the rotational and tidal perturbation (algorithm 3). Combining this algorithm with the analytical solution for the change in the moment of inertia presented in the present paper can give a semi-analytical solution for large angle reorientations of rotating tidally deformed bodies.

APPENDIX I: EXPRESSIONS FOR $A_{i,j}(t)$, $B_{i,j}(t)$, $C_{i,j}(t)$ AND $D_{i,j}(t)$

$$k^T(t) * \omega_i(t)\omega_j(t)|_{t=T_n} = A_{i,j}(T_n) + B_{i,j} \tag{4.30a}$$

$$\frac{d[k^T(t) * \omega_i(t)\omega_j(t)]}{dt}\Big|_{t=T_n} = C_{i,j}(T_n) + D_{i,j} \tag{4.30b}$$

where

$$A_{i,j}(t) = \sum_{p=1}^{n}\sum_{q=1}^{m} a_{i,j,p,q}(t) \tag{4.31}$$

$$\tag{4.32}$$

$$C_{i,j}(t) = \sum_{p=1}^{n}\sum_{q=1}^{m} c_{i,j,p,q}(t) \tag{4.33}$$

$$\tag{4.34}$$

and

$$B_{i,j} = k_e^T W_{i,n} W_{j,n} \tag{4.35a}$$

$$D_{i,j} = \frac{k_e^T \left(W_{i,n-1}W_{j,n} + W_{i,n}\left(W_{j,n-1} - 2W_{j,n}\right)\right)}{T_{n-1} - T_n} \tag{4.35b}$$

where for $t > T_p$

$$
\begin{aligned}
a_{i,j,p,q}(t) = \frac{k_q}{(T_{p-1} - T_p)^2 s_q^3} &\left(e^{s_q(t - T_{p-1})} (W_{i,n}(W_{j,n-1}((T_p - T_{p-1})s_q - 2) + 2W_{j,n}) \right. \\
&+ W_{i,n-1}\left(W_{j,n-1}\left((T_{p-1} - T_p)s_q\left((T_{p-1} - T_p)s_q + 2\right) + 2\right) + W_{j,n}\left((T_p - T_{p-1})s_q - 2\right)\right)) \\
&- e^{s_q(t - T_p)}(W_{i,n-1}(W_{j,n}((T_{p-1} - T_p)s_q - 2) + 2W_{j,n-1}) \\
&+ \left. W_{i,n}\left(\left((T_{p-1} - T_p)s_q - 2\right)\left((T_{p-1} - T_p)s_q W_{j,n} + W_{j,n-1}\right) + 2W_{j,n}\right))\right)
\end{aligned} \tag{4.36}
$$

$$
\begin{aligned}
c_{i,j,p,q}(t) = \frac{k_q e^{-s_q T_{p-1}}}{(T_{p-1} - T_p)^2 s_q^2} &\left(e^{t s_q} (W_{i,n}\left(W_{j,n-1}\left((T_p - T_{p-1})s_q - 2\right) + 2W_{j,n}\right) \right. \\
&+ W_{i,n-1}\left(W_{j,n-1}\left((T_{p-1} - T_p)s_q\left((T_{p-1} - T_p)s_q + 2\right) + 2\right) + W_{j,n}\left((T_p - T_{p-1})s_q - 2\right)\right)) \\
&- e^{s_q(T_{p-1} - T_p + t)}(W_{i,n-1}\left(W_{j,n}\left((T_{p-1} - T_p)s_q - 2\right) + 2W_{j,n-1}\right) \\
&+ \left. W_{i,n}\left(\left((T_{p-1} - T_p)s_q - 2\right)\left((T_{p-1} - T_p)s_q W_{j,n} + W_{j,n-1}\right) + 2W_{j,n}\right))\right)
\end{aligned} \tag{4.37}
$$

and for $t \leq T_p$

$$
\begin{aligned}
a_{i,j,p,q}(t) = \frac{k_q}{(T_{p-1} - T_p)^2 s_q^3} &\left(W_{i,n}(W_{j,n-1}(s_q(s_q\left(t - T_{p-1}\right)\left(t - T_p\right) + \left(T_p - T_{p-1}\right)e^{s_q(t - T_{p-1})} \right. \\
&- T_{p-1} - T_p + 2t) - 2e^{s_q(t - T_{p-1})} + 2) \\
&+ W_{j,n}(2(e^{s_q(t - T_{p-1})} - 1) - s_q\left(t - T_{p-1}\right)\left(s_q\left(t - T_{p-1}\right) + 2\right))) \\
&+ W_{i,n-1}(W_{j,n-1}(2(e^{s_q(t - T_{p-1})} - 1) + s_q((T_{p-1} - T_p)\left(\left(T_{p-1} - T_p\right)s_q + 2\right)e^{s_q(t - T_{p-1})} \\
&+ \left(t - T_p\right)\left(s_q\left(T_p - t\right) - 2\right))) \\
&+ W_{j,n}(s_q\left(s_q\left(t - T_{p-1}\right)\left(t - T_p\right) - T_{p-1} - T_p + 2t\right) \\
&+ \left. \left(\left(T_p - T_{p-1}\right)s_q - 2\right)e^{s_q(t - T_{p-1})}) + 2W_{j,n}))\right)
\end{aligned} \tag{4.38}
$$

$$
\begin{aligned}
c_{i,j,p,q}(t) = \frac{k_q e^{-s_q T_{p-1}}}{(T_{p-1} - T_p)^2 s_q^2} &\left(e^{t s_q} (W_{i,n}\left(W_{j,n-1}\left((T_p - T_{p-1})s_q - 2\right) + 2W_{j,n}\right) \right. \\
&+ W_{i,n-1}\left(W_{j,n-1}\left((T_{p-1} - T_p)s_q\left((T_{p-1} - T_p)s_q + 2\right) + 2\right) + W_{j,n}\left((T_p - T_{p-1})s_q - 2\right)\right)) \\
&- e^{T_{p-1} s_q}(W_{i,n}\left(W_{j,n-1}\left(s_q\left(T_{p-1} + T_p - 2t\right) - 2\right) + 2W_{j,n}\left(s_q\left(t - T_{p-1}\right) + 1\right)\right) \\
&+ \left. W_{i,n-1}\left(2W_{j,n-1}\left(s_q\left(t - T_p\right) + 1\right) + W_{j,n}\left(s_q\left(T_{p-1} + T_p - 2t\right) - 2\right)\right)))\right)
\end{aligned} \tag{4.39}
$$

APPENDIX III: GOVERNING EQUATION FOR THE CASE $B < C < A$ AND $B > C > A$

For the case $B > C > A$, we assume that the changes in the inertia tensor are linear:

$$\Delta I_{13}(t) = a_1 + b_1 t \tag{4.40a}$$

$$\Delta I_{23}(t) = a_2 + b_2 t \tag{4.40b}$$

Then equation 3.9 can be solved analytically which results in

$$
m'_1(t) = \sqrt{\frac{B}{A(C-A)^3(B-C)\Omega^2}} \sinh\left(\sqrt{\frac{(C-A)(B-C)}{AB}}\Omega\Delta t\right)\left((C-A)\Delta I_{23}(t) - C\Delta \dot{I}_{13}(t)\right)
$$
$$
- \cosh\left(\sqrt{\frac{(C-A)(B-C)}{AB}}\Omega\Delta t\right)\left(\frac{\Delta I_{13}(t)}{C-A} + \frac{C\Delta \dot{I}_{23}(t)}{\Omega(C-A)(B-C)}\right)
$$
$$
+ \left(\frac{\Delta I_{13}(t)}{C-A} + \frac{C\Delta \dot{I}_{23}(t)}{\Omega(C-A)(B-C)}\right) \tag{4.41}
$$

$$
m'_2(t) = \sqrt{\frac{A}{B(C-A)(B-C)^3\Omega^2}} \sinh\left(\sqrt{\frac{(C-A)(B-C)}{AB}}\Omega\Delta t\right)\left((C-B)\Delta I_{13}(t) + C\Delta \dot{I}_{23}(t)\right)
$$
$$
+ \cosh\left(\sqrt{\frac{(C-A)(B-C)}{AB}}\Omega\Delta t\right)\left(\frac{\Delta I_{23}(t)}{B-C} - \frac{C\Delta \dot{I}_{13}(t)}{\Omega(C-A)(B-C)}\right)
$$
$$
- \left(\frac{\Delta I_{23}(t)}{B-C} - \frac{C\Delta \dot{I}_{13}(t)}{\Omega(C-A)(B-C)}\right) \tag{4.42}
$$

Where $\sinh(u)$ and $\cosh(u)$ are hyperbolic functions

$$\sinh(u) = \frac{e^u - e^{-u}}{2} \tag{4.43a}$$

$$\cosh(u) = \frac{e^u + e^{-u}}{2} \tag{4.43b}$$

When Δt is small enough, we can apply approximation $\sinh(\theta) \approx \theta$ and $\cosh(\theta) \approx 1 - \theta^2/2$. Ignoring the derivative terms of the inertia tensor simplifies equation 4.41 and 4.42 into

$$m'_1(t) = \frac{(B-C)\Omega^2\Delta I_{13}(t)\Delta t^2 + 2B\Omega\Delta I_{23}(t)\Delta t}{2AB} \tag{4.44a}$$

$$m'_2(t) = \frac{-(C-A)\Omega^2\Delta I_{23}(t)\Delta t^2 - 2A\Omega\Delta I_{13}(t)\Delta t}{2AB} \tag{4.44b}$$

The same procedure can be applied to the case $A > C > B$, which results in

$$m_1''(t) = \frac{(C-B)\Omega^2 \Delta I_{13}(t)\Delta t^2 + 2B\Omega\Delta I_{23}(t)\Delta t}{2AB} \tag{4.45a}$$

$$m_2''(t) = \frac{-(A-C)\Omega^2 \Delta I_{23}(t)\Delta t^2 - 2A\Omega\Delta I_{13}(t)\Delta t}{2AB} \tag{4.45b}$$

4

5

PAPER 3: ROTATIONAL DYNAMICS OF TIDALLY DEFORMED PLANETARY BODIES AND VALIDITY OF FLUID LIMIT AND QUASI-FLUID APPROXIMATION

H.Hu,[1] W. van der Wal[1], L.L.A.Vermeersen[1]

To be submitted to *Icarus*

For a long time, the reorientation or true polar wander (TPW) of visco-elastic bodies has been studied with approximated solutions. Two types of methods are commonly addopted: those based on the quasi-fluid approximation (e.g. (Ricard et al., 1993)) and those that only consider the final reorientation (fluid limit) (e.g. (Matsuyama and Nimmo, 2007)). Recently, Hu et al. (2017b) generated a dynamic solution for calculating the reorientation of tidally deformed bodies but did not provide the links between the dynamic and the fluid limit solutions. This paper provides a semi-analytical method for calculating the reorientation of tidally deformed bodies and shows the relation between the dynamic and fluid limit solutions. Most importantly, we provide a criterion, the fluid limit process number $\mathscr{F}$, to test for a given model and estimated TPW speed if the quasi-fluid approximation or fluid limit solution is valid. This number is a quantitative description of how close the body stays in hydrostatic equilibrium during a reorientation process. We use this number to obtain the largest allowed TPW speed of Mars for various viscosities to use the approximated solution.

[1]Delft University of Technology

5.1. INTRODUCTION

For a rotating tidally locked planetary body, its orientation is stable when the rotational axis coincides with the principal axis with the largest moment of inertia and the tidal bulge is pointing towards the source of the tidal potential. This state corresponds to the minimum potential of the body when its viscoelastic part is fully relaxed. Perturbations such as mass redistribution, which changes the body's moment of inertia, will cause the body to reorient until a new minimal potential state is achieved. Such reorientation is often referred to as true polar wander (TPW) which is the displacement of the rotational/tidal axis with respect to surface topography or internal signatures. TPW is a common explanation for many surface features especially when they are present at or near the polar or equator such as the Tharsis plateau on Mars (Bouley et al., 2016), the tiger stripes on Enceladus (Nimmo and Pappalardo, 2006), the heart-shaped Sputnik Planitia on Pluto (Keane et al., 2016), etc.

The mathematical description of TPW includes the Liouville equation which represents the conservation of the angular momentum in the body-fixed frame and the moment of inertia equation which describes the change in the inertia tensor due to the deformation of the body and the mass redistribution. Due to the viscoelasticity of the body, computing the deformation involves convolution of the tidal Love number with the centrifugal and tidal potential, which increases the difficulty to solve these two equations analytically. Large angle TPW has been studied with approximated solutions such as those based on the quasi-fluid approximation which approximates the Love number with its first order Taylor expansion (e.g. (Spada et al., 1992a; Ricard et al., 1993; Cambiotti et al., 2010; Harada, 2012; Chan et al., 2014; Moore et al., 2017)). When a tidal bulge is present, the situation becomes even more difficult since the reorientation of the body does not only concern the relocation of the rotational axis, but also the tidal axis in which case the traditional rotational theory, linear or nonlinear, can not be applied anymore. Instead, most previous studies do not seek a dynamic solution for the reorientation of a tidally deformed body but only calculate the body's final reorientation given a perturbation. This approach considers the stabilizing effect of the lithosphere on the planetary body which was first brought up by Willemann (1984) and later studied by Mitrovica et al. (2005); Cambiotti et al. (2010); Harada (2012); Chan et al. (2014); Harada and Xiao (2015); Moore et al. (2017). Simply speaking, the viscoelastic body does not show any resistance to the change in the direction of the centrifugal or tidal force in the long-term since all the accumulated stress in the viscoelastic part eventually relaxes. As a result, the final reorientation of the body is only determined by the non-viscous part, usually the elastic lithosphere. Adopting this concept, Matsuyama and Nimmo (2007) provided a method to calculate the final state of a tidally deformed body with an elastic lithosphere. For a Heaviside load, the method from Matsuyama and Nimmo (2007) only provides the final position for the rotational and tidal axes but not the reorientation path. When the size of the load changes, e.g. if the mass anomaly is caused by accumulation of volatile material in which the size of the mass anomaly is a ramp function, the method from Matsuyama and Nimmo (2007) does provide a reorientation path, but the axes can only follow these paths when the body is fully relaxed at any moment of the reorientation. As a result, the method of Matsuyama and Nimmo (2007) is referred to as the fluid limit solution. If the speed of TPW is very slow, the body has more time to relax and will be closer to the fluid limit state. Then the fluid limit solution will be close to the dynamic solution. In this case, the body acts

like an inviscid body. On the other hand, as pointed out in (Hu et al., 2017a), as the change in the load decreases, deformation based on the quasi-fluid approximation approaches the fluid limit solution which itself is close to the dynamic solution. Based on this, the fluid limit solution and quasi-fluid approximation can both be valid when the TPW speed is slow enough. However, it is not known how slow the TPW needs to be so that these approximated solutions are accurate enough.

Recently, Hu et al. (2017b) developed an iterative procedure to provide a dynamic solution for calculating the reorientation of a rotating tidally deformed body without a lithosphere. However, Hu et al. (2017b) could not provide a comparison with the fluid limit solution because of lack of the lithosphere. This is because in (Hu et al., 2017b), the change in the moment of inertia is calculated numerically either by a finite-element package or by direct convolution. This is computationally expensive and is not suitable to deal with a lithosphere which is usually simulated with an extremely high viscosity (effectively elastic). Hu et al. (2017a) provided an analytical solution for calculating the inertia tensor without approximating the Love number and studied the effect of the lithosphere, referred to as a remnant bulge, on planetary bodies without a tidal bulge. Adding the tidal potential to the model and combining this analytical expression for the inertia tensor with the algorithm developed in Hu et al. (2017b) generates a semi-analytical method which can deal with tidally deformed bodies with a lithosphere. Including the influence of a lithosphere is crucial to give a correct prediction of TPW since it affects both the TPW speed and the final reorientation Mitrovica et al. (2005); Harada (2012); Chan et al. (2014); Moore et al. (2017); Hu et al. (2017a).

The first purpose of this paper is to establish a semi-analytical solution for reorientation of a rotating tidally deformed body with a lithosphere. The results will be compared with the fluid limit solution. Secondly, we want to provide a criterion to establish under which circumstances the approximated solutions, namely the fluid limit solution and those based on the quasi-fluid approximation, can be valid for a given interior model and estimated TPW speed. This can help us to either properly interpret previous studies based on approximated solutions or choose a valid method in future studies. In the next section, we first introduce the fluid limit solution from Matsuyama and Nimmo (2007) and establish our dynamic solution. In section 5.3, we compare both methods for a Heaviside load and show the effect of the size of the tidal bulge on the reorientation. The size of the tidal bulge can potentially change the path and speed of the TPW which has not been studied yet. In section 5.4, the reorientation for a ramp type load is compared between the two methods and we provide a criterion for testing the validity of the fluid limit solution. A Mars model is tested in section 5.5 and we show that the criterion can provide the condition for which both the fluid limit solution and solutions based on the quasi-fluid approximation are valid.

5.2. METHOD

In this section, we first introduce the fluid limit method by Matsuyama and Nimmo (2007) which calculates the final state of a reorientation of a planetary body with an elastic lithosphere. Then we establish our dynamic solution by combining the iterative algorithm introduced in Hu et al. (2017b) and the analytical solution of the change in the inertia tensor

given by (Hu et al., 2017a).

5.2.1. FLUID LIMIT SOLUTION OF WILLEMANN (1984); MATSUYAMA AND NIMMO (2007)

Willemann (1984); Matsuyama and Nimmo (2007) are concerned with the final state of a reorientation of a tidally deformed body with an elastic lithosphere. This kind of stratified body usually contains a layer of lithosphere, one or several layers of mantle and a core. Since the viscoelastic mantle and inviscid core (if it is liquid) do not show any resistance against a reorientation in the long-term, the final state of the body only depends on the initial stress-free shape of the lithosphere and the mass anomaly which causes the reorientation. The inertia tensor associated with the lithosphere of a tidally deformed body together with the mass anomaly can be written as (Matsuyama et al., 2014)

$$
I_{i,j} = \frac{\Delta k^T \Omega^2 a^5}{3G}\left(e_i^R e_j^R - \frac{1}{3}\delta_{ij}\right) - \frac{\Delta k^T \Omega^2 a^5}{3G}\left(\frac{3M_C}{M+M_C}\right)\left(e_i^T e_j^T - \frac{1}{3}\delta_{ij}\right)
$$
$$
+(1+k^L)C_{i,j} \tag{5.1}
$$

where the first term on the right-hand side stands for the deformation due to the centrifugal force, the second term is the contribution from the tidal deformation and the last term is from the mass anomaly. G is the gravitational constant and a is the radius of the planet. e^R and e^T are unit vectors giving the initial directions of the rotational and tidal axes. Ω is the initial rotational speed and M, M_C are the mass of the body and its orbiting host, respectively. Δk^T stands for either the mode strength associated with the slower transient mode (Sabadini et al., 2016) of the lithosphere (high viscous case) or the difference between the fluid tidal Love numbers of the body without and with the lithosphere (elastic case). k^L is the fluid load Love number. From the term $\frac{3M_C}{M+M_C}$, which will be called tidal potential factor, we can see that when $M_C >> M$, such as for satellites like Europa or Enceladus, the tidal deformation is about three times the magnitude of the centrifugal part. For Pluto, however, the tidal part contributes only about 11% of the magnitude of its centrifugal deformation considering the mass of the Charon is 12.2% of the Pluto. We will show in section 5.3 that this term has a significant influence on the reorientation path. When the inertia tensor of the lithosphere and mass anomaly is given by equation 5.1, the final reorientation can be obtained by diagonalizing the matrix I_{ij}. the largest and smallest eigenvectors represent the final direction of the rotational and tidal axes.

When a Heaviside load is applied, the fluid limit solution only gives the final state and we do not know the process or the path of the reorientation. When the load is varying and time-dependent, so that C_{ij} and I_{ij} in equation 5.1 become $C_{ij}(t)$ and $I_{ij}(t)$, the fluid limit solution can provide a time-dependent reorientation path. We will explore in section 5.4 in which case this path is valid to represent the real reorientation path.

5.2.2. A DYNAMIC SOLUTION

The difficulty to obtain a dynamic solution of the reorientation for a tidally deformed body is that the perturbation on both the rotational axis as well as the tidal axis need to be cal-

culated and the two perturbations need to be combined to fit the constraint that the angle between the rotational and tidal axes at a given moment is fixed (i.e. perpendicular when the axial tilt can be ignored). Hu et al. (2017b) established a method which treats the perturbation on the tidal axis in the same way as the rotational axis by applying the linearized Liouville equation. In (Hu et al., 2017b), the change in the inertia tensor is obtained by numerical convolution or with a finite element package, which makes the method not suitable for dealing with a lithosphere with extremely high viscosity. Hu et al. (2017a) provided an analytical way to obtain the change in the inertia tensor for a full-Maxwell rheology scheme, in contrast with approaches that based on the quasi-fluid approximation (e.g. Ricard et al. (1993)). The purpose of this subsection is to combine the analytical way of calculating change in the inertia tensor presented in (Hu et al., 2017a) and the iterative algorithm in Hu et al. (2017b) to obtain a semi-analytical solution for reorientation of a tidally deformed body with a high-viscous lithosphere.

For a centrifugally and tidally deformed body, the time-dependent change in the inertia tensor can be written as

$$
\begin{aligned}
I_{i,j}(t) = I\delta_{ij} + \frac{k^T(t)a^5}{3G} * \left[\omega_i^R(t)\omega_j^R(t) - \frac{1}{3}\omega_l^R\omega_l^R\delta_{ij} \right] \\
- \frac{k^T(t)a^5}{3G} * \left[\omega_i^T(t)\omega_j^T(t) - \frac{1}{3}\omega_l^T\omega_l^T\delta_{ij} \right] + [\delta(t) + k^L(t)] * C_{i,j}(t)
\end{aligned}
\tag{5.2}
$$

where I is the principle moment of inertia of the unloaded laterally homogeneous spherical body. $\boldsymbol{\omega^R} = (\omega_1^R, \omega_2^R, \omega_3^R)$ is the rotation vector whose magnitude is the rotational speed. $\boldsymbol{\omega^T} = (\omega_1^T, \omega_2^T, \omega_3^T)$ is the tidal vector whose magnitude satisfies

$$
|\boldsymbol{\omega^T}| = \sqrt{\frac{3GM_T}{a^3}}
\tag{5.3}
$$

Following the procedure shown in (Hu et al., 2017a), in order to solve equation 5.2, we approximate both $\boldsymbol{\omega^R}$ and $\boldsymbol{\omega^T}$ as piecewise linear functions

$$
\omega_i^R(t) = \sum_{p=1}^{n} \omega_{i,p}^R
\tag{5.4a}
$$

$$
\omega_i^T(t) = \sum_{p=1}^{n} \omega_{i,p}^T
\tag{5.4b}
$$

where

$$\omega_{i,p}^R = \left(W_{i,p-1}^R + \frac{W_{i,p}^R - W_{i,p-1}^R}{T_p - T_{p-1}} (t - T_{p-1}) \right) H(t - T_{p-1}) H(T_p - t) \tag{5.5a}$$

$$\omega_{i,p}^T = \left(W_{i,p-1}^T + \frac{W_{i,p}^T - W_{i,p-1}^T}{T_p - T_{p-1}} (t - T_{p-1}) \right) H(t - T_{p-1}) H(T_p - t) \tag{5.5b}$$

Here $H(t)$ is Heaviside function. At time $t = T_p$, $p = 1, 2, ... n$, we have $\boldsymbol{\omega}_i^R(T_p) = (W_{1,p}^R, W_{2,p}^R, W_{3,p}^R)$ and $\boldsymbol{\omega}_i^T(T_p) = (W_{1,p}^T, W_{2,p}^T, W_{3,p}^T)$. With equation 5.4, equation 5.2 and its derivative at time $t = T_n$ can be expressed analytically as

$$I_{i,j}(T_n) = I\delta_{i,j} + \frac{a^5}{3G} [(A_{i,j}(T_n) + B_{i,j}) - \frac{1}{3} \sum_{k=1}^{3} (A_{k,k}(T_n) + B_{k,k})]$$
$$- \frac{a^5}{3G} [(\bar{A}_{i,j}(T_n) + \bar{B}_{i,j}) - \frac{1}{3} \sum_{k=1}^{3} (\bar{A}_{k,k}(T_n) + \bar{B}_{k,k})] + E_{i,j}(T_n) \tag{5.6}$$

$$\dot{I}_{i,j}(T_n) = \frac{a^5}{3G} [(C_{i,j}(T_n) + D_{i,j}) - \frac{1}{3} \sum_{k=1}^{3} (C_{k,k}(T_n) + D_{k,k})]$$
$$+ \frac{a^5}{3G} [(\bar{C}_{i,j}(T_n) + \bar{D}_{i,j}) - \frac{1}{3} \sum_{k=1}^{3} (\bar{C}_{k,k}(T_n) + \bar{D}_{k,k})] + \dot{E}_{i,j}(T_n) \tag{5.7}$$

The expressions for $A_{ij}, B_{ij}, C_{ij}, D_{ij}$ and $\bar{A}_{ij}, \bar{B}_{ij}, \bar{C}_{ij}, \bar{D}_{ij}$ can be found in (Hu et al., 2017a).

As shown in (Hu et al., 2017a), for a given hydrostatic state the model needs to be loaded with a corresponding centrifugal and tidal force (not necessarily the same as the present-day values) for a time span T_h after which all the modes are sufficiently relaxed. So for the first two time steps, we have

$$T_0 = 0 \tag{5.8a}$$
$$T_1 = T_h \tag{5.8b}$$
$$(W_{1,0}^R, W_{2,0}^R, W_{3,0}^R) = (W_{1,1}^R, W_{2,1}^R, W_{3,1}^R) = \boldsymbol{\omega}_0^R \tag{5.8c}$$
$$(W_{1,0}^T, W_{2,0}^T, W_{3,0}^T) = (W_{1,1}^T, W_{2,1}^T, W_{3,1}^T) = \boldsymbol{\omega}_0^T \tag{5.8d}$$

where $\boldsymbol{\omega}_0^R$ and $\boldsymbol{\omega}_0^T$ are the initial rotational and tidal vectors before the reorientation is triggered by the mass anomaly. When the T_p, $W_{i,p}^R$ and $W_{i,p}^T$ are known for $p = 1, 2, .. n - 1$, given a new time step step T_n, the new reorientation $W_{i,n}^R$ and $W_{i,n}^T$ can be obtained by the iterative algorithm given by Hu et al. (2017b). The procedure is shown in appendix I of chapter 3.

Comparing with the original procedure in Hu et al. (2017b), the main feature of the method presented in this section is that we can deal with layers with extremely high viscosity. As a result, we can validate the iterative algorithm by comparing the results with those obtained by the fluid limit method from Matsuyama and Nimmo (2007) which will be discussed in the following sections.

5.3. Reorientation due to a Heaviside load

As a first comparison and validation for the dynamic method, we simulate the reorientation of a tidally deformed body with an effectively elastic (very high viscosity) lithosphere due to a Heaviside load. In this case, the fluid limit solution only provides the final reorientation, but we can test if the dynamic solutions approach the predicted end positions. We use the same Triton model which was used in (Hu et al., 2017b) and add a 10 km lithosphere which has the same density and rigidity as the Ice I layer but with a viscosity of 10^{32} Pa s which guarantees that this layer behaves elastic during the simulated period. The interior model is shown in table 5.1.

Table 5.1: Properties of Triton

Layer	Outer Radius (km)	Density (kg m^{-3})	Shear Modulus (Pa)	Viscosity (Pa s)
Ice Shell	1352	937	3.6×10^9	1×10^{32}
Ice I	1342	937	3.6×10^9	1×10^{21}
Ice II	1100	1193	6.2×10^9	1×10^{21}
Mantle	950	3500	65×10^9	1×10^{19}
Core	600	5844.8	0	0

We first calculate the fluid limit solution for a positive mass anomaly of magnitudes ranging from 0 to 6×10^{17} kg, which is large enough to be relocated close to the sub-Neptune point for the Triton model used. In order to show the complete reorientation, both the displacements of the rotational and tidal axes need to be shown in the body-fixed frame. As a result, we show the reorientation by the relocation of the mass anomaly in the bulge-fixed frame whose Z-axis and X-axis are aligned with the rotational and tidal axes. The results are shown in figure 5.1, in which the fluid limit and dynamic solutions of three magnitudes of the mass anomaly: 1.5×10^{17} kg, 3×10^{17} kg and 6×10^{17} kg are shown separately. We can see that the dynamic solutions approach the end solution given by the fluid-limit method. Irrespective of the magnitude of the mass anomaly, the reorientation of a body with lithosphere shows similar behaviour to that without a lithosphere as shown in Hu et al. (2017b). The process is first dominated by a relative fast reorientation around the tidal axis to relocate the mass anomaly close to the equator, then followed by a relatively slow reorientation around the rotational axis to push the mass anomaly close to the sub-host point. When positive mass anomalies are larger than certain values, it can be pushed towards the equator and further increasing the mass anomaly only changes its position to be more close to the sub-host or anti-host point. As a result, the conclusion in (Hu et al., 2017b) that positive mass anomalies are more likely to be found around the equator, still holds for models with a lithosphere. The reason behind the fast reorientation around the tidal axis and the slow reorientation around the rotational axis has been discussed in detail by Hu et al. (2017b) as the stronger

resistance of the body against the reorientation around the rotational axis compared to that around the tidal axis. It can also be seen in figure 5.1 that for the Heaviside load, the path of the fluid limit solution can only be close to the dynamic solution when the magnitude of the mass anomaly is relatively small.
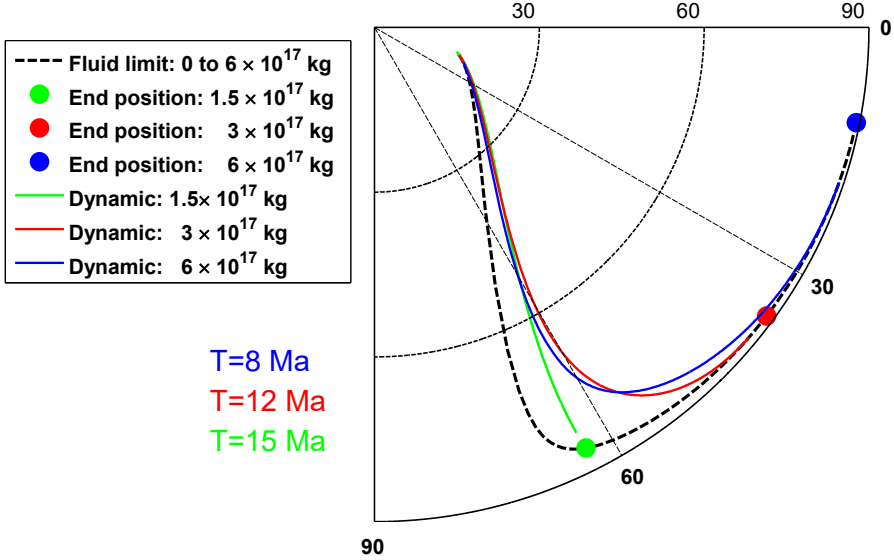

Figure 5.1: The movement of the mass anomaly in the bulge-fixed frame in which the Z-axis and X-axis always align with the rotational (at the origin) and tidal axes (0 degree longitude line), respectively. The mass anomaly is originally located at 15 degree colatitude and 15 degree longitude. The black dashed line represents the fluid limit solution of the mass anomaly changing from 0 kg to 6×10^{17} kg where the green, red and blue dots give the end location predicted by the fluid limit method for a Heaviside load with a magnitude of 1.5×10^{17} kg, 3×10^{17} kg and 6×10^{17} kg, respectively. The coloured lines represent the dynamic solutions of the corresponding magnitude simulated with period T.

Next, we demonstrate the effect of the tidal potential factor $\alpha = \frac{3M_C}{M+M_C}$, which represents the proportion of the magnitude of the tidal potential to that of the centrifugal potential for a tidally locked body, on the path and speed of a reorientation. We use the same Triton model as in figure 5.1 but without the elastic lithosphere and trigger TPW by a constant surface mass anomaly of 6×10^{17} kg. The tidal potential factor is scaled from 0 (no tidal bulge) to 3 (the largest and realistic case). When $\alpha = 0$, the TPW path is calculated by the method from (Hu et al., 2017a). The period of the Chandler wobble can be calculated as

$$T = \frac{2\pi}{\Omega} \sqrt{\frac{AB}{(C-A)(C-B)}} \tag{5.9}$$

where A,B and C can be obtained by the time limit of equation 5.2 for components I_{11}, I_{22} and I_{33} and setting tidal potential factor α to 0 in this case. With the rotational speed of Triton, it can be calculated that its Chandler wobble has a period of about 50 years which is far shorter than the dominant relaxation time of the body. Thus even without the tidal bulge, the TPW path on Triton would be like that of the Earth or Mars, instead of a mega-wobble like on Venus. We simulate the reorientation with a period at which the mass anomaly

reaches 5 degrees away from its predicted end position. The results are shown in figure 5.2. It can be noticed that with a larger tidal potential factor α, the path of the mass anomaly is more likely to be dominated by the reorientation around the tidal-axis first which gives the detour on the path. As a result, for satellites like Europa, Enceladus and Triton, the reorientation path should be like the blue line while for Pluto ($\alpha \approx 0.1$), the path is almost a straight line towards the sub-Charon point or its antipodal. Because the tidal bulge provides an extra stabilizing effect in addition to the centrifugal bulge, as the tidal bulge shrinks, the speed of the reorientation increases. The decrease of α also causes an increase of the elastic jump in the beginning of the reorientation (the gap between the initial position of the mass anomaly and the start of the coloured lines) which is very large (4 to 16 degrees) in this case. Such elastic jump represents the amplitude of the Chandler wobble triggered by the mass anomaly in the beginning, so a mass anomaly with the magnitude of 6×10^{17} kg will trigger a very large Chandler wobble and a larger tidal bulge decreases the magnitude of the wobble. From figure 5.2, it can be understood that the reorientation on icy satellites like Enceladus or Europa will look completely different than the reorientation on Pluto despite their similar internal structure (ice shell lithosphere, water ocean and a silicon mantle/core) and rotational state (tidally locked and rotational period in days).

α=3   T=2715 ka
α=2.5 T=2238 ka
α=2   T=1779 ka
α=1.5 T=1348 ka
α=1   T=978 ka
α=0.5 T=696 ka
α=0.1 T=440 ka
α=0   T=355 ka
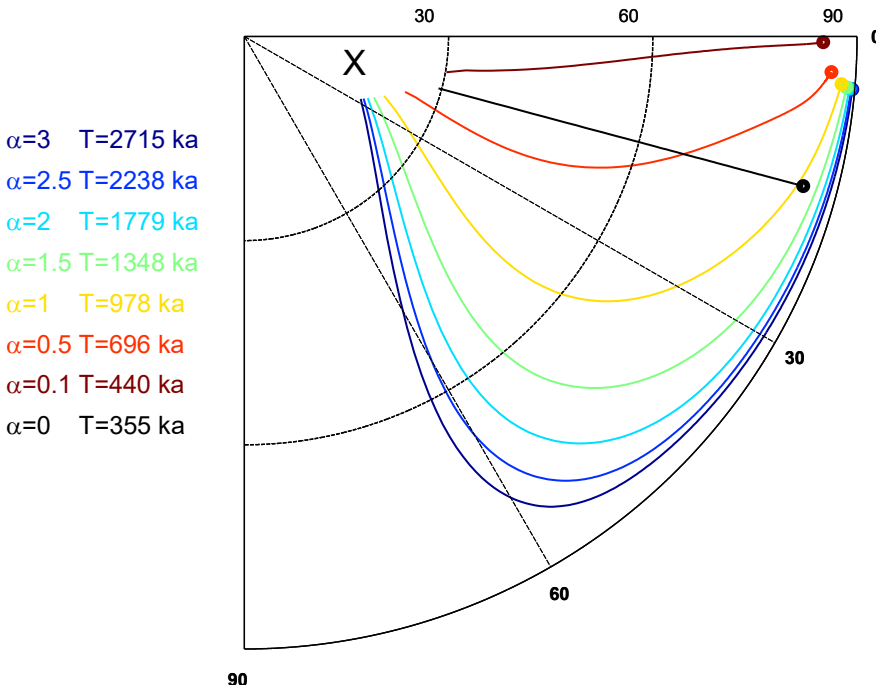
Figure 5.2: The movement of the mass anomaly in the bulge-fixed frame of a Triton model with its tidal deformation factor α scaled from 0 (no tidal bulge) to 3 (the real case). The simulation for each α runs for a period of T with which the mass anomaly reaches 5 degrees away from its end position. The black cross represents the initial position of the mass anomaly (15 degrees colatitude and 15 degrees longitude) while the coloured dots are the end positions for each α.

5.4. REORIENTATION DUE TO A RAMP LOAD AND CRITERION FOR A FLUID LIMIT PROCESS

As we have seen from last section, the reorientation path generated by the fluid-limit method with a changing load does not represent the actual path for a Heaviside load. A natural question following this would be: will the dynamic solution for a changing load match the result from the fluid-limit solution? For the same load, the key factor here is how fast the reorientation is. If the rotational and tidal axes change slowly and the equatorial and tidal bulges have more time to readjust to the new position (the fluid limit position), then the process of the reorientation would be more like as on a fluid(inviscid) body (without considering the convective motions). As a result, we can expect that the dynamic solution of a very slowly changing load will be similar to the fluid-limit solution. The purpose of this section is to test this hypothesis and more importantly, to provide a criterion to determine how slow the changes in the rotational and tidal axes need to be so that the reorientation process can be considered as a fluid limit process.

We first test the hypothesis. The same type of model as in figure 5.1 is used and the dynamic solutions are calculated for a ramp load where the positive mass anomaly increases linearly from 0 to 6×10^{17} kg for different durations: $5, 20, 60, 120, 360$ million and 1 billion years. The results are shown in figure 5.3. For the model we used, it can be shown that it takes about 50 million years for its degree 2 potential Love number to reach about 99.95% of its fluid Love number. Thus for 1 billion years, the process is already very slow compared to the dominant relaxation time of the model. Another important information obtained in figure 5.3 is that for a tidally deformed body, different load changing speed results in different reorientation path. As a result, a specific reorientation path is a very strong constraint for the loading history as well as the viscosity of the model.

In figure 5.3, we see that as the change in the load slows down, the dynamic solution approaches the fluid limit solution. However, even for the period of 360 million years, the difference is still visible, which suggests that the validity of the fluid limit solution for a changing load is also limited. Consequently, we want to provide a simple quantitative criterion to test that, given an interior model, how slow the reorientation must be so that the process can be considered as a fluid limit process. Or the other way around, given a reorientation process, e.g. estimated from geographic analysis, how low the viscosity of the interior must be so that the model stays in hydrostatic equilibrium during the process of a reorientation. This allows future studies to rely on the simple fluid limit method.

When a layered model is given, the tidal Love number in the Laplace domain for a given harmonic degree can be expressed as (Peltier, 1974):

$$k^T(s) = k_e^T + \sum_{i=1}^{m} \frac{k_i^T}{s - s_i} \tag{5.10}$$

where k_e^T is the elastic Love number, k_i^T are the residues of each mode and s_i are the inverse
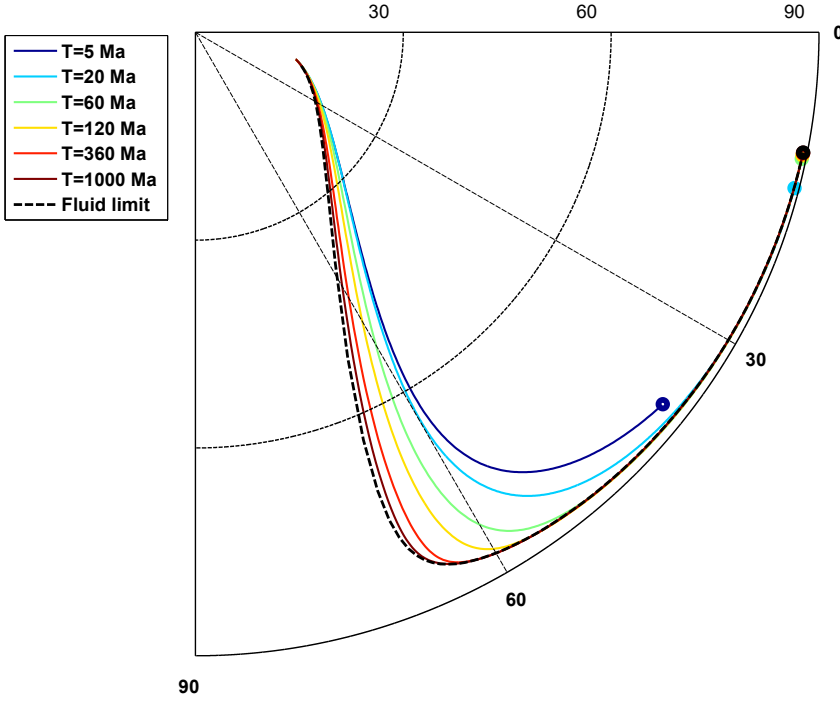
Figure 5.3: The movement of the mass anomaly in the bulge-fixed frame of the Triton model ($\alpha = 3$) in which the Z-axis and X-axis always align with the rotational (at the origin) and tidal axes (0 degree longitude line), respectively. The mass anomaly is originally located at 15 degrees latitude and 15 degrees longitude. The black dashed line represents the fluid limit solution of the mass anomaly changing from 0 kg to 6×10^{17} kg. The coloured lines represent the dynamic solutions for the load changes linearly during the period of T.

relaxation times. In the following, we omit the superscript T which stands for "tidal". The fluid Love number is the sum of the strength of the elastic part k_e and the viscous relaxation characterised for each mode as $-k_i/s_i$:

$$k_f = \quad k_e - \sum_{i=1}^{m} \frac{k_i}{s_i} \tag{5.11}$$

If the Love number only contains the elastic part k_e^T, then any deformation will happen instantaneously. This means that during a reorientation or TPW, the equatorial bulge readjusts immediately following the change of the rotational axis. Then any process will be a fluid limit process in this case. Because of the viscous relaxation characterized by $k_i^T/(s-s_i)$, which represents a delayed readjustment in the time domain, the axis of the principle moment of inertia of the body lags behind the rotational axis. Mathematically, when the principle axis of moment does not coincide with the rotational axis, the inertia tensor in the frame of the rotational and tidal axes will have non-zero cross products. From this aspect, a reorientation or TPW process can only be considered as a fluid limit process when the magnitudes of the cross products are small enough. Therefore, we want to formulate and

approximate the cross products in the inertia tensor using the tidal Love number. We need to be aware that since we only consider the readjustment of the body itself, the inertia tensor should not include the mass anomaly which triggers the reorientation.

We consider a case where the rotational axis is with a unit rotating speed. We let the rotational axis move with a constant speed V in the X-Z plane of the body fixed frame:

$$\boldsymbol{\omega}^R = \quad (\sin(V t), 0, \cos(V t)) \tag{5.12}$$

The inertia tensor associated with the equatorial readjustment can be written as

$$\boldsymbol{I_N} \quad = \quad \frac{k^T(t) a^5}{3G} * \left[\omega_i^R(t) \omega_j^R(t) - \frac{1}{3} \omega_l^R \omega_l^R \delta_{ij} \right] \tag{5.13}$$

We fully normalized the change in the inertia tensor for the equatorial bulge readjustment, which means that the gravitational constant and radius are set to one and the tidal Love number is scaled with its fluid Love number. With $G = a = 1$ and

$$k^T(t) = \frac{k(t)}{k_f} \tag{5.14}$$

we have

$$\boldsymbol{I_N} \quad = \quad \frac{k(t)}{k_f} * \begin{bmatrix} \sin^2(V t) - 1/3 & 0 & \sin(V t)\cos(V t) \\ 0 & -1/3 & 0 \\ \sin(V t)\cos(V t) & 0 & \cos^2(V t) - 1/3 \end{bmatrix} \tag{5.15}$$

This equation can be solved analytically using the Laplace transform. We transform this matrix in the frame whose Z'-axis is the rotational axis. With the transformation matrix

$$\boldsymbol{Q} \quad = \quad \begin{bmatrix} \cos(V t) & 0 & \sin(V t) \\ 0 & 1 & 0 \\ -\sin(V t) & 0 & \cos(V t) \end{bmatrix} \tag{5.16}$$

we have

$$\boldsymbol{I_N'} \quad = \quad \boldsymbol{Q'} \mathscr{L}^{-1}\{\mathscr{L}\{\boldsymbol{I_N}\}\} \boldsymbol{Q} \tag{5.17}$$

where $\mathscr{L}^{-1}$ and $\mathscr{L}$ are the inverse Laplace transform and Laplace transform, respectively. As the time t proceeds, $\boldsymbol{I_N'}$ approaches a stable state which gives the characteristic values when all the modes are sufficiently relaxed. We take the limit of infinite time of $\boldsymbol{I_N'}$ and obtain

$$\boldsymbol{I}^* = \lim_{t \to \infty} \boldsymbol{I}'_N =$$

$$\frac{1}{k_f} \begin{bmatrix} -\frac{1}{3}(k_e - \sum_{i=1}^{m} \frac{k_i(s_i^2 - 2V^2)}{s_i^3 + 4s_i^2 V^2}) & 0 & \sum_{i=1}^{m} \frac{k_i V}{s_i^2 + 4V^2} \\ 0 & -\frac{1}{3}(k_e - \sum_{i=1}^{m} \frac{k_i}{s_i}) & 0 \\ \sum_{i=1}^{m} \frac{k_i V}{s_i^2 + 4V^2} & 0 & \frac{2}{3}(k_e - \sum_{i=1}^{m} \frac{k_i(s_i^2 + V^2)}{s_i^3 + 4s_i^2 V^2}) \end{bmatrix}$$

It can be easily seen that when $V = 0$, $\boldsymbol{I}^*$ degenerates into the matrix

$$\boldsymbol{I}^*|_{V=0} = \begin{bmatrix} -\frac{1}{3} & 0 & 0 \\ 0 & -\frac{1}{3} & 0 \\ 0 & 0 & \frac{2}{3} \end{bmatrix}$$

which is the fully normalized change in the principle moment of inertia for the equatorial bulge. The non-diagonal component of $\boldsymbol{I}^*$, $\sum_{i=1}^{m} \frac{k_i V}{s_i^2 + 4V^2}$, can now represent the scale of the delayed readjustment due to the viscous response.

We define a dimensionless *fluid limit process number*

$$\mathcal{F} = \frac{1}{(1+\alpha)k_f} \sum_{i=1}^{m} \frac{k_i V_{max}}{s_i^2 + 4V_{max}^2} \tag{5.18}$$

where α is the tidal potential factor, V_{max} is the maximum velocity of the polar wander estimated either from geographic analysis or from fluid limit solution. When only the centrifugal bulge is present ($\alpha = 0$), $\mathcal{F}$ is the normalized product of inertia and this number needs to be small enough so that the process in which the rotational axis changes with speed V can be considered as a fluid limit process. When calculating $\mathcal{F}$ for models whose lithosphere has a high viscosity instead of being elastic, the transient mode associated with the lithosphere needs to be removed. Thus in equation 5.18, $m - 1$ instead of m modes need to be considered. For the situations presented in figure 5.3, it can be shown that the ramp loads with periods 20, 60, 360 million and 1 billion years correspond to the fluid process number being about $2.7 \times 10^{-2}, 1.5 \times 10^{-2}, 2.9 \times 10^{-3}$ and 1×10^{-3}.

Fluid limit process number provides a quantitative description of how close the body stays in hydrostatic equilibrium during a reorientation process. However, it is difficult to directly link the fluid process number to the error level of an approximated solution. From the example shown in figure 5.3 and other experiments we have conducted on models of terrestrial planets the Earth, Mars and Venus as well as icy moons, we can conclude that $\mathcal{F}$ needs to be smaller than about 10^{-3} so that the fluid limit solutions are within an acceptable global error level. When $\mathcal{F}$ is larger than 1×10^{-3}, the TPW speed of a body without tidal bulge or both the path and speed of the reorientation for a tidally deformed body will have large errors. This will be further discussed in the next section.

5.5. VALIDITY OF FLUID AND QUASI-FLUID APPROXIMATION

Physically, the fluid limit solution assumes that the equatorial and tidal bulge readjust to the new directions of the rotational and tidal axes instantaneously. This means that for a viscous body the fluid limit solution always overestimates the speed of the readjustment. In contrast with this, the TPW solution based on the quasi-fluid approximation (e.g. Ricard et al. (1993); Spada et al. (1992a); Harada (2012); Harada and Xiao (2015); Chan et al. (2014)), underestimates the readjustment speed of the bulge (Hu et al., 2017a). As pointed out by (Hu et al., 2017a), when the change in the load is slow enough, the solution based on the quasi-fluid approximation will approach the fluid limit solution. In this section, we want to confirm this statement and show that the fluid process number $\mathscr{F}$ can provide a criterion for which both the fluid-limit solution and the quasi-fluid approximation are valid.

We choose a model which does not have a significant tidal bulge, Mars, so that we can apply the non-linear methods based on the quasi-fluid approximation. When the tidal bulge is small or can be neglected and the period of the Chandler wobble is much shorter than the dominant relaxation time of the interior and the characteristic time of the loading or forcing, based on figure 5.2 we know that the reorientation path for the rotational axis is almost a straight line within the great circle of the surface. In this case, the reorientation paths obtained from different methods are almost the same but the speed can show large differences. We demonstrate this with the Mars model. The interior model of Mars (thickness of each layer, density, rigidity) is chosen according to (Zharkov and Gudkova, 2005) and divided into 5 layers which contain a 50 km lithosphere. The viscosity of the model is divided into an effectively elastic lithosphere, a uniform mantle of viscosities 10^{20} Pa s and an inviscid core. The interior properties are shown in table 5.2.

Table 5.2: Properties of Mars

Layer	Outer Radius (km)	Density (kg m^{-3})	Shear Modulus (Pa)	Viscosity (Pa s)
Lithosphere	3389.5	2004	0.180×10^{11}	1×10^{32}
Upper mantle	3339.5	3605	0.900×10^{11}	1×10^{20}
Shallow lower mantle	2800	3620	0.942×10^{11}	1×10^{20}
Deeper lower mantle	2200	3808	1.030×10^{11}	1×10^{20}
Core	1700	6500	0	0

Again, we test a ramp type load which increases from 0 to 3.5×10^{19} kg linearly in a certain time span. This amount of the mass anomaly is the estimated total mass of the Tharsis plateau which is about $10^{19} \sim 10^{20}$ kg (Hynek and Phillips, 2001; Nimmo and Tanaka, 2005). We compare the dynamic solution obtained by the method presented in (Hu et al., 2017a) with the fluid limit solution and the one which is based on the quasi-fluid approximation from (Chan et al., 2014). The results are shown in figure 5.4. As expected, the speed of TPW from the fluid limit solution is faster while that obtained based on the quasi-fluid approximation is slower. It is also clear that only when the change in the load is slow enough, specifically when $\mathscr{F} < 0.001$, the speed of TPW from the two approximated solutions starts to match the complete dynamic solution.
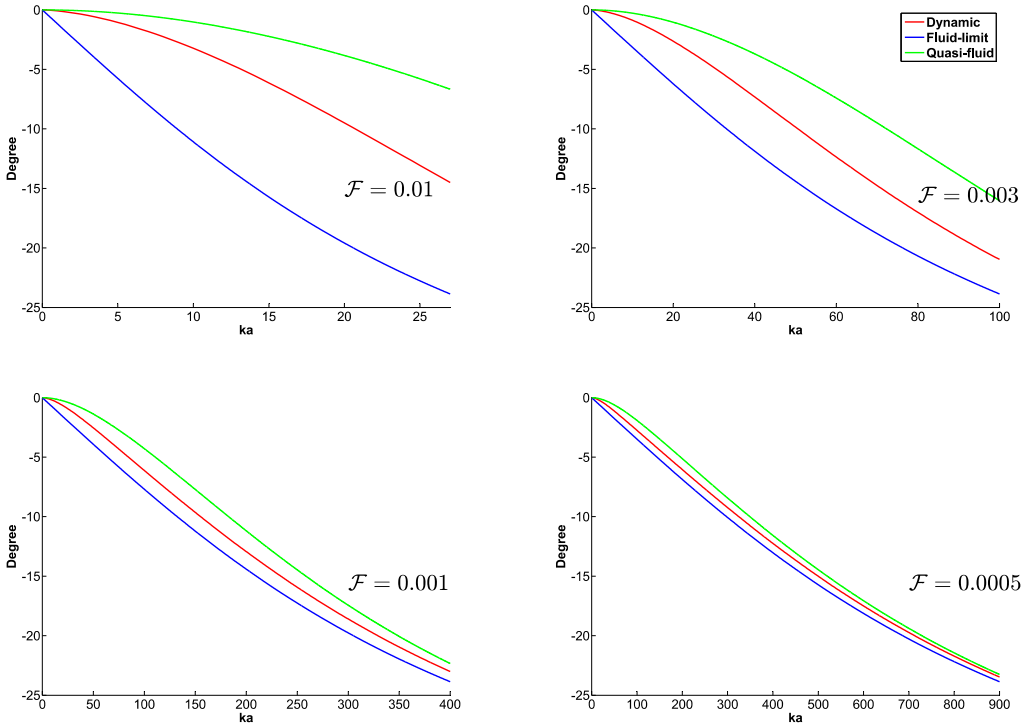
Figure 5.4: TPW on Mars triggered by a mass anomaly changing from 0 to 3.5×10^{19} kg linearly in 27, 100, 400 and 900 thousand years respectively. The mass anomaly is attached at the surface at 45 degrees colatitude. The results are obtained by the dynamic method from this paper (red), fluid-limit solution (blue) and method based on the quasi-fluid approximation (green). The corresponding fluid process number $\mathcal{F}$ for each case is shown in the figure. The viscosity of the Martian mantle is set to 10^{20} Pa s.

From the definition and effect of the fluid limit process number, it can be seen that the following statements are equivalent:

- The fluid limit process number is small enough.

- The axis of the principle moment of inertia of the body and the rotational axis can be considered to coincide.

- The model can be considered to be in hydrostatic equilibrium during the reorientation.

The validity of the approximated method is dependent on the model we use and the fluid limit process number provides a direct indication for the specific case in which the reorientation can be considered as a fluid limit process. This can help us to properly interpret the validity of previous studies of TPW on various planetary bodies or choose an accurate method for future studies.

For Mars, estimates for the viscosities of the mantle range from 10^{19} Pa s to 10^{22} Pa s (Hauck

and Phillips, 2002; Breuer and Spohn, 2006) and the formation history of Tharsis is uncertain. Since the fluid process number is dependent on the largest TPW speed, the largest possible formation speed of Tharsis instead of the average speed should determine the fluid process number. For instance, a quick early formation by volcanic activities followed by a slow upwelling due to tectonic activities results in a larger fluid process number than a constant process with the same average formation speed. Similar to the results in figure 5.4, it can be shown that when the Martian mantle has viscosities of 10^{19}, 10^{20} ,10^{21} or 10^{22} Pa s, the allowed maximum TPW speed for the approximated method to be valid is 0.8 degree/ka, 0.075 degree/ka, 8 degree/ma and 0.8 degree/ma, respectively. Due to all these uncertainties, we need to take caution to use an approximated method for future studies of TPW on Mars.

Planetary bodies which are currently intensively studied such as the Moon of the Earth and icy satellites such as Enceladus and Europa also have large uncertainty on its viscosity. As a result, when TPW is studied on these objects, an estimation of the fluid process number should be conducted first before the choice of the method.

5.6. CONCLUSIONS

We present a semi-analytical method for calculating the dynamic solution for the reorientation of a rotating tidally deformed body. By comparing with the fluid-limit solution, we validate the algorithm developed in (Hu et al., 2017b) for obtaining a time-dependent solution. It is confirmed that the fluid-limit solution and the quasi-fluid approximation are only valid when the reorientation/TPW speed is slow enough.

We provide a simple criterion, the fluid process number $\mathcal{F}$, to test if the fluid-limit solution or the quasi-fluid approximation can be adopted given a specific model and estimated maximum reorientation/TPW speed. The fluid process number can also be used the other way around: if a reorientation/TPW path history is confirmed, the criterion that fluid process number is small enough actually gives a constraint on the viscosity of the model. Concerning previous studies of TPW based on approximated solutions, calculating the fluid process number helps evaluate the validity of the results. For future studies concerning the TPW or reorientation of terrestrial planets or moons, estimating the fluid process number helps to decide whether an approximated solution can be adopted. For instance, when studying a specific planetary body, the mass distribution information can be derived from the gravity data, with which the magnitude of the TPW can be easily estimated by the fluid limit method, given the information about the lithosphere. After this, if the reorientation path or speed is required, e.g. to compare the stress pattern during the TPW with surface geological features, calculating the fluid process number helps to decide whether the reorientation path obtained from the fluid limit method can be directly adopted or a more complex method like in this paper needs to be applied.

6

CONCLUSIONS AND RECOMMENDATIONS

Summarizing the conclusions drawn in chapters 3-5, the first part of this chapter addresses the research questions raised in section 2.6. The second part of this chapter provides an outlook to possible further research and applications.

6.1. CONCLUSIONS

The main purpose of this dissertation is to establish a more general and accurate method to study the rotational variation of planetary bodies and evaluate the approximations taken in previous studies. We established both a numerical iterative procedure which can be combined with a finite element package where lateral heterogeneity and complex rheology can be adopted, as well as a semi-analytical approach by which the influence of the lithosphere and hydrostatic state of the body can be taken into account. With the help of the new method, we explored the influence of the assumptions taken in existing methods, which are introduced in chapter 2, for calculating true polar wander (TPW). More importantly, we can specify under which conditions these assumptions can be adopted and when they give biased results. In the following context, we first summarize the new method in terms of its background, validation and applicability in contrast with the previous methods. We show that the new method satisfies the research goals stated in section 2.6. Next, the specific research questions listed in section 2.6 are answered. At the end of this section, we also summarize the applications shown in chapters 3-5, which provide new insights in rotational variations of various planetary bodies based on the new method.

The new method

As shown in chapter 2, the complete rotational dynamics of a viscoelastic planetary body is governed by two equations: the Liouville equation and the moment of inertia (MoI) equation. In previous studies, three major types of methods for studying TPW were used:

1. Linear method, which linearises the Liouville equation 2.1.

2. Non-linear method, which approximates the Love numbers in order to simplify the moment of inertia equation 2.7.

3. Fluid-limit method, which only calculates the new equilibrium position of the rotational axis when a perturbation in mass distribution is introduced.

Compared with these methods, the main idea of the new method presented in this thesis is to decouple the governing equations 2.1 and 2.7, and combine them in an iterative procedure, as shown in section 2.5.
Solving the MoI equation can either be done analytically (chapter 4) or numerically with a finite element method (chapter 3). In order to solve the Liouville equation in an iterative manner, two situations are considered:

1. The period of the Chandler wobble is much smaller than the dominant relaxation time of the body.

2. The period of the Chandler wobble is comparable to or larger than the dominant relaxation time of the body.

In the first case, the linearized Liouville equation can be used to study the long-term secular change of the reorientation on planets such as the Earth and Mars as well as most of the icy moons. The Chandler wobble periods of these bodies are in the order of years while the

dominant relaxation time of the bodies is above thousands of years. The second case concerns the long-term rotational behaviour of slow-rotating objects such as Venus or studies on short-term rotational behaviour, the Chandler wobble, for fast-rotating objects such as the Earth or Mars.

The new method is validated in three stages:

1. In chapter 3, for small angle TPW on objects without a tidal bulge, the obtained result can match the analytical solution from the linear methods (Wu and Peltier, 1984) to less than 0.1% difference in degree if the step size is chosen to be much smaller (e.g. 1%) than the dominating relaxation time and if we do not update the MoI for the mass anomaly during the TPW. Updating the MoI of the mass anomaly in the bulge-fixed frame actually corrects the intrinsic error in the linear method. This issue will be discussed in more detail in the answer to the first research question.

2. For large angle TPW on objects without a tidal bulge, it has been shown in chapter 5 that if the model does not contain relatively slow modes and the speed of TPW is slow enough, the non-linear method based on the quasi-fluid approximation can be accurate (we answer research question 4 later to show how "slow" the TPW needs to be). And in chapter 3, we show that the TPW obtained by our new method matches that from the non-linear method (Ricard et al., 1993) for models that satisfy these conditions. An example case is the two layer Earth model from table 3.1 (Wu and Wang, 2006) triggered by a mass anomaly with magnitude of 2×10^{19} kg. This mass anomaly is equivalent to the estimated total ice loss during the last ice age (Ricard et al., 1993). We provide a quantitative criterion, the fluid limit process number $\mathscr{F}$ as equation 5.18, to predict for which cases the result from the non-linear method will approach that obtained by our method (chapter 5). This verifies the accuracy of previous studies (Chan et al., 2014; Moore et al., 2017) which are based on the simpler quasi-fluid method.

3. For a tidally deformed body, the obtained reorientation path is validated by the fluid-limit method (Matsuyama and Nimmo, 2007) in the case where the reorientation speed is relatively slow ($\mathscr{F} < 0.001$) compared to the dominant relaxation time of the body (chapter 5). The reason that the validation only applies to a slowly reorienting case is due to the limitation of the fluid limit approximation and this will be discussed in the answer to research question 4. Again, the criterion that the fluid limit process number $\mathscr{F}$ should be less than 0.001 can tell in which case this approximation is valid.

Compared to previous approaches, the established method has the following advantages:

• It can calculate both small and large angle TPW.

• Both long-term secular trend as well as the short-term Chandler wobble for fast-rotating bodies can be obtained.

• The long-term mega wobble for slowly rotating objects can also be dealt with.

• A dynamic solution for reorientation of tidally deformed bodies can be obtained.

• The effect of the lithosphere can be directly included and models which are not in hydrostatic equilibrium can also be taken into account.

- Complex rheology and lateral heterogeneity of the model can be dealt with.

As discussed in chapter 1, understanding TPW is crucial to provide a link between the formation of some observed planetary features and the interior properties of the body. Simply speaking, for non-tidally deformed bodies, the new method provides a more accurate simulation of TPW compared with previous methods. For tidally deformed (locked) bodies, the time-dependent solution for the reorientation of the body can be obtained by the new method. This extra accuracy and applicability can provide us with new insight on the rotational variations of various planetary bodies, which can further contribute to the understanding of the interior and dynamics of the bodies themselves.

Answer to question 1: Intrinsic error in the linear method

In the linear method, the MoI is always calculated in the body-fixed frame which is not updated in the bulge-fixed frame. This creates an intrinsic error which may not be small even when only small angle TPW is considered. This is because the value of the MoI of a mass anomaly is very sensitive to the latitude of the anomaly (section 3.3) when it is close to the poles or equator. Thus, the applicable range of the linear method is not only constrained by the linearisation of the Liouville equation but also by the error introduced by the manner in which the MoI of the mass anomaly is calculated. For example, TPW on the Earth partly originates from ice loss which mainly originates from Antarctica and Greenland that is close to the pole, e.g. (Chen et al., 2013). For mass anomalies located at this high latitude, if the estimated TPW angle is beyond 0.8 degree, then the linear method will result in an error beyond 1.5 %, see figure 3.7. This error can result in an incorrect estimation of the ice loss in these areas if TPW is used as a constraint.

Answer to question 2 and 4: Validity of the quasi-fluid approximation

As has been discussed in Chapters 3 and 4, in order to solve the MoI equation which contains the convolution of the Love number with the centrifugal/tidal potential, the non-linear method (Ricard et al., 1993) adopts the quasi-fluid approximation to simplify the Love number. Mathematically, this approximation is the first order Taylor expansion in the Laplace domain. The cost of this approximation is that viscoelasticity is not perfectly accounted for. For the polar wander case on the Earth or Mars, taking the quasi-fluid approximation can underestimate the speed of the equatorial bulge readjustment, which leads to an underestimation of the TPW speed by a factor of about 4, see figures 3.8 and 4.9. On the other hand, for slowly rotating objects such as Venus, the quasi-fluid approximation overestimates the equatorial bulge readjustment speed in the latitudinal direction, causing too much damping of the mega wobble. This results in an overestimation of a factor of 3 to 5.

It was also shown in chapter 5 that the quasi-fluid approximation can only be adopted when the speed of TPW is slow enough so that the body is sufficiently relaxed to be close to a fluid-limit state during the TPW. In the same chapter, we state that the product of inertia of the body in the bulge-fixed frame describes whether the body has relaxed sufficiently (a fully relaxed body has product of the inertia in the bulge-fixed frame that is equal to zero). As a result, a quantitative criterion, that the fluid limit process number $\mathscr{F}$ must be less than

0.001, is also provided in chapter 5 to test if for a given situation, model and TPW speed, the method based on the quasi-fluid approximation can provide an accurate result. The fluid limit process number can be calculated when the tidal Love number and the estimated TPW speed is given. We conclude that the fluid limit process number must be smaller than 0.001 for the quasi-fluid approximation to be adopted.

Answer to question 3 and 4: Validity of the fluid limit approximation

Similar to the quasi-fluid approximation, the fluid limit method is only valid when the speed of TPW is relatively slow, as discussed in chapter 5. The fluid limit approximation assumes that during the TPW the non-lithospheric part of the body is fully relaxed. This requires that either the body is less viscous so the readjustment of the body is fast enough or the TPW speed itself is slow enough. The fluid limit process number $\mathscr{F}$ can also be the criterion for the validity of the fluid limit approximation and the standard, $\mathscr{F} < 0.001$, still applies in this case. As shown in chapter 5, if $\mathscr{F}$ is larger than this value, the obtained reorientation path for a tidally deformed body given by the fluid limit method (Matsuyama and Nimmo, 2007) for a time-dependent load can have a large bias. For bodies without a tidal bulge, failing this criterion means a large overestimation of the TPW speed, in contrast with an underestimation of TPW speed for the quasi-fluid approximation.

TPW on various planetary bodies

In this part, we want to focus on the polar wander behaviour on various planetary bodies in our solar system which has been introduced in chapter 1 based on the new method.

Earth. For TPW on the Earth, currently the speed and direction of present day TPW is of high interest. Many studies concerning this topic focus on the effect on TPW from post-glacial rebound (Spada et al., 1992b) or ongoing ice loss in Greenland or Antarctica (Besse and Courtillot, 2002). On a million year time scale, these factors only cause a small angle TPW (Ricard et al., 1993). Providing a realistic model, such as the Preliminary reference Earth model (PREM) (Dziewonski and Anderson, 1981), both the linear method and our approach can yield an accurate present day TPW speed. However, due to the intrinsic error of the linear method, predicting future TPW behaviour for more than 0.8 degree with the linear approach can result in erroneous conclusions.

Mars. Due to the presence of the Tharsis plateau, Mars is believed to have experienced a large angle TPW (Schultz and Lutz, 1988; Bouley et al., 2016). The TPW history of Mars cannot be modeled accurately because of the uncertainties in both the viscosity of the body and the formation history of the Tharsis plateau, as discussed in section 1.2.2. What can be said is that previous predictions of the TPW speed (about 1 degree/Ma) based on the quasi-fluid approximations, e.g. Chan et al. (2014), can be underestimated by a factor of 4, given the possible range of the Martian viscosities (see chapter 4 and figure 4.9). An incorrectly estimated TPW speed on Mars can results in an erroneous estimation for the age of the Tharsis

plateau or the interior viscosity.

Venus. TPW on Venus is dominated by the long-term wobble, as shown in section 4.3. Different from the phenomena on Earth and Mars, the rotational axis of the Venus will circle around the mass anomaly that triggers the TPW instead of going towards it. The influence of taking the quasi-fluid approximation in studying the mega wobble on Venus is significant. A previous study (Spada et al., 1996) overestimated the speed of a mass anomaly on Venus approaching the pole or equator. If we assume that Venus has similar viscosity as the Earth or Mars, a mass anomaly of the same scale will take a factor of 10 to 15 longer on Venus to reach the pole or equator than on the Earth or Mars. And this time scale is underestimated by previous studies by a factor of 3-5.

Icy moons. Most known icy moons are tidally locked to a much more massive host body, which creates a tidal bulge that is about 3 times the magnitude of the centrifugal bulge. We have shown in chapter 3 and 5 that the reorientation of such bodies triggered by a positive mass anomaly has a preference of first reorienting around the tidal axis to place the mass anomaly close to the equator, see figures 3.10 and 5.1. Then the speed of the reorientation slows down and the mass anomaly is pushed slowly towards the sub-host or anti-host points. Consequently, TPW on an icy moon triggered by ice caps on the poles would see the body reorient around the tidal axis first, different from what is predicted by the fluid-limit methods (Rubincam, 2003; Matsuyama and Nimmo, 2007). The presence of a lithosphere mostly determines how far the positive mass anomalies can be pushed towards the sub- and anti-host points (see figure 4.7) but the mass anomalies are still more likely to be found around the equator.

Pluto. Although Pluto is tidally locked with its moon Charon, the mass of Charon is only about 12% of that of Pluto which creates a relatively small tidal bulge compared to most of the icy moons. As a result, the reorientation on Pluto only has part of the features of TPW on other tidally deformed bodies. Positive mass anomalies tend to be relocated towards the sub- and anti-host points and negative mass anomalies tend to be pushed towards the poles. However, the reorientation path on Pluto does not have a strong preference of firstly reorienting around the tidal axis. Instead the path of the mass anomaly is almost a straight line (see figure 5.2). This means the reorientation path obtained in previous studies based on the fluid-limit method, e.g. (Keane et al., 2016), is likely to be accurate. However, the speed of the reorientation can still be biased by the fluid limit method depending on the viscosity of the planet as well as by the load history: how fast the volatiles accumulate in the Sputnik Planitia (Keane et al., 2016) and the ocean wells up (Nimmo et al., 2016).

To sum up this part, TPW on various planetary bodies, either the path or the speed, estimated by previous methods can contain large biases. Such errors can lead to erroneous estimations, such as on viscosity of the planet, the age of certain observed features or the stress distribution/history of the surface. The new method established in this thesis provides a more advanced tool for planetary scientists to properly interpret rotational variations on various bodies.

6.2. RECOMMENDATIONS

The research presented in this thesis can be followed by further studies in two aspects: applications of the developed method or a further development of the method. Both will be discussed in the following.

Possible applications

- Constraining the age of the Sputnik Planitia and the viscosity of Pluto. Similar to studies such as Nimmo et al. (2016); Keane et al. (2016), we can use the developed method in this thesis instead of the fluid limit approach to further constrain the history of mass accumulation in the Sputnik Planitia, e.g. how fast the volatiles accumulate or the ocean wells up, to obtain further insight on Pluto. Another constraint on the load such as the energy flux from the Sun during the formation history of this area (Hamilton et al., 2016) can also provide useful information to constrain the formation history of this area.

- Constraining Martian viscosity from its TPW history. To constrain the viscosity of a planet by TPW theory, a time-dependent TPW history is required. This information on Mars can be estimated from various studies such as its topography, e.g. (Bouley et al., 2016), or surface hydrogen distribution, e.g. (Feldman et al., 2004). Once a TPW history is known, given an assumed loading history, the viscosity of the body can be constrained.

- Constraining the interior model of Enceladus and Europa. Topographic data on these icy satellites can provide a detailed reorientation path (Tajeddine et al., 2017). Since icy moons are tidally deformed, for each specific load the reorientation path is unique (see figure 5.3). A detailed reorientation path on a tidally deformed body gives a very strong constraint on both the load and the interior model compared to bodies without a tidal bulge (see section 5.4). However, these studies on icy moons likely require modelling differential rotation. This issue will be discussed in the next part about further model development.

- Studying the effect of varying shell thickness on icy moons on its reorientation such as Enceladus on the TPW. This can help us to gain further knowledge on the formation of Enceladus' south pole region. The numerical model based on the finite element method (chapter 3) can deal with the lateral heterogeneity introduced by an outer shell of varying thickness. However, current models can only deal with the case in which the shell and interior co-rotate, see also the next section for recommendations for further development of models for differential rotation.

Model development

The new method developed in this thesis still has limitations. For instance, only torque-free rotational variations are considered and differential rotation is ignored. In order to take these issues into account, further model development is required. This is discussed in the following.

The first possible extension of the developed method would be introducing torque into our model for dealing with torque driven rotational variations, such as libration and non-synchronous rotation (NSR). NSR has not been discussed in this thesis but, just like TPW, is believed to be the cause of many observed surface features, such as the longitudinal migration of tectonic patterns on Europa (Hurford et al., 2007; Rhoden et al., 2010; Jara-Orué and Vermeersen, 2011).

A finite element model can deal with a lateral heterogeneous planet. However, a further development of the numerical model is required for dealing with an elastic or highly viscous lithosphere in the finite element package. As mentioned in chapter 4, currently, it is very difficult to introduce the correct 'background shape' for the elastic or highly viscous part of the body in a finite element framework. One possible way to solve this problem is to first obtain the correct shape for the lithosphere with a model which has much lower viscosity, then continue the simulation by setting the viscosity to the desired value. In this way, the extremely long calculation time caused by the viscosity contrast between the lithosphere and the rest of the body can be avoided.

Another interesting phenomenon that is not discussed in this thesis is differential rotation of the shell and the interior. This issue is crucial for the study of rotational variations of icy moons which are believed to have a global sub-surface ocean. For the topic of differential rotation, previous studies mostly adopted an analytical approach and only focused on the small short-term perturbations where a linear scheme can be used (Mathews et al., 1991; Dehant et al., 1993; Dumberry, 2009; Jara-Orué and Vermeersen, 2011). The semi-analytical approach in this thesis can be extended, e.g. adding the ocean dynamics and torques between the shell and inner core (Hoolst et al., 2008) into the iterative procedure, to cope with differential rotation. Since the governing equations are decoupled in our method, the influence of the fluid layer and associated fluid dynamics can be directly included into the iteration. For instance, we can apply the method developed in this thesis to both the inner solid part of the body and the outer shell with an initial condition for the interface of the fluid layer. The result of these two parts provides the boundary condition to the fluid layer where a fluid dynamic model needs to be applied and new interface conditions are obtained. This forms an iterative procedure which includes two solid models and one fluid model.

BIBLIOGRAPHY

Arkani-Hamed, J. (2009). Polar wander of Mars: Evidence from giant impact basins. *Icarus*, 204(2):489 – 498.

Armann, M. and Tackley, P. J. (2012). Simulating the thermochemical magmatic and tectonic evolution of Venus's mantle and lithosphere: Two-dimensional models. *Journal of Geophysical Research: Planets*, 117(E12). E12003.

Arvo, J. (1992). Graphics Gems III. chapter Fast Random Rotation Matrices, pages 117–120. Academic Press Professional, Inc., San Diego, CA, USA.

Besse, J. and Courtillot, V. (1991). Revised and synthetic apparent polar wander paths of the African, Eurasian, North American and Indian Plates, and true polar wander since 200 ma. *Journal of Geophysical Research: Solid Earth*, 96(B3):4029–4050.

Besse, J. and Courtillot, V. (2002). Apparent and true polar wander and the geometry of the geomagnetic field over the last 200 myr. *Journal of Geophysical Research: Solid Earth*, 107(B11):EPM 6–1–EPM 6–31. 2300.

Bouley, S., Baratoux, D., Matsuyama, I., Forget, F., Séjourné, A., Turbet, M., and Costard, F. (2016). Late Tharsis formation and implications for early Mars. *Nature*, 531(7594):344–347.

Breuer, D. and Spohn, T. (2006). Viscosity of the Martian mantle and its initial temperature: Constraints from crust formation history and the evolution of the magnetic field. *Planetary and Space Science*, 54(2):153 – 169.

Cambiotti, G., Ricard, Y., and Sabadini, R. (2010). Ice age true polar wander in a compressible and non-hydrostatic Earth. *Geophysical Journal International*, 183(3):1248–1264.

Cambiotti, G., Ricard, Y., and Sabadini, R. (2011). New insights into mantle convection true polar wander and rotational bulge readjustment. *Earth and Planetary Science Letters*, 310(3–4):538 – 543.

Chan, N.-H., Mitrovica, J. X., Daradich, A., Creveling, J. R., Matsuyama, I., and Stanley, S. (2014). Time-dependent rotational stability of dynamic planets with elastic lithospheres. *Journal of Geophysical Research: Planets*, 119(1):169–188.

Chen, J. L., Wilson, C. R., Ries, J. C., and Tapley, B. D. (2013). Rapid ice melting drives earth's pole to the east. *Geophysical Research Letters*, 40(11):2625–2630.

Dehant, V., Hinderer, J., Legros, H., and Lefftz, M. (1993). Analytical approach to the computation of the Earth, the outer core and the inner core rotational motions. *Physics of the Earth and Planetary Interiors*, 76:259–282.

Dehlinger, P. (1978). *Marine Gravity*. Elsevier Scientific Pub. Co. New York.

Dumberry, M. (2009). Influence of elastic deformations on the inner core wobble. *Geophysical Journal International*, 178(1):57–64.

Dziewonski, A. M. and Anderson, D. L. (1981). Preliminary Reference Earth Model. *Physics of the Earth and Planetary Interiors*, 25(4):297 – 356.

Evans, J. (1866). On a possible geological cause of changes in the position of the axis of the Earth's crust. *Proceedings of the Royal Society of London*, 15:46–54.

Farrell, W. E. (1972). Deformation of the Earth by surface loads. *Reviews of Geophysics*, 10(3):761–797.

Feldman, W. C., Prettyman, T. H., Maurice, S., Plaut, J. J., Bish, D. L., Vaniman, D. T., Mellon, M. T., Metzger, A. E., Squyres, S. W., Karunatillake, S., Boynton, W. V., Elphic, R. C., Funsten, H. O., Lawrence, D. J., and Tokar, R. L. (2004). Global distribution of near-surface hydrogen on Mars. *Journal of Geophysical Research: Planets*, 109(E9). E09006.

Garrick-Bethell, I., Wisdom, J., and Zuber, M. T. (2006). Evidence for a past high-eccentricity lunar orbit. *Science*, 313(5787):652–655.

Gold, T. (1955). Instability of the Earth's axis of rotation. *Nature*, 175(4456):526–529.

Goldreich, P. and Toomre, A. (1969). Some remarks on polar wandering. *Journal of Geophysical Research*, 74(10):2555–2567.

Goossens, S., Sabaka, T. J., Genova, A., Mazarico, E., Nicholas, J. B., and Neumann, G. A. (2017). Evidence for a low bulk crustal density for mars from gravity and topography. *Geophysical Research Letters*, 44(15):7686–7694. 2017GL074172.

Gross, R. S. (2000). The excitation of the Chandler wobble. *Geophysical Research Letters*, 27(15):2329–2332.

Hamilton, D. P., Stern, S. A., Moore, J. M., Young, L. A., and the New Horizons Geology, Geophysics and Imaging Theme Team (2016). The rapid formation of sputnik planitia early in pluto's history. *Nature*, 540(7631):97–99.

Harada, Y. (2012). Long-term polar motion on a quasi-fluid planetary body with an elastic lithosphere: Semi-analytic solutions of the time-dependent equation. *Icarus*, 220(2):449–465.

Harada, Y. and Xiao, L. (2015). A timescale of true polar wander of a quasi-fluid Earth: An effect of a low-viscosity layer inside a mantle. *Physics of the Earth and Planetary Interiors*, 240:25 – 33.

Hauck, S. A. and Phillips, R. J. (2002). Thermal and crustal evolution of Mars. *Journal of Geophysical Research: Planets*, 107(E7):6–1–6–19.

Hinderer, J., Legros, H., and Amalvict, M. (1982). A search for Chandler and nearly diurnal free wobbles using Liouville equations. *Geophysical Journal International*, 71(2):303–332.

Hoolst, T. V., Rambaux, N., Karatekin, Ö., Dehant, V., and Rivoldini, A. (2008). The librations, shape, and icy shell of Europa. *Icarus*, 195(1):386 – 399.

Hu, H., van der Wal, W., and Vermeersen, L. L. A. (2017a). A Full-Maxwell approach for large-angle polar wander of viscoelastic bodies. *Journal of Geophysical Research: Planets*, 122(12):2745–2764. 2017JE005365.

Hu, H., van der Wal, W., and Vermeersen, L. L. A. (2017b). A numerical method for reorientation of rotating tidally deformed viscoelastic bodies. *Journal of Geophysical Research: Planets*, 122(1):228–248. 2016JE005114.

Hurford, T., Sarid, A., and Greenberg, R. (2007). Cycloidal cracks on europa: Improved modeling and non-synchronous rotation implications. *Icarus*, 186(1):218–233.

Hynek, B. M. and Phillips, R. J. (2001). Evidence for extensive denudation of the Martian highlands. *Geology*, 29(5):407.

Iess, L., Stevenson, D. J., Parisi, M., Hemingway, D., Jacobson, R. A., Lunine, J. I., Nimmo, F., Armstrong, J. W., Asmar, S. W., Ducci, M., and Tortora, P. (2014). The gravity field and interior structure of Enceladus. *Science*, 344(6179):78–80.

Jara-Orué, H. M. and Vermeersen, B. L. (2011). Effects of low-viscous layers and a non-zero obliquity on surface stresses induced by diurnal tides and non-synchronous rotation: The case of Europa. *Icarus*, 215(1):417 – 438.

Jurdy, D. (1978). An alternative model for early tertiary absolute plate motions. *Geology*, 6(1).

Keane, J. T., Matsuyama, I., Kamata, S., and Steckloff, J. K. (2016). Reorientation and faulting of Pluto due to volatile loading within Sputnik Planitia. *Nature*, 540(7631):90–93.

Kite, E. S., Matsuyama, I., Manga, M., Perron, J. T., and Mitrovica, J. X. (2009). True Polar Wander driven by late-stage volcanism and the distribution of paleopolar deposits on Mars. *Earth and Planetary Science Letters*, 280:254–267.

Lambeck, K. (1988). *Geophysical Geodesy: The Slow Deformations of the Earth*. Oxford science publications. Clarendon Press.

Lambeck, K. (2005). *The Earth's Variable Rotation: Geophysical Causes and Consequences*. Cambridge Monographs on Mechanics. Cambridge University Press.

Malcuit, R. (2014). *The Twin Sister Planets Venus and Earth: Why Are They so Different?* SpringerLink: Bücher. Springer International Publishing.

Mansinha, L. and Smylie, D. E. (1967). Effect of earthquakes on the chandler wobble and the secular polar shift. *Journal of Geophysical Research*, 72(18):4731–4743.

Mathews, P. M., Buffett, B. A., Herring, T. A., and Shapiro, I. I. (1991). Forced nutations of the Earth: Influence of inner core dynamics: 1. theory. *Journal of Geophysical Research: Solid Earth*, 96(B5):8219–8242.

Matsuyama, I. (2013). Fossil figure contribution to the lunar figure. *Icarus*, 222(1):411 – 414.

Matsuyama, I., Mitrovica, J. X., Daradich, A., and Gomez, N. (2010). The rotational stability of a triaxial ice-age Earth. *Journal of Geophysical Research: Solid Earth*, 115(B5):B05401. B05401.

Matsuyama, I. and Nimmo, F. (2007). Rotational stability of tidally deformed planetary bodies. *Journal of Geophysical Research: Planets*, 112(E11).

Matsuyama, I., Nimmo, F., and Mitrovica, J. X. (2014). Planetary reorientation. *Annual Review of Earth and Planetary Sciences*, 42(1):605–634.

McKay, C. P., Anbar, A. D., Porco, C., and Tsou, P. (2014). Follow the plume: The habitability of Enceladus. *Astrobiology*, 14(4):352–355.

Miettinen, K. (1999). *Nonlinear Multiobjective Optimization*. International Series in Operations Research & Management Science. Springer US.

Mitrovica, J. X. and Wahr, J. (2011). Ice age Earth rotation. *Annual Review of Earth and Planetary Sciences*, 39(1):577–616.

Mitrovica, J. X., Wahr, J., Matsuyama, I., and Paulson, A. (2005). The rotational stability of an ice-age Earth. *Geophysical Journal International*, 161(2):491–506.

Moore, K., Chan, N.-H., Daradich, A., and Mitrovica, J. (2017). Time-dependent rotational stability of dynamic planets with viscoelastic lithospheres. *Icarus*, 289(C):34 – 41.

Mound, J. E., Mitrovica, J. X., and Forte, A. M. (2003). The equilibrium form of a rotating Earth with an elastic shell. *Geophysical Journal International*, 152(1):237.

Munk, W. and MacDonald, G. (1960). *The Rotation of the Earth: A Geophysical Discussion*. Cambridge monographs on mechanics and applied mathematics. University Press.

Murray, B. C. and Malin, M. C. (1973). Polar wandering on Mars? *Science*, 179(4077):997–1000.

Murray, C. and Dermott, S. (2000). *Solar System Dynamics*. Cambridge University Press.

Nakada, M. (2002). Polar wander caused by the Quaternary glacial cycles and fluid Love number. *Earth and Planetary Science Letters*, 200(1–2):159 – 166.

Nakada, M. (2007). True polar wander associated with continental drift on a hypothetical Earth. *Earth, Planets and Space*, 59(6):513–522.

Nakiboglu, S. M. and Lambeck, K. (1980). Deglaciation effects on the rotation of the Earth. *Geophysical Journal of the Royal Astronomical Society*, 62(1):49–58.

Nimmo, F., Hamilton, D. P., McKinnon, W. B., Schenk, P. M., Binzel, R. P., Bierson, C. J., Beyer, R. A., Moore, J. M., Stern, S. A., Weaver, H. A., Olkin, C. B., Young, L. A., Smith, K. E., and New Horizons Geology, Geophysics and Imaging Theme Team (2016). Reorientation of Sputnik Planitia implies a subsurface ocean on Pluto. *Nature*, 540(7631):94–96.

Nimmo, F. and Pappalardo, R. T. (2006). Diapir-induced reorientation of saturn's moon Enceladus. *Nature*, 441(7093):614–616. 10.1038/nature04821.

Nimmo, F. and Tanaka, K. (2005). Early crustal evolution of Mars. *Annual Review of Earth and Planetary Sciences*, 33(1):133–161.

Ojakangas, G. W. and Stevenson, D. J. (1989). Polar wander of an ice shell on Europa. *Icarus*, 81(2):242 – 270.

Peltier, W. R. (1974). The impulse response of a Maxwell Earth. *Reviews of Geophysics*, 12(4):649–669.

Peltier, W. R. and Jiang, X. (1996). Glacial isostatic adjustment and Earth rotation: Refined constraints on the viscosity of the deepest mantle. *Journal of Geophysical Research: Solid Earth*, 101(B2):3269–3290.

Press, F. and Briggs, P. (1975). Chandler wobble, earthquakes, rotation, and geomagnetic changes. *Nature*, 256(5515):270–273. 10.1038/256270a0.

Renaud, J. P. and Henning, W. G. (2017). Increased Tidal Dissipation using Realistic Rheological Models: the Thermal History of Io and Tidally Active Extrasolar Planets. *ArXiv e-prints*.

Rhoden, A. R., Militzer, B., Huff, E. M., Hurford, T. A., Manga, M., and Richards, M. A. (2010). Constraints on europa's rotational dynamics from modeling of tidally-driven fractures. *Icarus*, 210(2):770 – 784.

Ricard, Y., Spada, G., and Sabadini, R. (1993). Polar wandering of a dynamic Earth. *Geophysical Journal International*, 113(2):284–298.

Rouby, H., Greff-Lefftz, M., and Besse, J. (2010). Mantle dynamics, geoid, inertia and TPW since 120 myr. *Earth and Planetary Science Letters*, 292(3–4):301 – 311.

Rubincam, D. P. (2003). Polar wander on Triton and Pluto due to volatile migration. *Icarus*, 163(2):469 – 478.

Sabadini, R. and Peltier, W. R. (1981). Pleistocene deglaciation and the Earth's rotation: Implications for mantle viscosity. *Geophysical Journal of the Royal Astronomical Society*, 66(3):553–578.

Sabadini, R., Vermeersen, B., and Cambiotti, G. (2016). *Global Dynamics of the Earth: Applications of Viscoelastic Relaxation Theory to Solid-Earth and Planetary Geophysics, 2nd edition*. Springer Netherlands.

Sabadini, R., Yuen, D. A., and Boschi, E. (1982). Polar wandering and the forced responses of a rotating, multilayered, viscoelastic planet. *Journal of Geophysical Research: Solid Earth*, 87(B4):2885–2903.

Schenk, P., Matsuyama, I., and Nimmo, F. (2008). True polar wander on europa from global-scale small-circle depressions. *Nature*, 453(7193):368–371. 10.1038/nature06911.

Schultz, P. H. and Lutz, A. B. (1988). Polar wandering of Mars. *Icarus*, 73(1):91–141.

Seidelmann, P. K. (1982). 1980 IAU theory of nutation - The final report of the IAU Working Group on Nutation. *Celestial Mechanics*, 27:79–106.

Showman, A. P., Han, L., and Hubbard, W. B. (2013). The effect of an asymmetric core on convection in enceladus' ice shell: Implications for south polar tectonics and heat flux. *Geophysical Research Letters*, 40(21):5610–5614.

Siegler, M. A., Miller, R. S., Keane, J. T., Laneuville, M., Paige, D. A., Matsuyama, I., Lawrence, D. J., Crotts, A., and Poston, M. J. (2016). Lunar true polar wander inferred from polar hydrogen. *Nature*, 531(7595):480–484.

Smith, D. E., Zuber, M. T., Solomon, S. C., Phillips, R. J., Head, J. W., Garvin, J. B., Banerdt, W. B., Muhleman, D. O., Pettengill, G. H., Neumann, G. A., Lemoine, F. G., Abshire, J. B., Aharonson, O., David, C., Brown, Hauck, S. A., Ivanov, A. B., McGovern, P. J., Zwally, H. J., and Duxbury, T. C. (1999). The global topography of mars and implications for surface evolution. *Science*, 284(5419):1495–1503.

Spada, G., Ricard, Y., and Sabadini, R. (1992a). Excitation of true polar wander by subduction. *Nature*, 360(6403):452–454.

Spada, G., Sabadini, R., and Boschi, E. (1996). Long-term rotation and mantle dynamics of the Earth, Mars, and Venus. *Journal of Geophysical Research: Planets*, 101(E1):2253–2266.

Spada, G., Sabadini, R., Yuen, D. A., and Ricard, Y. (1992b). Effects on post-glacial rebound from the hard rheology in the transition zone. *Geophysical Journal International*, 109(3):683–700.

Spencer, J. R. and Nimmo, F. (2013). Enceladus: An active ice world in the Saturn System. *Annual Review of Earth and Planetary Sciences*, 41(1):693–717.

Spohn, T., Breuer, D., and Johnson, T. (2014). *Encyclopedia of the Solar System*. Elsevier Science.

Steinberger, B. and O'Connell, R. J. (1997). Changes of the Earth's rotation axis owing to advection of mantle density heterogeneities. *Nature*, 387(6629):169–173. 10.1038/387169a0.

Tajeddine, R., Soderlund, K. M., Thomas, P. C., Helfenstein, P., Hedman, M. M., Burns, J. A., and Schenk, P. M. (2017). True polar wander of Enceladus from topographic data. *Icarus*, 295:46 – 60.

Thomas, P, Tajeddine, R., Tiscareno, M., Burns, J., Joseph, J., Loredo, T., Helfenstein, P., and Porco, C. (2016). Enceladus's measured physical libration requires a global subsurface ocean. *Icarus*, 264:37 – 47.

Šrámek, O. and Zhong, S. (2012). Martian crustal dichotomy and Tharsis formation by partial melting coupled to early plume migration. *Journal of Geophysical Research: Planets*, 117(E1).

van der Wal, W., Whitehouse, P. L., and Schrama, E. J. O. (2015). Effect of GIA models with 3D composite mantle viscosity on GRACE mass balance estimates for Antarctica. *Earth and Planetary Science Letters*, 414:134 – 143.

Vermeersen, L. L. A. and Sabadini, R. (1996). Significance of the fundamental mantle rotational relaxation mode in polar wander simulations. *Geophysical Journal International*, 127(2):F5–F9.

Wahr, J. M. (1983). The effects of the atmosphere and oceans on the Earth's wobble and on the seasonal variations in the length of day - II. Results. *Geophysical Journal of the Royal Astronomical Society*, 74(2):451–487.

Wang, H., Wu, P., and van der Wal, W. (2008). Using postglacial sea level, crustal velocities and gravity-rate-of-change to constrain the influence of thermal effects on mantle lateral heterogeneities. *Journal of Geodynamics*, 46:104–117.

Willemann, R. J. (1984). Reorientation of planets with elastic lithospheres. *Icarus*, 60:701–709.

Williams, J.-P., Nimmo, F., Moore, W. B., and Paige, D. A. (2008). The formation of Tharsis on Mars: What the line-of-sight gravity is telling us. *Journal of Geophysical Research: Planets*, 113(E10). E10011.

Wu, P. (2004). Using commercial finite element packages for the study of Earth deformations, sea levels and the state of stress. *Geophysical Journal International*, 158(2):401–408.

Wu, P. and Peltier, W. R. (1984). Pleistocene deglaciation and the Earth's rotation: A new analysis. *Geophysical Journal of the Royal Astronomical Society*, 76(3):753–791.

Wu, P. and van der Wal, W. (2003). Postglacial sealevels on a spherical, self-gravitating viscoelastic Earth: effects of lateral viscosity variations in the upper mantle on the inference of viscosity contrasts in the lower mantle. *Earth and Planetary Science Letters*, 211(1–2):57 – 68.

Wu, P. and Wang, H. (2006). Effects of mode coupling and location of rotational axis on glacial induced rotational deformation in a laterally heterogeneous viscoelastic Earth. *Geophysical Journal International*, 167(2):853–859.

Zahnle, K. and Walker, J. C. (1987). A constant daylength during the Precambrian era? *Precambrian Research*, 37(2):95 – 105.

Zharkov, V. N. and Gudkova, T. V. (2005). Construction of Martian interior model. *Solar System Research*, 39(5):343–373.

Zhong, S., Paulson, A., and Wahr, J. (2003). Three-dimensional finite-element modelling of earth's viscoelastic deformation: effects of lateral variations in lithospheric thickness. *Geophysical Journal International*, 155(2):679–695.

CURRICULUM VITAE

Haiyang Hu was born in Chengdu, China on 9th of July, 1984. He attended secondary school at Chengdu Experimental Foreign Language School in 1997. In 2003, he started his bachelor in Mechanics at Peking University in Bejing with a double major in Fundamental Mathematics. After he graduated in 2007, he trolled for two years around many places in China. He came to the Netherlands in 2009 and entered Hogeschool Fontys in Eindhoven, with major Electrical Engineering. He did an internship in GE security in 2010 for 6 months where he designed a motion detector to distinguish between a human and a pet. He entered TU Delft for a master study in 2010, with major Control and Simulation in the faculty Aerospace Engineering and obtained his MSc. diploma with *cum laude* in 2012. His master thesis was entitled *The stability of uncertain systems and application of interval analysis.*

He started his PhD in 2013, working on an NWO funded project entitled: *Transient Rotational Variations of Icy Moons.* The main goal of this project was to use 3D finite element modeling to study the effect of heterogeneity on rotational behaviours of icy moons. For the first two years of his PhD work, he established a new finite element framework using Abaqus, which can be used to calculate the deformation of planetary bodies. Now, this program is used by other PhD and master students in the department of Astrodynamics and Space Missions. For the second two years, he changed the original plan of the proposal and focused on the theoretical development of rotational variations of planetary bodies, both numerically and analytically. These works have led to the content of this dissertation.

LIST OF PUBLICATIONS

Journal Publications:

Hu, H., van der Wal, W., & Vermeersen, L. L. A. (2018). Rotational dynamics of tidally deformed planetary bodies and validity of fluid limit and quasi-fluid approximation. *Icarus* (submitted).

Hu, H., van der Wal, W., & Vermeersen, L. L. (2017b). A full-Maxwell approach for large-angle polar wander of viscoelastic bodies. *Journal of Geophysical Research: Planets*, 122(12):2745-2764.

Hu, H., van der Wal, W., & Vermeersen, L. L. A. (2017a). A numerical method for reorientation of rotating tidally deformed viscoelastic bodies. *Journal of Geophysical Research: Planets*, 122, 228-248.

Conference Papers:

Hu, H., van Kampen, E., & Chu, Q.P. (2013). Stability of uncertain LTI systems and application of interval analysis. *AIAA Guidance, Navigation, and Control (GNC) Conference.*

Popular Science Writings:

Time, Tides and Wandering poles. *Earth & Space Science News (EOS).*